TECHNICAL REPORT STANDARD TITLE PAGE

1. Report No.	2. Government Accession No.	3. Recipient's Catalog No.
FHWA/TX-86/79+350-2		

4. Title and Subtitle	5. Report Date
DISTRIBUTION OF GIRDER LOADS IN A COMPOSITE HIGHWAY BRIDGE	December 1985
	6. Performing Organization Code
7. Author(s)	8. Performing Organization Report No.
C. W. Elling, R. E. Klingner, and N. H. Burns	Research Report 350-2
9. Performing Organization Name and Address	10. Work Unit No.
Center for Transportation Research The University of Texas at Austin Austin, Texas 78712-1075	11. Contract or Grant No. Research Study 3-5-83-350
12. Sponsoring Agency Name and Address	13. Type of Report and Period Covered
Texas State Department of Highways and Public Transportation; Transportation Planning Division P. O. Box 5051 Austin, Texas 78763	Interim
	14. Sponsoring Agency Code

15. Supplementary Notes

Study conducted in cooperation with the U. S. Department of Transportation, Federal Highway Administration. Research Study Title: "Behavior of Concrete Bridge Decks on Steel Beams—Verification of the Ontario Bridge Deck Design (With and Without Panels)"

16. Abstract

Background material on refined and simplified methods for the analysis of bridge superstructures was presented. Seven methods were briefly described: five refined methods and two simplified methods. Using the full-scale experimental specimen of Project 350, subjected to vertical loads at 4 points on the deck surface, the variation of bending moments along the length of center girder was determined, both before and after deck cracking. These experimentally determined girder moments were compared with the moments obtained from the AASHTO Specifications, from the Ontario Highway Bridge Design Code, and from a finite element model of the bridge.

The experimentally determined values were approximated fairly closely by those of the Ontario Code and the finite element analysis. The peak moment predicted using the AASHTO procedure exceeded the corresponding experimental value by about 80 percent.

In assessing the proper role of these methods for estimating girder moments, it is important to recognize that each method has its place. An AASHTO-type method (or perhaps a simplification of the Ontario procedure) is necessary for preliminary design. After preliminary deck and girder sizes have been picked, an Ontario-type procedure can be used to produce a more efficient revised design. The finite element method appears advantageous primarily for checking local behavior.

17. Key Words	18. Distribution Statement
bridge, composite, girder, load, distribution, tests	No restrictions. This document is available to the public through the National Technical Information Service, Springfield, Virginia 22161.

19. Security Classif. (of this report)	20. Security Classif. (of this page)	21. No. of Pages	22. Price
Unclassified	Unclassified	164	

Form DOT F 1700.7 (8-69)

DISTRIBUTION OF GIRDER LOADS IN A COMPOSITE HIGHWAY BRIDGE

by

C. W. Elling, R. E. Klingner, and N. H. Burns

Research Report No. 350-2

Research Project 3-5-83-350

"Behavior of Concrete Bridge Decks on Steel Beams - Verification of the Ontario Bridge Deck Design (With and Without Panels)"

Conducted for

Texas

State Department of Highways and Public Transportation

In Cooperation with the
U.S. Department of Transportation
Federal Highway Administration

by

CENTER FOR TRANSPORTATION RESEARCH
BUREAU OF ENGINEERING RESEARCH
THE UNIVERSITY OF TEXAS AT AUSTIN

December 1985

The contents of this report reflect the view of the authors who are responsible for the facts and accuracy of the data presented herein. The contents do not necessarily reflect the views or policies of the Federal Highway Administration. This report does not constitute a standard, specification, or regulation.

P R E F A C E

Recent research in the U.S. and Canada has suggested that the flexural capacity of bridge decks is increased by in-plane compressive forces, created when the cracked deck is restrained by supports that cannot move laterally. This phenomenon, commonly referred to as "arching action," is the basis for the semi-empirical design provisions of the current Ontario (Canada) Bridge Design Code. That code permits the use of less flexural steel than would be required by current AASHTO Specifications, resulting in bridge decks which are generally more economical and resistant to corrosion.

Previous research on arching action has been carried out mainly using small-scale models with artificial boundary conditions. The overall objective of Research Project 3-5-83-350 was to study the performance of full-scale bridge decks designed taking arching action into account. Using a full-scale model of a realistic prototype highway bridge, both cast-in-place and precast, prestressed panel decks were considered.

During the course of Project 3-5-83-350, an opportunity became available to study the distribution of loads to the girders of the bridge. In the United States, slab and girder bridges are usually designed according to the AASHTO Specifications, which consider the slab and girders to act independently, and involve the use of empirical moment distribution coefficients. Several other procedures are also available. The specific objectives addressed in Report 350-2 were:

1. To measure the girder loads and bending moments in a full-scale bridge;

2. To compare the girder bending moments with those predicted using some of the available methods;

3. Based on this comparison, to assess the relative merits of the procedures studied.

S U M M A R Y

Background material on refined and simplified methods for the analysis of bridge superstructures was presented. Seven methods were briefly described: five refined methods and two simplified methods. Using the full-scale experimental specimen of Project 350, subjected to vertical loads at 4 points on the deck surface, the variation of bending moments along the length of center girder was determined, both before and after deck cracking. These experimentally determined girder moments were compared with the moments obtained from the AASHTO Specifications, from the Ontario Highway Bridge Design Code, and from a finite element model of the bridge.

The experimentally determined values were approximated fairly closely by those of the Ontario Code and the finite element analysis. The peak moment predicted using the AASHTO procedure exceeded the corresponding experimental value by about 80 percent.

In assessing the proper role of these methods for estimating girder moments, it is important to recognize that each method has its place. An AASHTO-type method (or perhaps a simplification of the Ontario procedure) is necessary for preliminary design. After preliminary deck and girder sizes have been picked, an Ontario-type procedure can be used to produce a more efficient revised design. The finite element method appears advantageous primarily for checking local behavior.

I M P L E M E N T A T I O N

While the results discussed in this report were not included in the original objectives of Project 350, they were obtained during that Project's investigation into the behavior of Ontario-type bridge decks. The distribution of girder loads and moments in composite highway bridges is a current topic of several research projects being conducted in the United States. Because the results discussed here represent a valid set of data regarding the distribution of moments in composite bridges, it was believed worthwhile to present them in the form of a research report.

TABLE OF CONTENTS

TABLE OF CONTENTS (continued)

LIST OF TABLES

LIST OF FIGURES

LIST OF FIGURES (continued)

LIST OF FIGURES (continued)

CHAPTER 1

INTRODUCTION

1.1 General

Slab and girder bridges, which carry loads by the combined action of the slab and the girders, are a common element in modern highway systems. Because such structures are usually statically indeterminate, girder moments and loads cannot easily be determined. Estimates of girder loads in slab and girder bridges are important both for evaluating existing bridges and for designing new ones. As will be discussed later, the theoretical methods which can be used to analyze slab and girder bridges are rather complicated.

In the United States, slab and girder bridges are usually designed according to the Specifications of the American Association of State Highway and Transportation Officials (AASHTO) [1]. This design procedure for slab and girder bridges, described in Section 3 of Reference 1, considers the slab and girders to act independently.

The deck slab is usually designed as a one-way slab spanning transversely between the girders. In computing design moments for the slab, no longitudinal distribution of live load bending moments is assumed. Under live load, transverse moments per foot of width of slab are calculated using the load on one rear wheel of a truck. Once the transverse moments in the slab are obtained, the size and spacing of the main transverse reinforcement are determined. Longitudinal distribution reinforcement, placed perpendicular to the main reinforcement, is calculated as a percentage of the transverse reinforcement.

Bending moments in the longitudinal girders are calculated according to Section 3.23 of the AASHTO Specifications. An individual girder is first isolated from the structure; if shear connectors are used to provide composite action, then an effective width of the slab is included as part of the girder. A single line of wheel loads from one truck is applied to the girder. The loads are placed on the span so as to produce maximum stress, and multiplied by an empirical distribution factor. Values of these empirical distribution factors for various types of bridges are listed in Table 3.23.1 of the AASHTO Specification (Table 1.1 on the following page). Design moments for the girder are calculated from these factored loads.

TABLE 1.1 AASHTO Empirical Load Distribution Factors
(Table 3.23.1, Ref. 1)

TABLE 3.23.1 Distribution of Wheel Loads in Longitudinal Beams

Kind of Floor	Bridge Designed for One Traffic Lane	Bridge Designed for Two or More Traffic Lanes
Timber:[a]		
Plank[b]	S/4.0	S/3.75
Nail laminated[c] 4" thick or multiple layer[d] floors over 5" thick	S/4.5	S/4.0
Nail laminated[c] 6" or more thick	S/5.0 If S exceeds 5' use footnote f.	S/4.25 If S exceeds 6.5' use footnote f.
Glued Laminated[e] Panels On Glued Laminated Stringers		
4" thick	S/4.5	S/4.0
6" or more thick	S/6.0 If S exceeds 6' use footnote f.	S/5.0 If S exceeds 7.5' use footnote f.
On Steel Stringers		
4" thick	S/4.5	S/4.0
6" or more thick	S/5.25 If S exceeds 5.5' use footnote f.	S/4.5 If S exceeds 7' use footnote f.
Concrete:		
On Steel I-Beam Stringers[g] and Prestressed Concrete Girders	S/7.0 If S exceeds 10' use footnote f.	S/5.5 If S exceeds 14' use footnote f.
On Concrete T-Beams	S/6.5 If S exceeds 6' use footnote f.	S/6.0 If S exceeds 10' use footnote f.
On Timber Stringers	S/6.0 If S exceeds 6' use footnote f.	S/5.0 If S exceeds 10' use footnote f.
Concrete Box Girders[h]	S/8.0 If S exceeds 12' use footnote f.	S/7.0 If S exceeds 16' use footnote f.
On Steel Box Girders	See Article 10.39.2.	
On Prestressed Concrete Spread Box Beams	See Article 3.28.	
Steel Grid:		
(Less than 4" thick)	S/4.5	S/4.0
(4" or more)	S/6.0 If S exceeds 6' use footnote f.	S/5.0 If S exceeds 10.5' use footnote f.
Steel Bridge Corrugated Plank[i] (2" min. depth)	S/5.5	S/4.5

S = average stringer spacing in feet.

[a]Timber dimensions shown are for nominal thickness.

[b]Plank floors consist of pieces of lumber laid edge to edge with the wide faces bearing on the supports (see Article 20.17—Division II).

[c]Nail laminated floors consist of pieces of lumber laid face to face with the narrow edges bearing on the supports, each piece being nailed to the preceding piece (see Article 20.18—Division II).

[d]Multiple layer floors consist of two or more layers of planks, each layer being laid at an angle to the other (see Article 20.17—Division II).

[e]Glued laminated panel floors consist of vertically glued laminated members with the narrow edges of the laminations bearing on the supports (see Article 20.1.1—Division II).

[f]In this case the load on each stringer shall be the reaction of the wheel loads, assuming the flooring between the stringers to act as a simple beam.

[g]"Design of I-Beam Bridges" by N. M. Newmark—Proceedings, ASCE, March 1948.

[h]The sidewalk live load (see Article 3.15) shall be omitted for interior and exterior box girders designed in accordance with the wheel load distribution indicated herein.

[i]Distribution factors for Steel Bridge Corrugated Plank set forth above are based substantially on the following reference:

Journal of Washington Academy of Sciences, Vol. 67, No. 2, 1977 "Wheel Load Distribution of Steel Bridge Plank," by Conrad P. Heins, Professor of Civil Engineering, University of Maryland.

These distribution factors were developed based on studies using 6" × 2" steel corrugated plank. The factors should yield safe results for other corrugation configurations provided primary bending stiffness is the same as or greater than the 6" × 2" corrugated plank used in the studies.

A qualitative example of this AASHTO procedure is illustrated in Fig. 1.1, and described below. The structure is a slab and steel girder bridge, simply supported, and loaded by four concentrated loads P which could represent the concentrated loads from a standard AASHTO H-20 truck loading. In this example, the center girder is chosen for design. As shown in Fig. 1.1b, two wheel loads are applied to that girder so as to produce maximum stress. The loads are multiplied by a distribution factor S/C, where S is the stringer spacing in ft, and C is a constant whose value depends on the bridge type. In the case of a slab and steel girder bridge designed for two or more lanes of traffic, the constant is 5.5, resulting in a distribution factor of about 1.0 for typical girder spacings. The resulting moments (Fig. 1.1c) are used to design the center (interior) girder. The design moments in the exterior girders can be obtained similarly. Girder design moments can also be calculated using the lane loading described in Section 3.6 of the AASHTO Specifications. The larger moment from either the lane loading or the truck loading should be used for design.

In addition to the AASHTO procedure, distribution factors can be obtained from the Ontario Highway Bridge Design Code [2]. Alternatively, the designer can calculate girder moments using one of the more accurate analytical techniques described in Chapter 3 of this thesis.

1.2 Objectives

As will be discussed subsequently, the current AASHTO procedure for determining girder moments usually provides a conservative estimate of the actual moments. To assess the validity of the AASHTO procedure, it was decided to investigate experimentally the distribution of girder moments and loads in a typical bridge. The specimen selected for study was a full-scale composite highway bridge on steel girders, constructed in the laboratory as part of another investigation [3]. In this thesis, some aspects of the testing of that bridge model will be described. The experimentally determined girder moments will be compared with the values obtained by theoretical analyses, both exact and approximate. This study has the following objectives:

1. to measure the girder loads and bending moments in a full-scale bridge;

2. to compare the girder bending moments with those predicted using some of the available methods; and

3. based on this comparison, to assess the relative merits of the procedures studied.

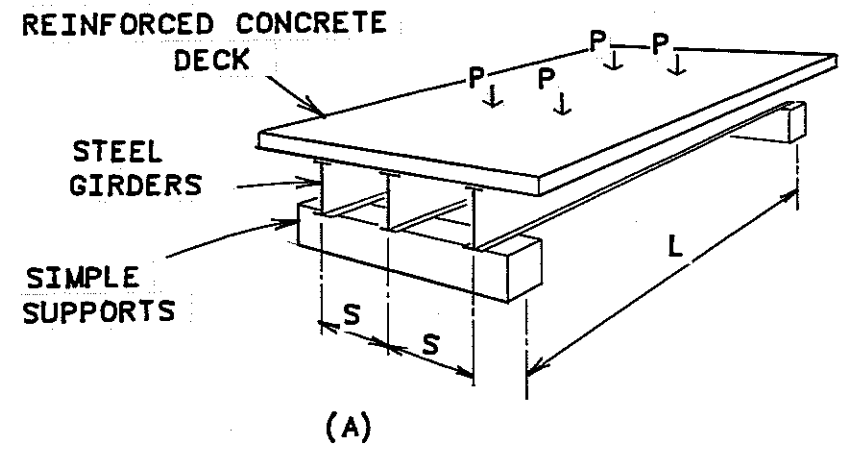

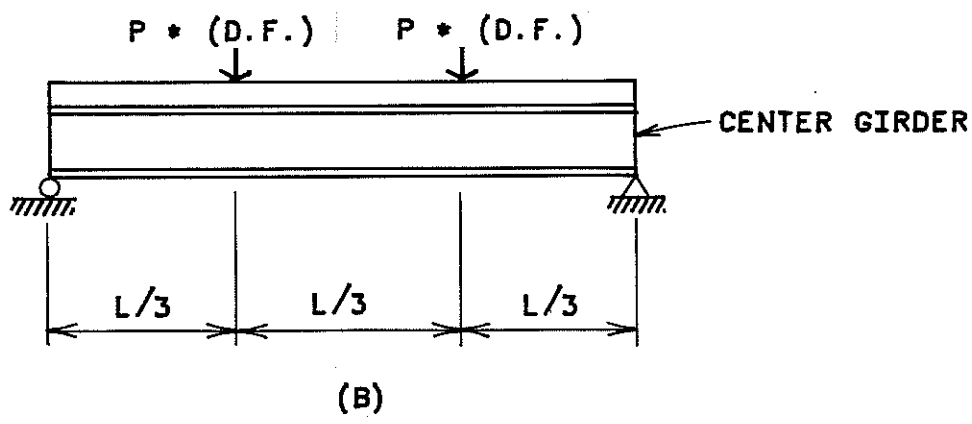

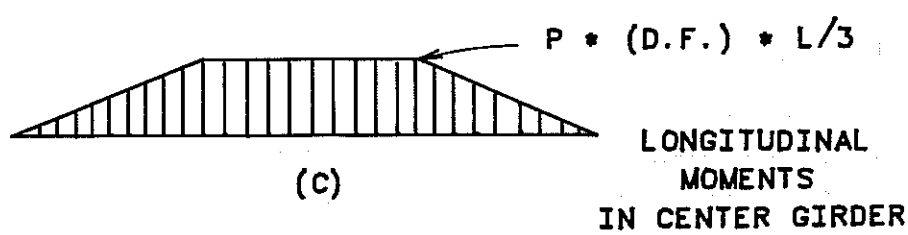

MAXIMUN MOMENT
IN CENTER GIRDER = PL * (S/C)(1/3)
= PL * (S/5.5)(1/3)

Fig. 1.1 Qualitative example of AASHTO load distribution procedure

1.3 Scope

In Chapter 2, background material is presented on various theoretical methods used to analyze bridge superstructures. The experimental test program and test results are discussed in Chapters 3 and 4, and the observed and predicted girder moment distributions are compared in Chapter 5. In Chapter 6, the findings are summarized, and conclusions are presented.

CHAPTER 2

THEORETICAL BACKGROUND

2.1 Refined Methods of Analysis

Refined methods of analysis for analyzing highway bridge superstructures and determining girder moments and loads can be classified into six categories:

1. orthotropic plate theory methods [4,5,6];
2. harmonic analysis methods [7];
3. grillage analogy methods [8,9,10,11];
4. finite element methods [12,13,14];
5. finite strip methods [15,16,17]; and
6. folded plate methods [18,19,20].

Refined methods of analysis with general applications are well reported in the technical literature. The references listed above are representative of a large number of published papers.

The orthotropic plate approach idealizes the actual bridge structure as an equivalent orthotropic plate, which is then treated by classical theory [21]. This approach was first developed by Guyon for grillages with negligible torsional stiffness [22] and later for isotropic slabs [23]. Massonnet [24] extended this approach by including the effects of torsion. The combined work of Guyon and Massonnet, referred to as the Guyon-Massonnet load distribution theory [25], has been extended by others [26,27,28,29].

The harmonic analysis procedure, developed in the 1950's by Hendry and Jaeger [7], considers the same flexural and torsional rigidities as the orthotropic plate analysis, but neglects the torsional rigidity in the transverse direction [30]. Loads are distributed to the individual girders as though the slab were a continuous beam over non-deflecting supports. The loading is expressed as a harmonic series or Fourier sine series. Expressions for shear, moment, slope, and deflection are found by successive integration of this load series. Girder bending moments are determined by considering the above series in conjunction with transverse force equilibrium and slope-deflection expressions in the transverse direction [30].

The grillage analogy method idealizes the bridge structure using an equivalent grid system, which is then analyzed [30] by:

a) slope-deflection and compatibility equations;

b) moment or torque distribution;

c) shear distribution; or

d) reaction distribution.

This method usually involves the solution of a large number of simultaneous equations or numerous arithmetic calculations [30].

The finite element and finite strip methods are widely used in the analysis of structures. A discussion of the theory and application of the finite element method to two-dimensional and three-dimensional systems involving plane stress, plane strain, plate bending, shells, and solids is given by Zienkiewicz [31]. The finite element and finite strip methods are general techniques for obtaining numerical solutions to boundary value problems. As discussed in Ref. 31, the finite element method involves dividing the structure to be analyzed into a finite number of simple elements, whose deformations are assumed to follow prescribed basis functions. The basis functions are selected to ensure compatibility between adjacent elements. Using variational concepts, the combination of basis functions (for each element) is found which minimizes the static potential of the entire idealized structure. The resulting solution is an approximation to the exact response.

Folded plate theory can be divided into two categories: a) the ordinary method [32], in which the longitudinal behavior of the plate is calculated according to beam theory, and the transverse behavior according to one-way theory; and b) the stiffness method [33], which combines slab theory and plane stress theory. The bridge is considered as an assembly of individual, elastic, isotropic rectangular plate elements interconnected at the longitudinal joints, and simply supported at the ends [34].

Six refined methods of analysis have been briefly discussed. A more rigorous description of these methods can be found in the cited references. As will be discussed later, the power and versatility of the finite element method led to its choice for modeling the bridge specimen described in this report.

2.2 Simplified Methods of Analysis

Simplified methods have been developed from these more complex theories. The AASHTO distribution procedure, discussed in Section 1.1,

was developed over several years. The first edition of the AASHTO Specifications, published in 1931 [35], provided load fractions to be used for calculating design moments in interior stringers (of any type) with concrete or timber floors. The 7th edition of the AASHTO Specifications [36] introduced a separate modification factor for moments in interior steel stringers. This modification resulted from analytical and experimental studies conducted in the 1940's by Newmark [37]. The load distribution fractions for concrete decks on steel or prestressed concrete stringers in the current 13th edition of the AASHTO Specifications [1] are based on Newmark's work. According to that procedure, each girder is designed to carry a fraction, K, of the wheel load, where

$$K = S/C \tag{1.1}$$

and S = average girder spacing in ft; and

C = specified constant depending on bridge type.

The constant C is 5.5 for a slab and girder bridge designed for two or more lanes of traffic, and is 7.0 for one lane. Equation 1.1 usually provides a conservative estimate of the actual girder loads, and is easy for the designer to apply to specific bridge types [34].

Another simplified method, developed in the 1970's by the Ontario (Canada) Ministry of Transportation and Communication, is described in Section 3.7 of the Ontario Bridge Design Code [2]. The distribution factor procedure of this method is comparable to that described in Section 3 of the current AASHTO Specifications, except that the distribution factors are selected from charts. Most of the key parameters affecting load distribution are considered: bridge span, bridge geometry, bridge width, girder spacing, number of loaded lanes, and bridge stiffness properties [34]. This is intended to provide improved accuracy. The charts were derived using orthotropic plate theory, and checked using the grillage analogy method.

CHAPTER 3

EXPERIMENTAL TEST PROGRAM

3.1 General

As explained in the introduction, one objective of this study was to measure the girder loads and bending moments in a full-scale highway bridge. As part of another investigation [3], a full-scale composite highway bridge was constructed and tested at the Phil M. Ferguson Structural Engineering Laboratory at The University of Texas at Austin. In the following sections, a description will be given of the bridge components, the construction procedure, the testing procedure, and the instrumentation. Appendix A lists the material properties.

3.2 Specimen Description

3.2.1 Steel Girders. As shown in Figs. 3.1 through 3.4, the three steel girders were W36x150 sections, 60 ft long, simply supported on a 48-ft span. The girders, donated to the project by the Texas State Department of Highways and Public Transportation (District 14), had been recovered from a bridge that had been replaced, and were in excellent condition. To ensure composite action, 7/8-in. diameter studs were welded to the top flange of each girder. The studs were placed in rows of three along the top flange, as shown in Figs. 3.5, 3.6 and 3.7. In the southern half of the bridge, the rows of studs were placed diagonally to allow adequate spacing between the panels. The girders were connected by steel diaphragms, shown in Figs. 3.8 and 3.9. The girders were simply supported on neoprene bearing pads, resting on anchor blocks, which in turn rested on the laboratory floor.

3.2.2 Cast-in-Place Deck. Cast-in-place concrete with #4 reinforcement was used for the entire deck on the northern half of the bridge, the deck above the precast, prestressed panels, and the cantilever overhangs. The design strength of the concrete was 4000 psi. The concrete used for the deck, supplied by Texas Readymix (Austin) met the Specifications of the Texas Department of Highways and Public Transportation for Class C concrete [38]. The deck thickness averaged 7-1/2 in. To facilitate construction and subsequent evaluation of test results, the deck was cast with a uniform thickness.

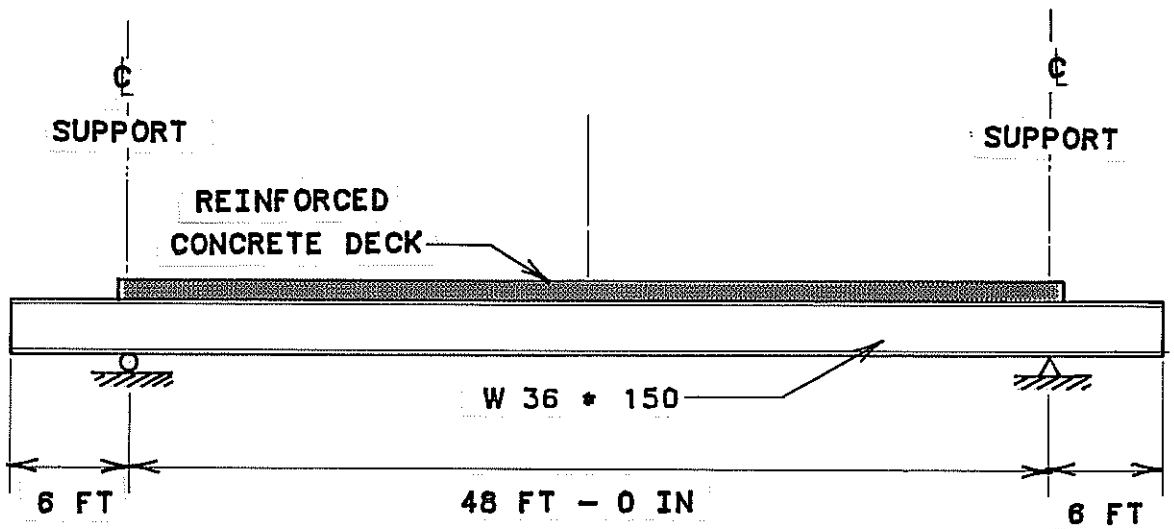

Fig. 3.1 Elevation view of laboratory specimen

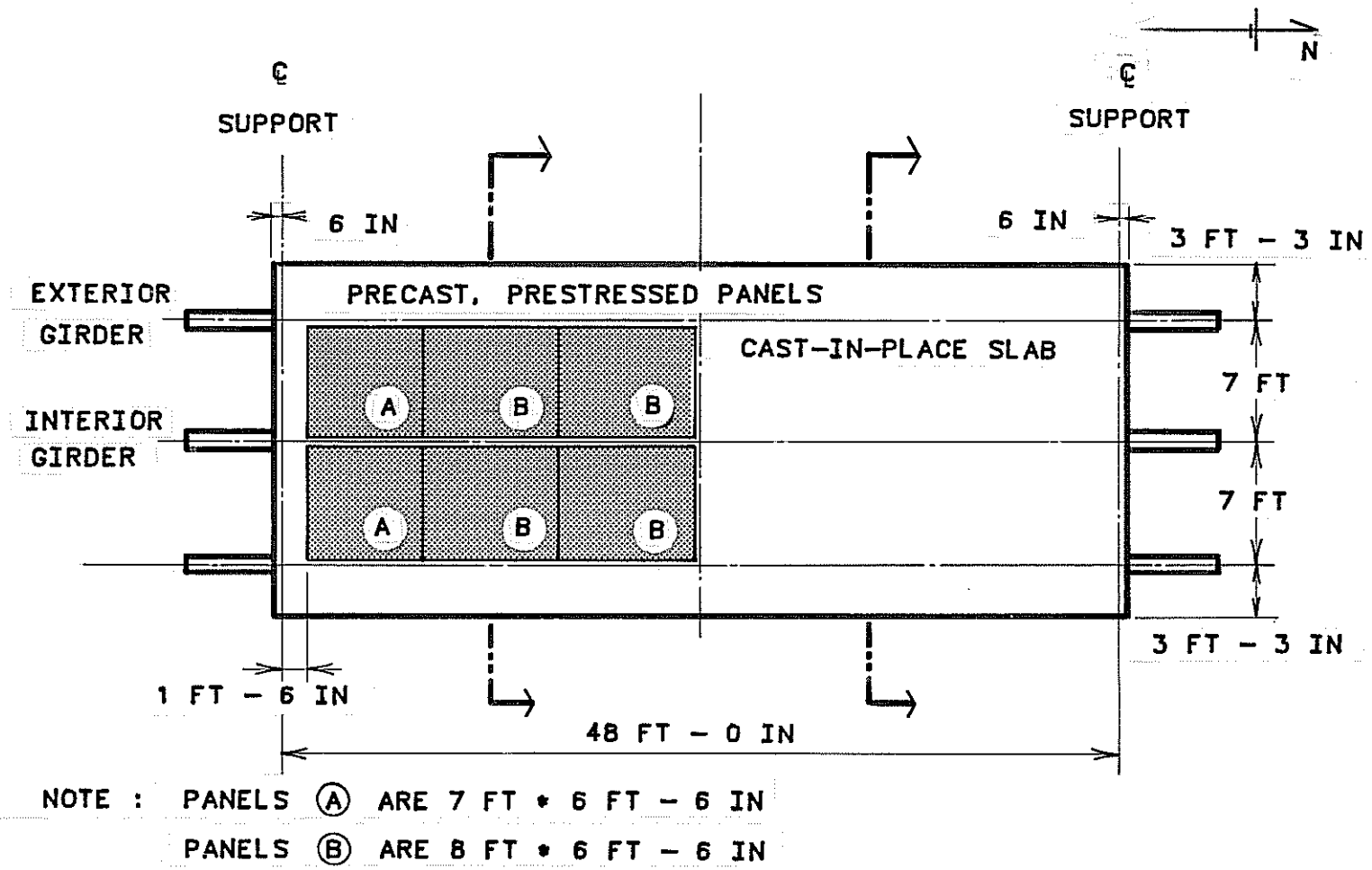

Fig. 3.2 Plan view of laboratory specimen

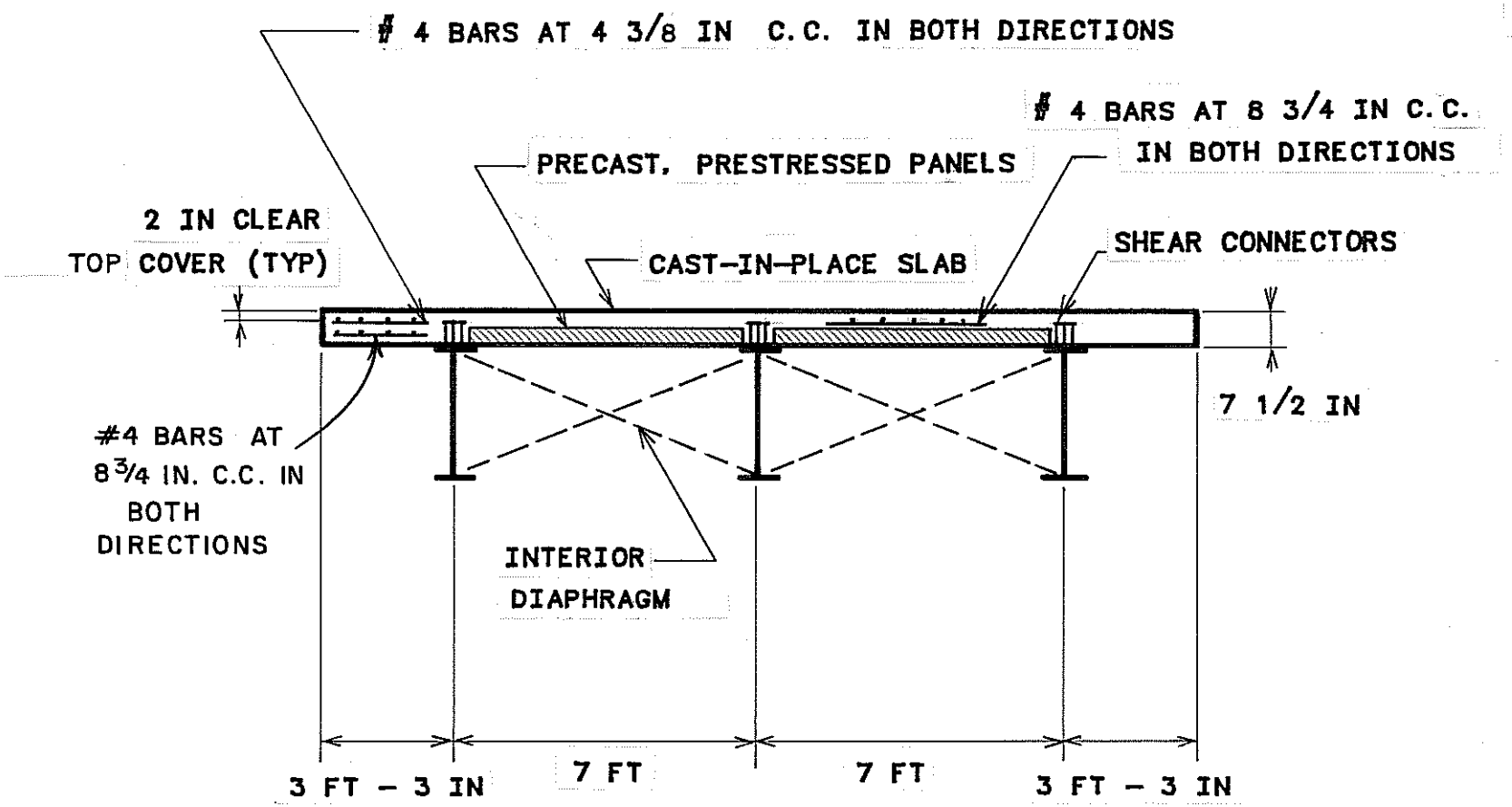

Fig. 3.3 Cross section of laboratory specimen showing precast, prestressed panels

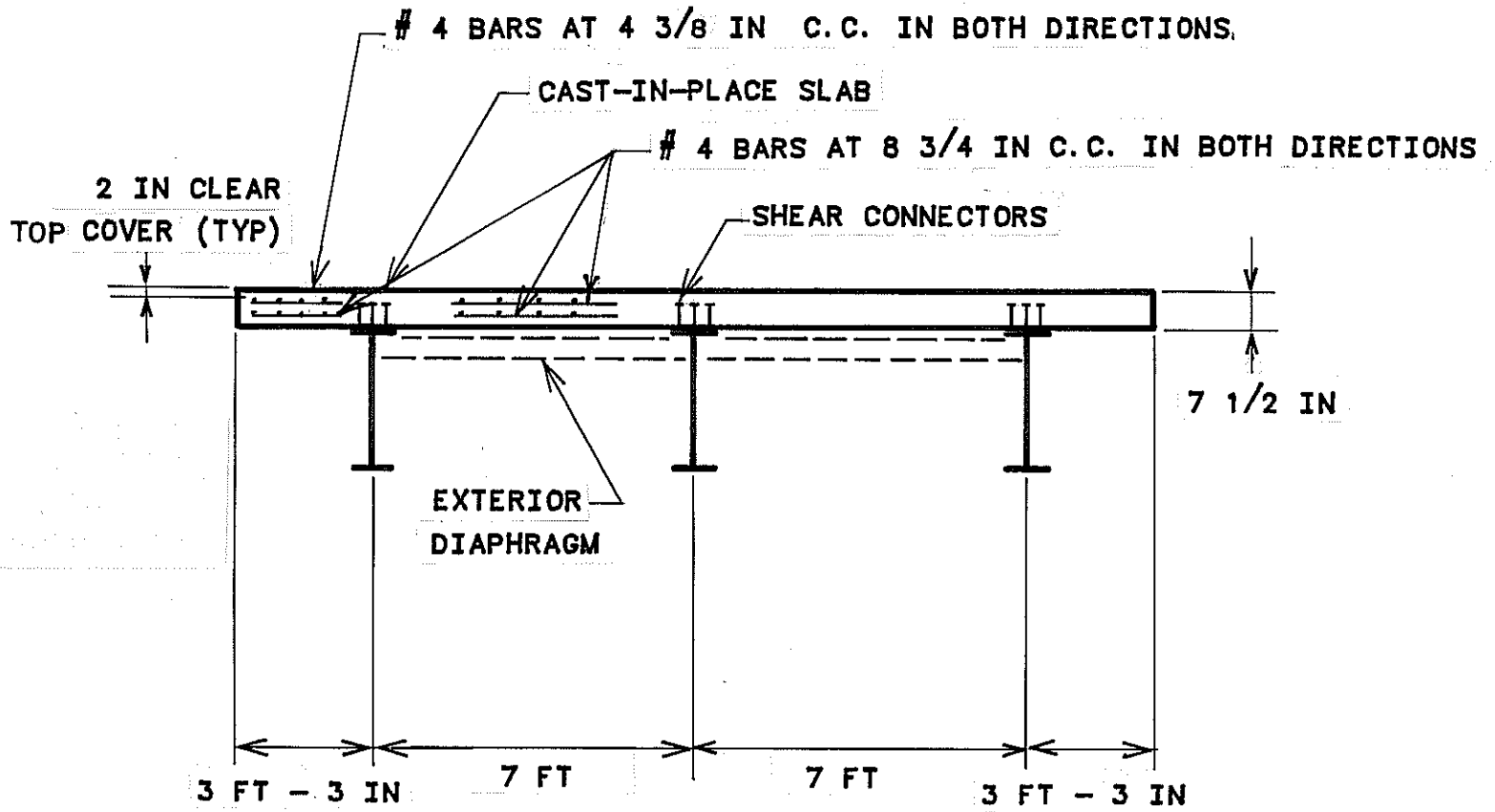

Fig. 3.4 Cross section of laboratory specimen showing cast-in-place deck

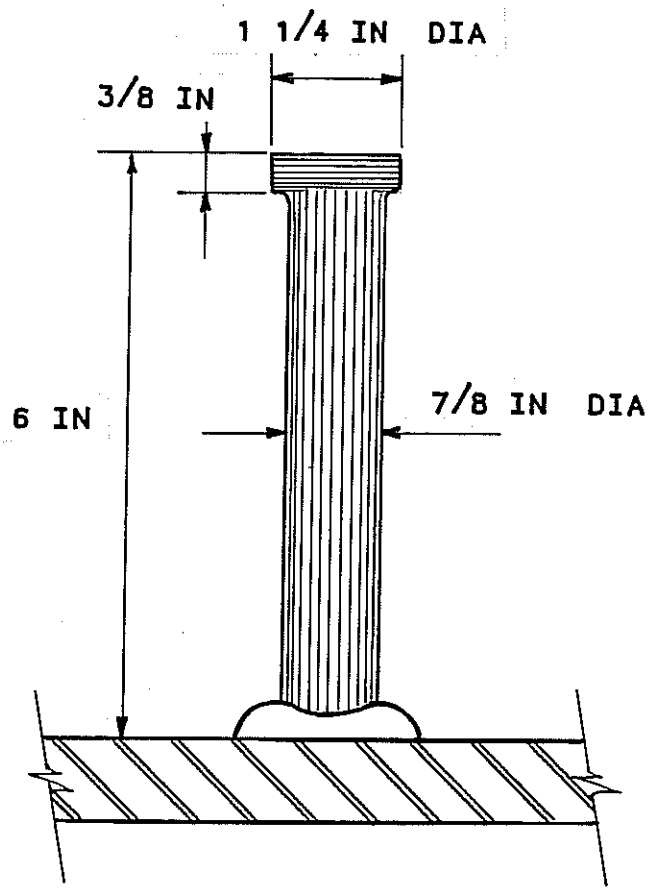

Fig. 3.5 Typical shear stud

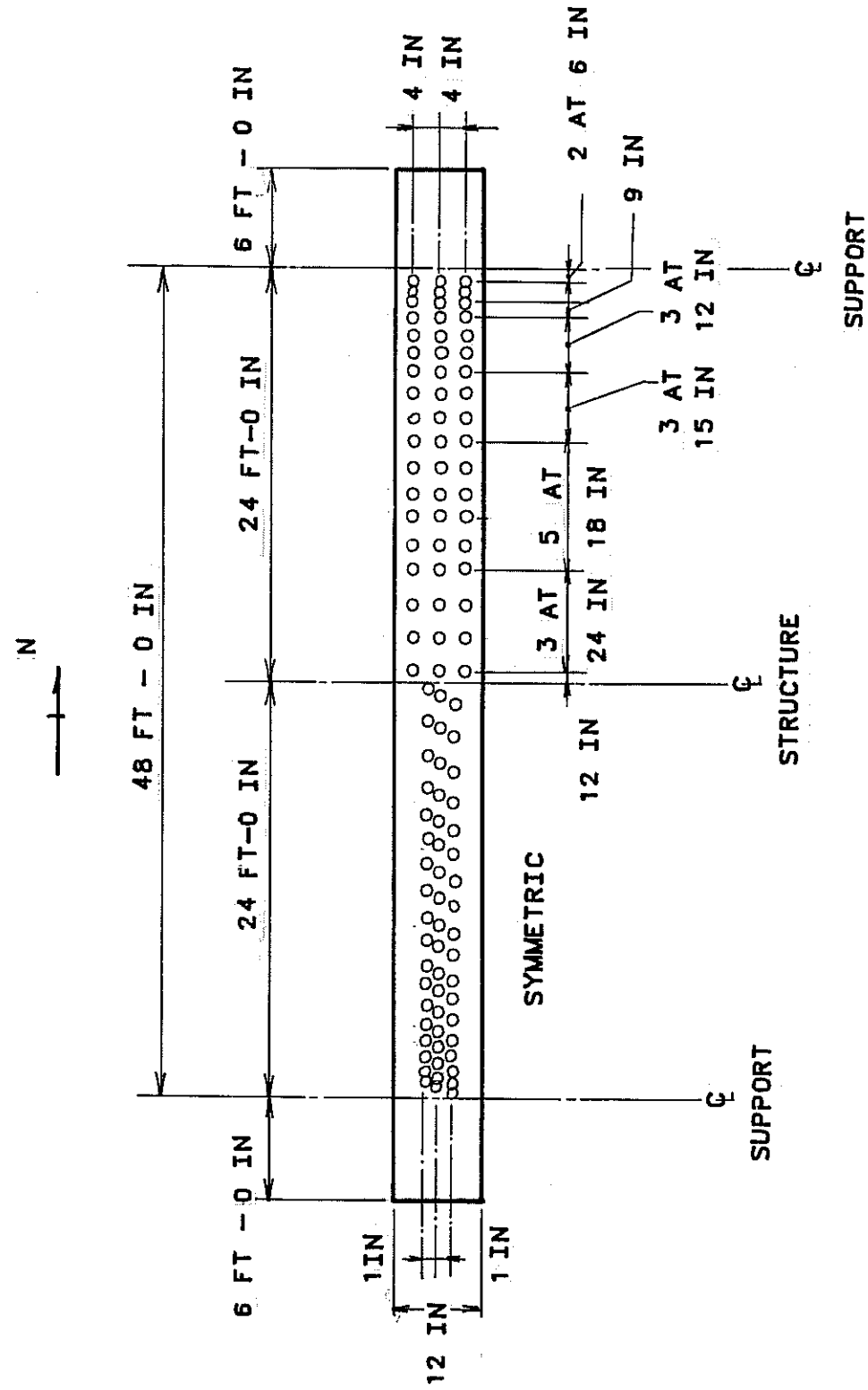

Fig. 3.6 Layout of shear studs on the steel girders

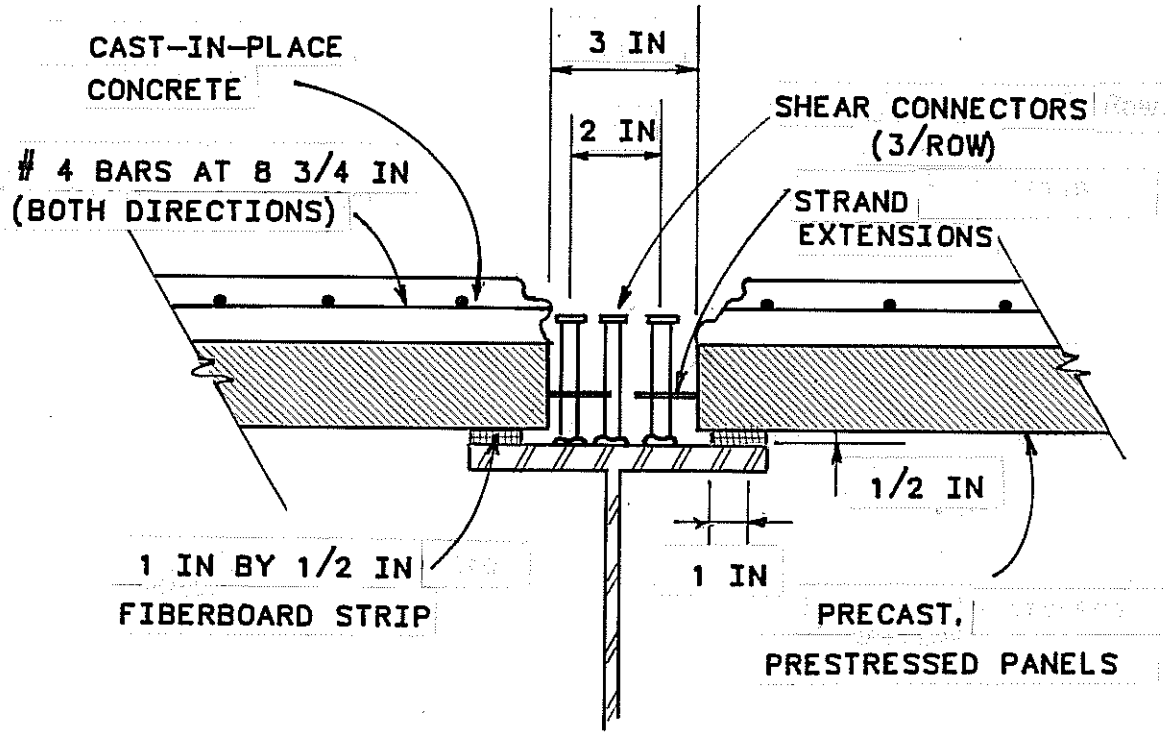

Fig. 3.7 Detail of connection between girders and panels

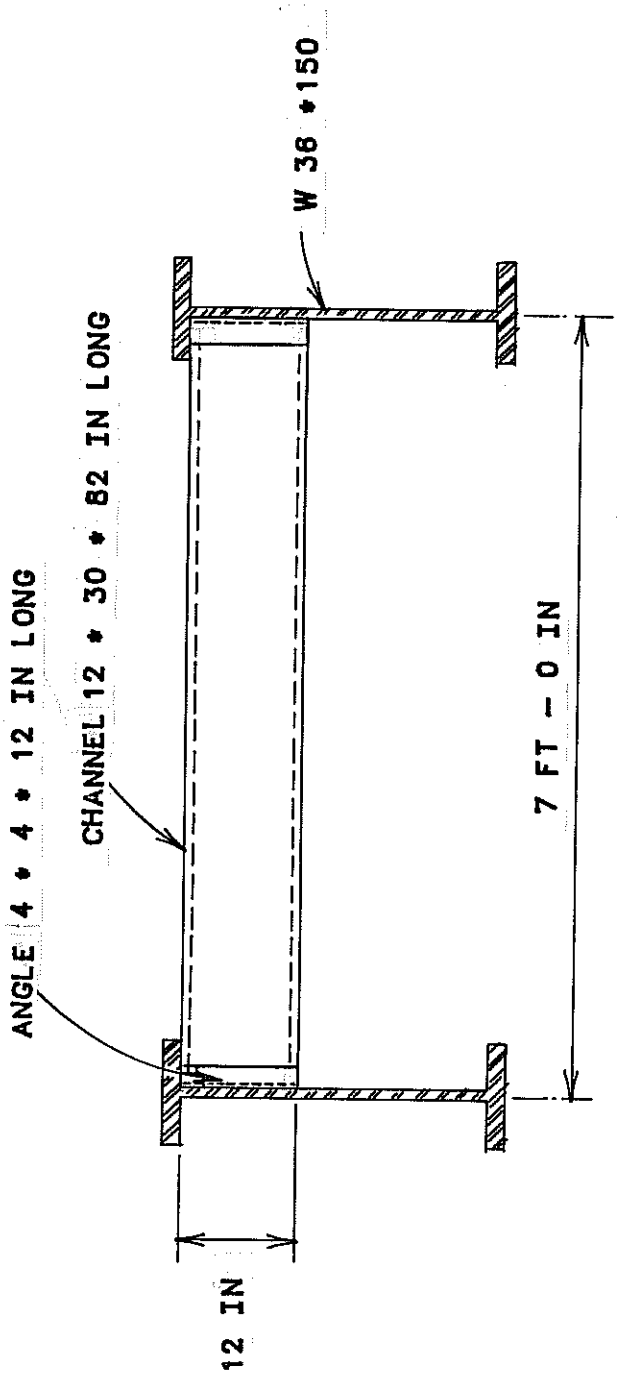

Fig. 3.8 Typical exterior diaphragm

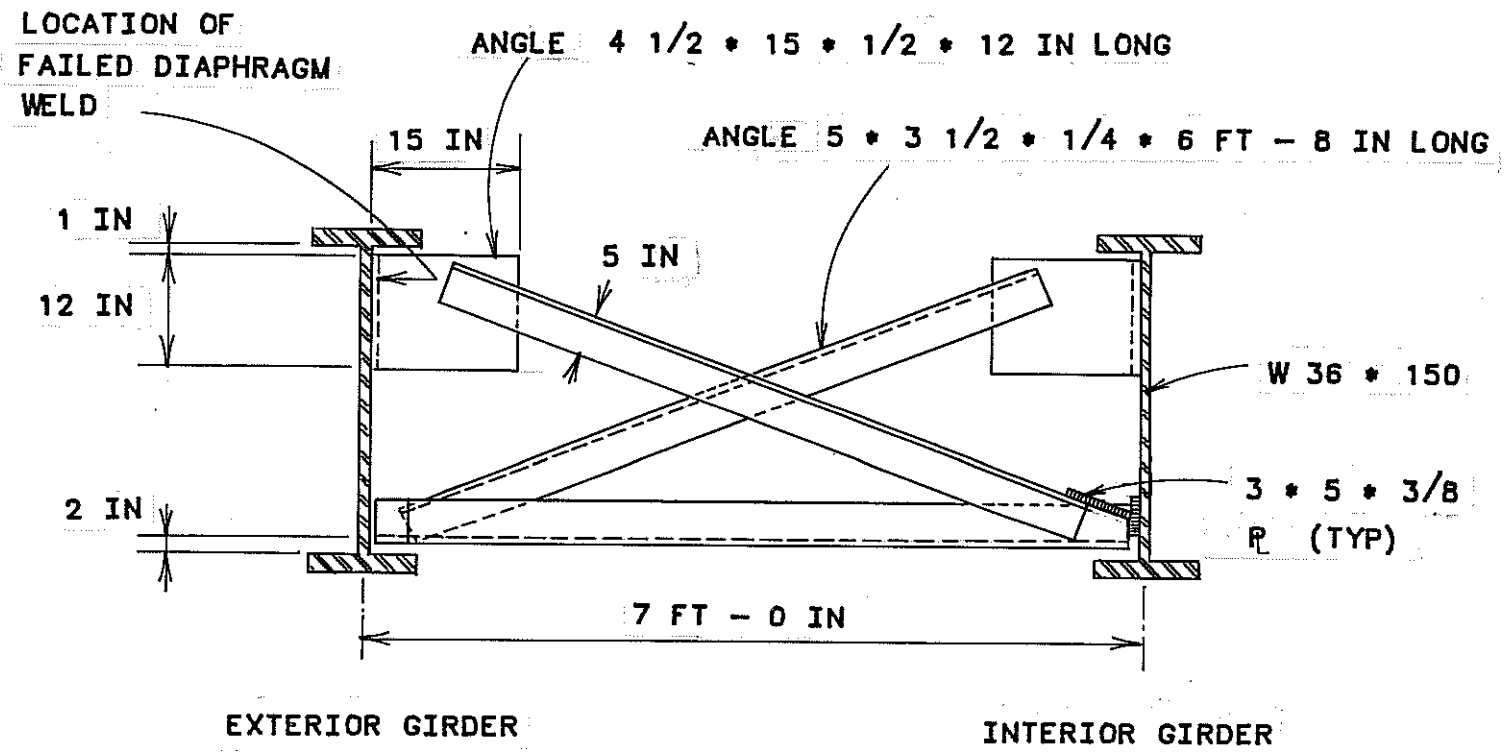

Fig. 3.9 Typical interior diaphragm

3.2.3 Precast, Prestressed Panels. Six precast, transversely-prestressed panels, fabricated by J.D. Abrams Precast (Austin) spanned between the longitudinal girders. These panels, illustrated in Figs. 3.2 and 3.10, rested on 1 x 1/2-in., asphalt-impregnated fiberboard strips. The panels were 6.5 ft wide by either 7 or 8 ft long. They were of 6000-psi concrete, 4 in. thick, and were later covered by a 3-1/2 in. topping of 4000-psi concrete.

3.3 Construction

3.3.1 Steel Girders. Construction began in the summer of 1983 with the placement of the three girders on top of the neoprene pads and anchor blocks. After positioning the three girders at a 7-ft spacing, the interior and exterior diaphragms were welded to the girder webs. The shear studs were then welded to the top flanges of the girders with a portable stud welding machine, and all welds were checked for soundness.

3.3.2 Precast, Prestressed Panels. The six precast, prestressed panels were transported by truck to the laboratory, lifted into position with an overhead crane, and placed between the girders as shown in Fig. 3.7.

3.3.3 Formwork. The bridge was unshored. Wooden formwork was installed between the girders on the northern (cast-in-place) half of the bridge, and was supported by the girders using steel hangers. On the southern half of the bridge, the panels spanned between the girders, and served as formwork. Wooden formwork was used for short sections of deck underneath the north and south ends, and along the entire length of the bridge for the cantilever overhangs.

Wooden formwork consisted of 1/2-in. plywood stiffened with 2x4 and 2x6 lumber, lacquered and oiled. Care was exercised to prevent the form oil from getting onto the steel reinforcement. Caulking and styrofoam were used to seal cracks and prevent leaks, and all removable bolts and inserts were coated with grease to facilitate removal.

3.3.4 Reinforcement for Cast-in-Place Deck. Steel reinforcement for the cast-in-place deck was supplied by Alamo Steel and Machine Company (Austin). Chairs provided 1-1/2 in. cover between the bottom formwork and the bottom layer of reinforcement. Top reinforcement was supported on 4-1/2 in. chairs. The mat of reinforcement lying on top of the precast, prestressed panels was elevated 1/2 in. above the surface of the panels with short lengths of #4 bar placed between the panels and the mat. Most of the deck was reinforced by #4 bars at 8-3/4 in. in both directions. The cantilever overhangs had #4 bars at 4-3/4 in. spacing in both directions, top and bottom. The layout of the steel reinforcement, shown in Fig. 3.11, conformed to Texas Standard Department of Highways and Public

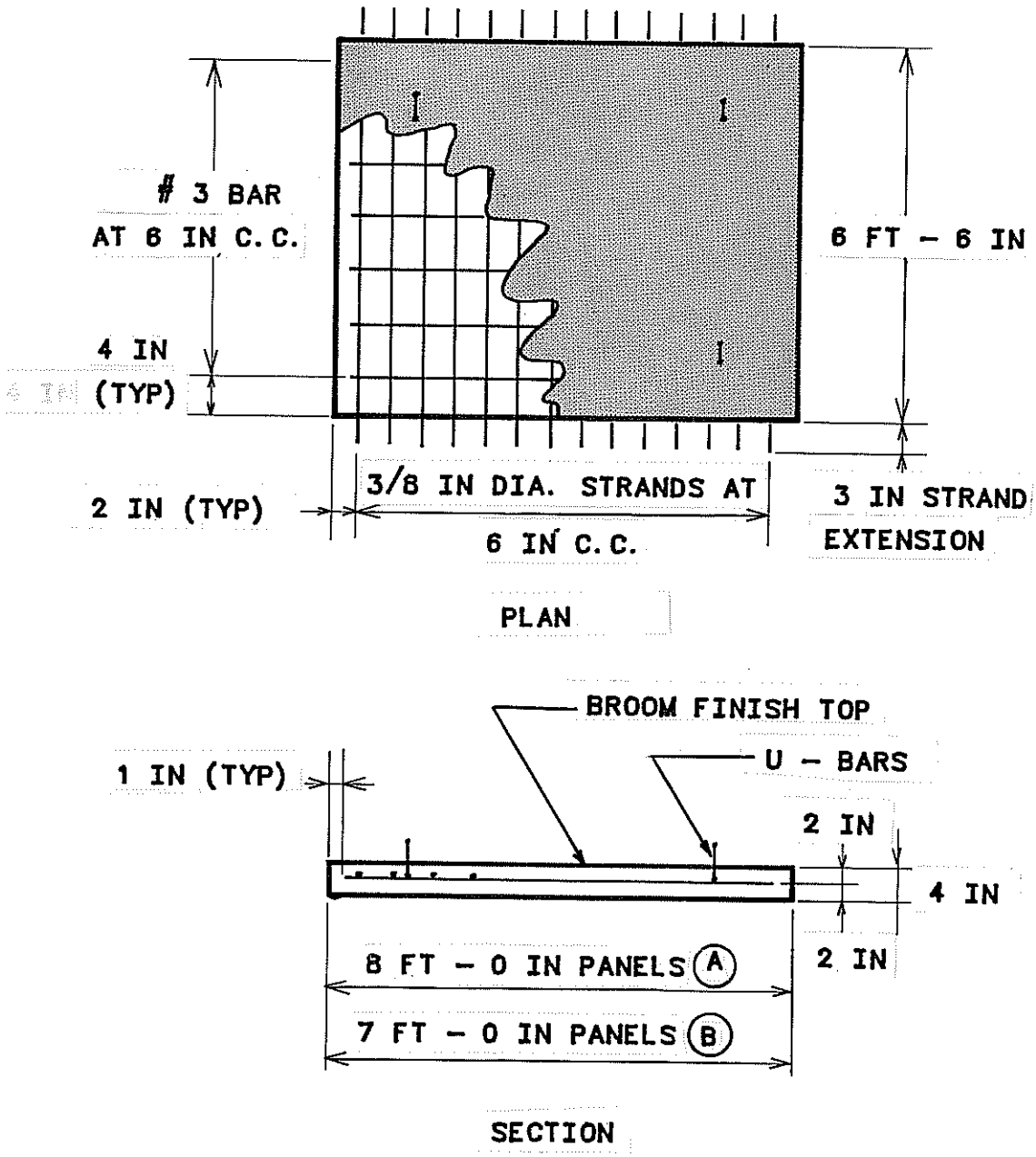

Fig. 3.10 Precast, prestressed panels

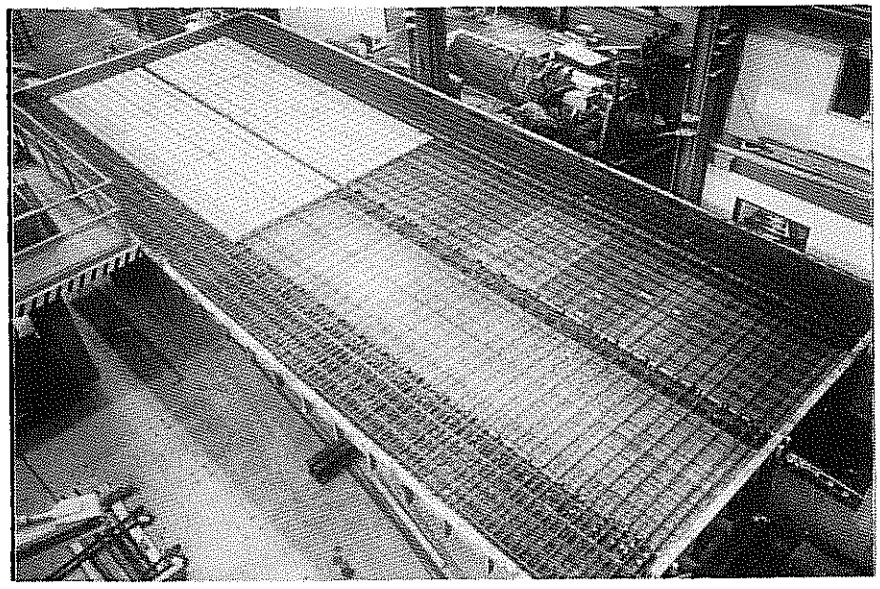

Fig. 3.11 Layout of steel reinforcement

Transportation Drawing Number 1284 (Texas State Department of Highways and Public Transportation, Bridge Division, Drawing File 1284, Research Project 3-5-83-50, April 14, 1982) [39].

The transverse and longitudinal bars were continuous (without splices). The additional transverse steel in the overhangs extended 21 in. inside of the top edge of the exterior girders.

3.3.5 Placement and Curing of Concrete. The concrete deck was cast monolithically using ready-mix concrete, placed with a 1-yd. bucket on an overhead travelling crane. The concrete was vibrated with two portable vibrators, and finished with a 25-ft long vibratory screed, moved longitudinally. Additional finishing was unnecessary Twenty-one standard 6x12-in. cylinders were cast, as well as nine 6x6x18-in. beams. Polyethylene sheets as well as a membrane curing compound were used to cure the deck. The test cylinders and beams were cured under the same conditions as the deck.

3.3.6 Removal of Formwork. Wooden formwork was removed about seven days after the deck was cast. Four 3-in. diameter cores were removed from the deck to permit attachment of the hydraulic loading rams.

3.4 Test Setup

The test setup, shown in Figs. 3.12 and 3.13, consisted of four identical 72-kip hydraulic rams attached to two reaction beams. The rams were supplied by two hydraulic pumps with a combined capacity of 55 gpm at 3000 psi [40,41]. The hydraulic lines on the rams were interconnected to a single servovalve, so that an equal pressure could be applied to all four rams, producing an equal load in each ram. A schematic diagram of the loading system is shown in Fig. 3.14. A servocontroller and strain gage actuated load cell controlled the loading.

Each of the two 21-ft reaction beams consisted of two S10x24.5 sections attached together, and bolted at 4-ft intervals to the tie-down points on the test slab (Figs. 3.15 and 3.16).

3.5 Instrumentation

3.5.1 Beam Strain Measurement. The distribution of loads to the girders was determined using 54 electrical resistance strain gages, located as shown in Figs. 3.17, 3.18, and 3.19. Before the strain gages were applied, the steel surface was polished and cleaned. The strain gages were Precision Measurements W32 [42], attached to the steel with M-Bond 200 adhesive. The lead wires for these strain gages were soldered to shielded cable. The connection to the lead wires, and the

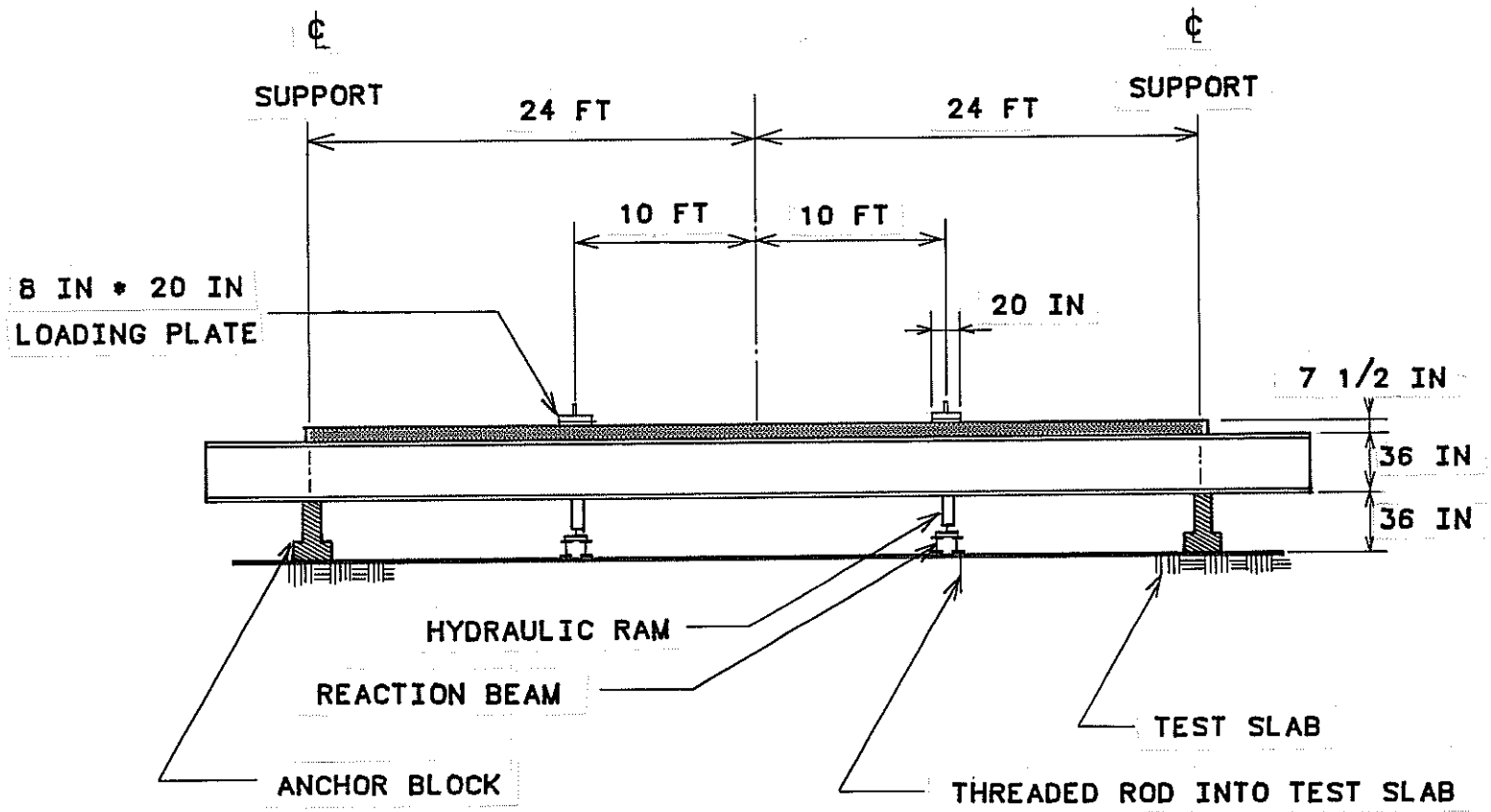

Fig. 3.12 Elevation of test setup

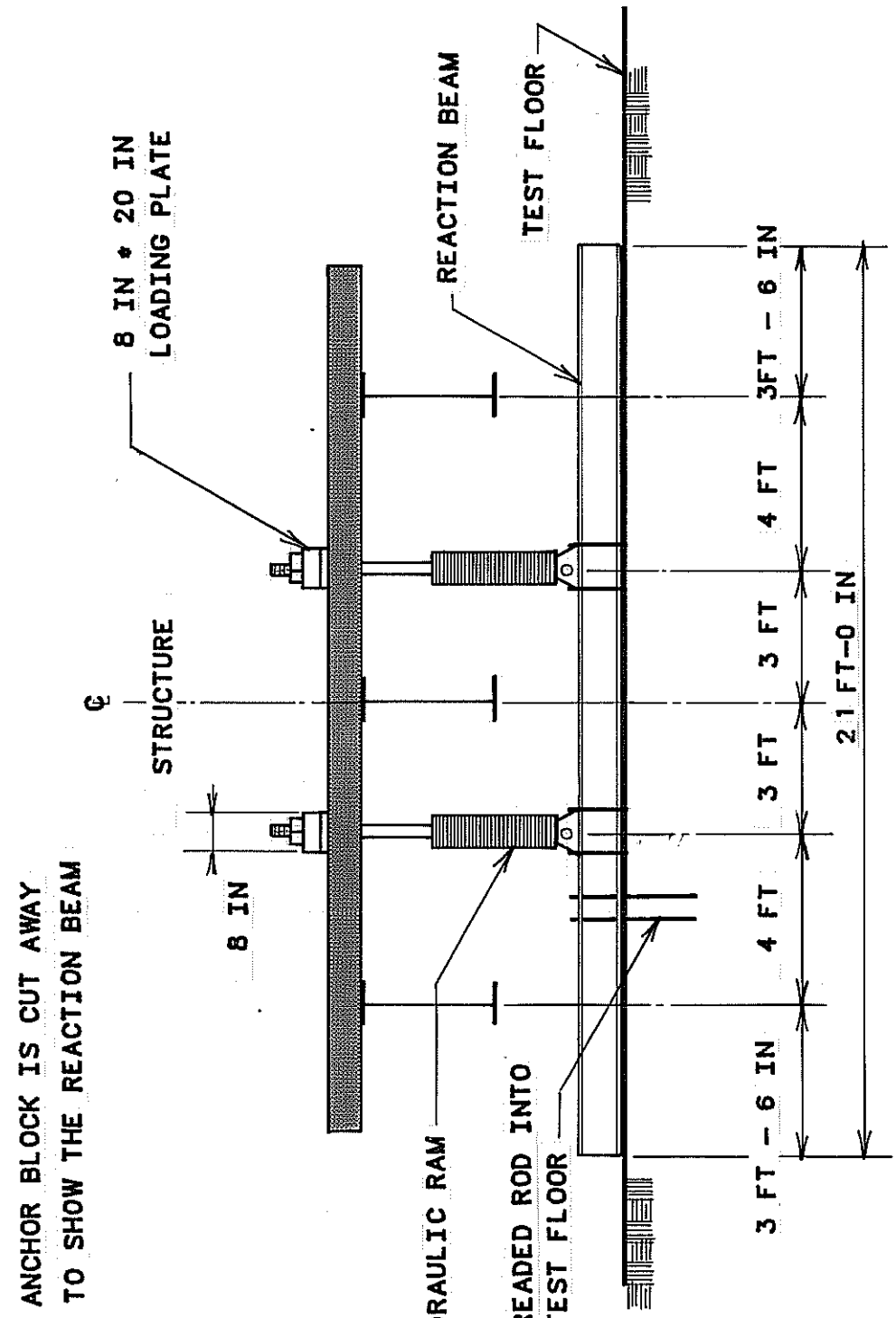

Fig. 3.13 Cross-section of test setup

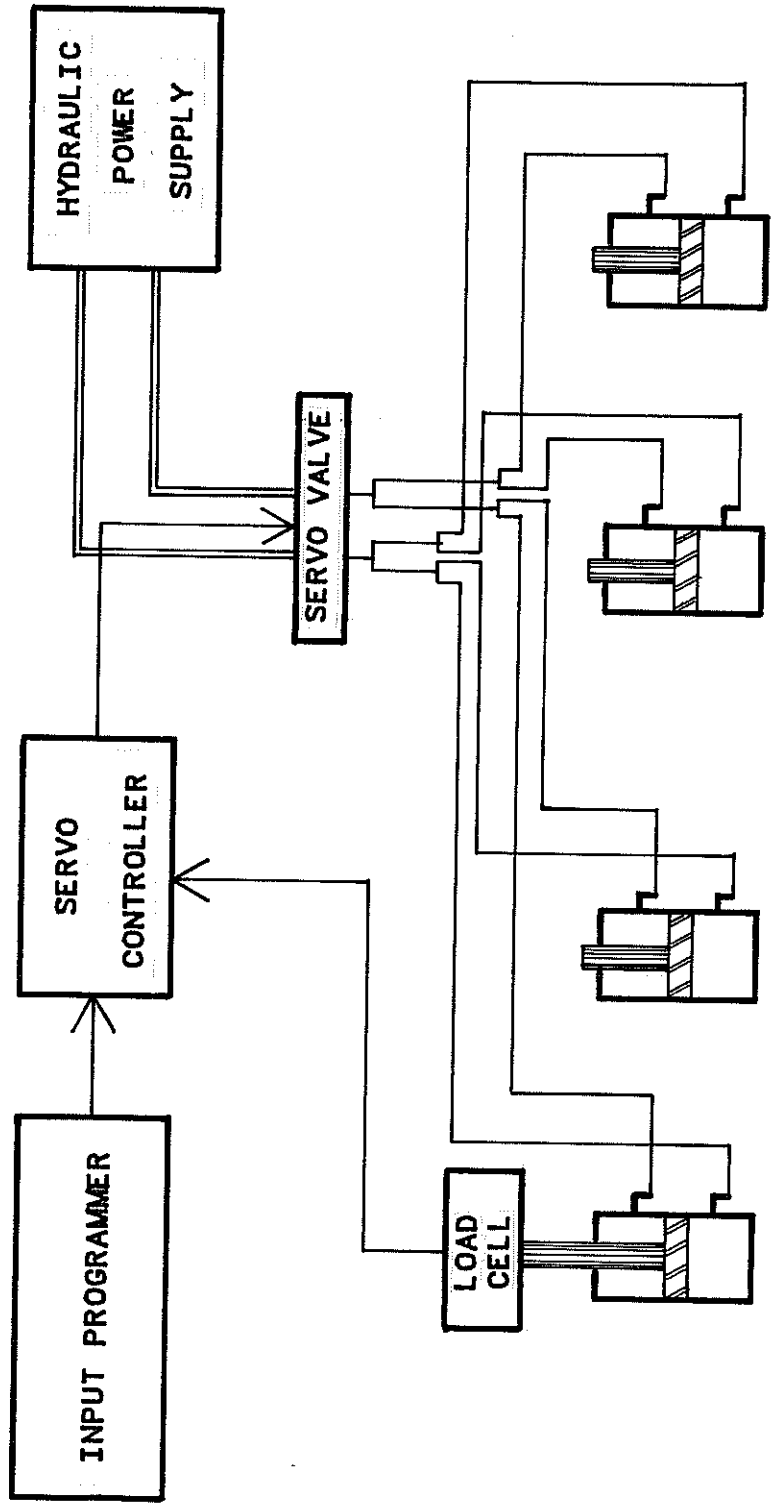

Fig. 3.14 Schematic of loading system

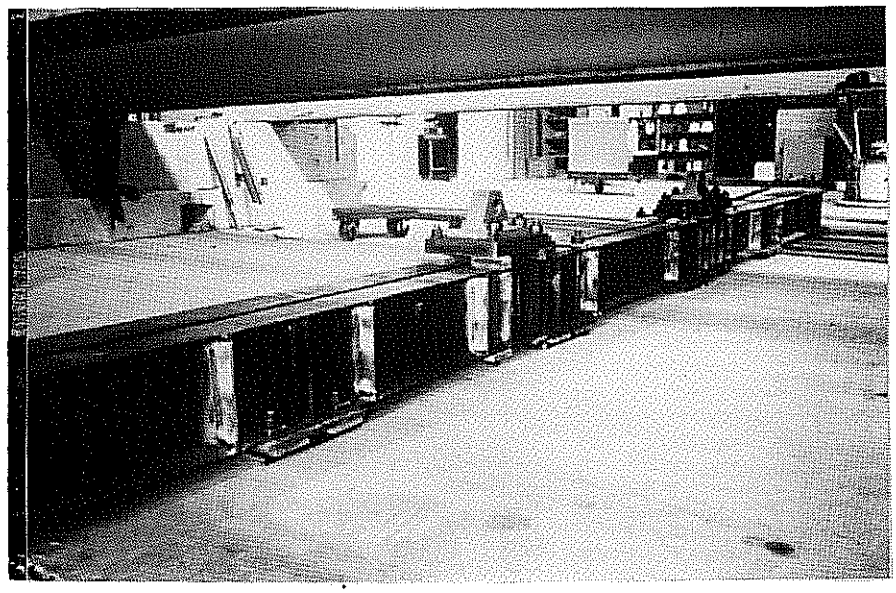

Fig. 3.15 Reaction beam

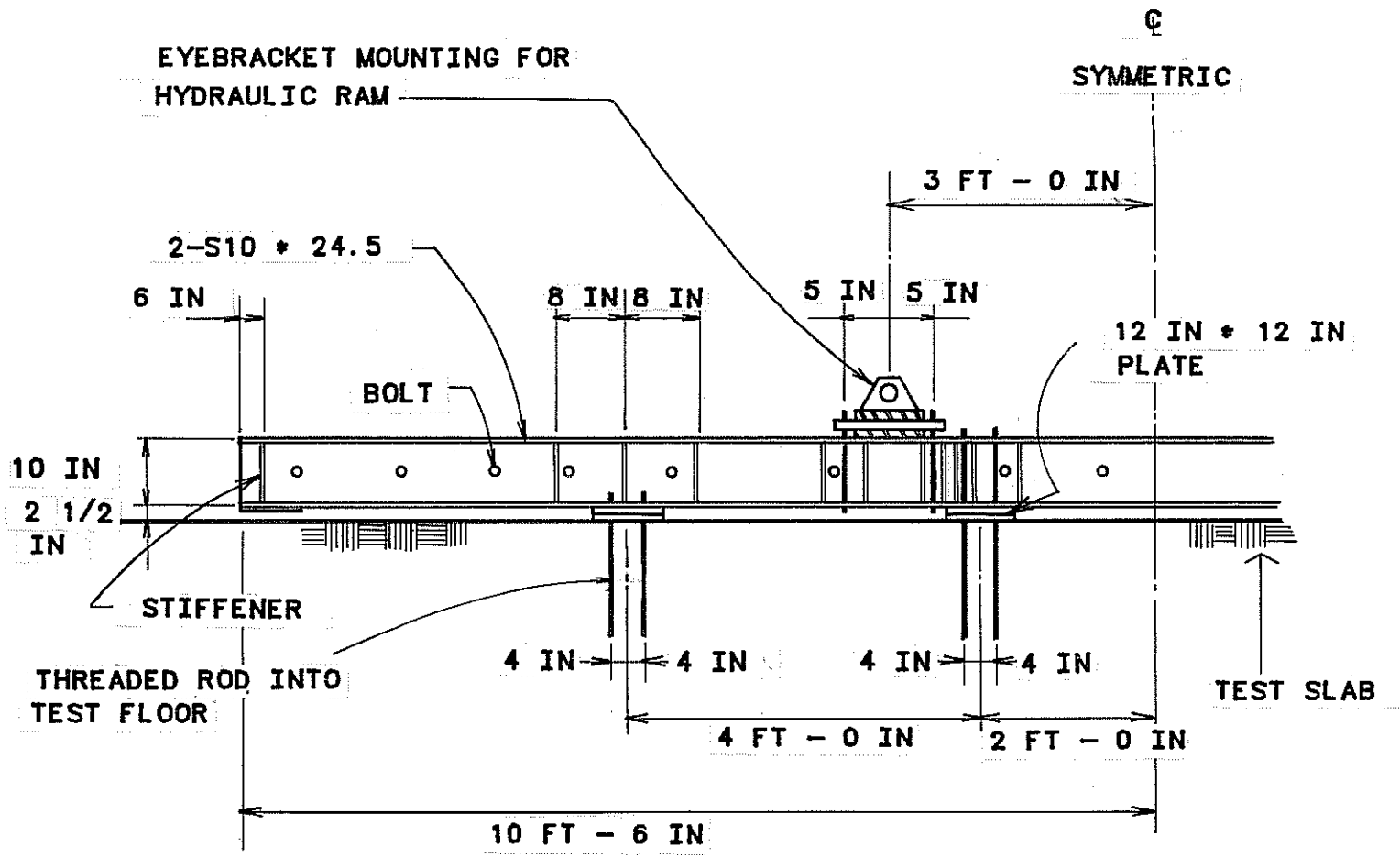

Fig. 3.16 Side view of reaction beam

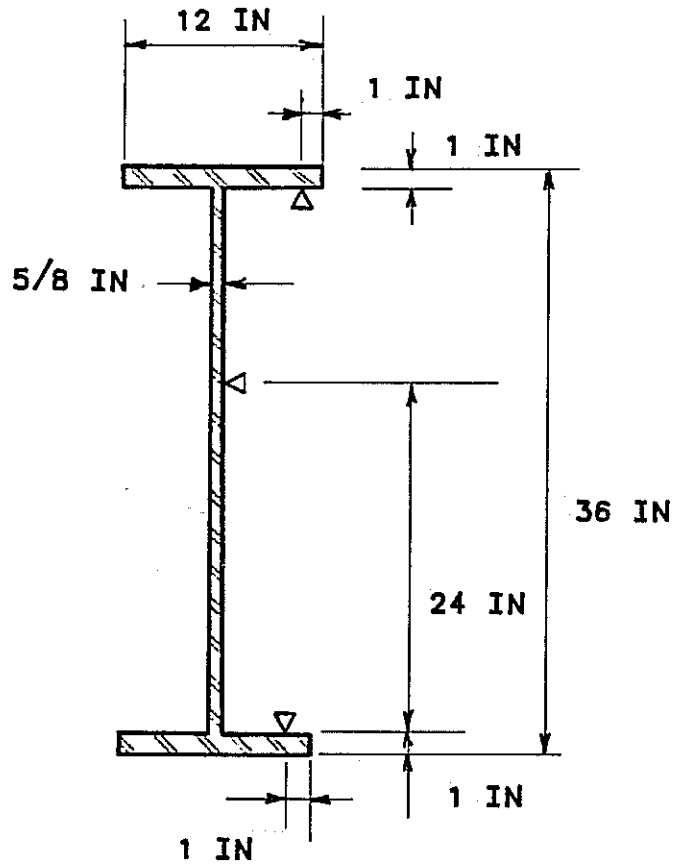

Fig. 3.17 Location of strain gage on the steel girder

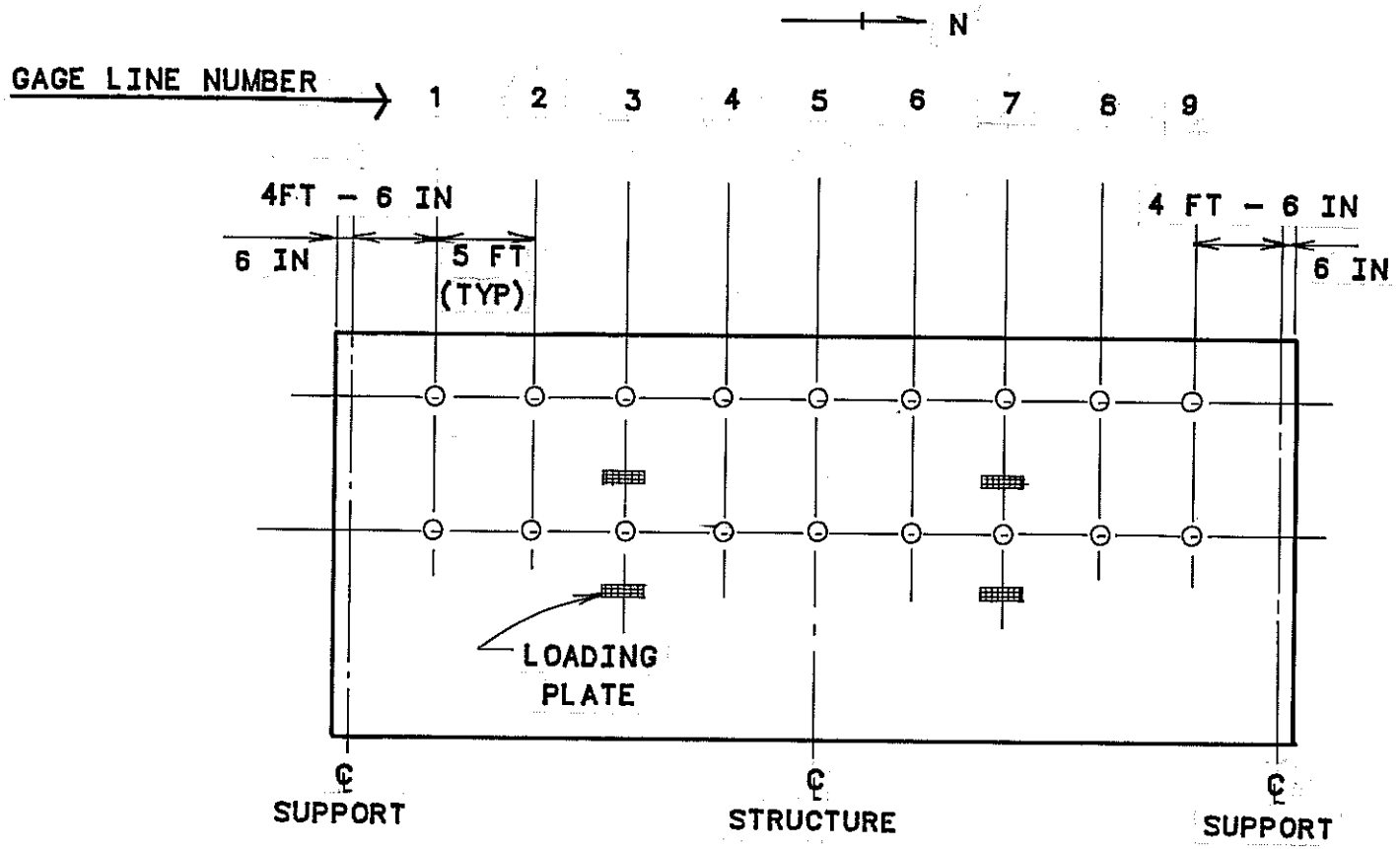

NOTE : ○ DENOTES THE LOCATION OF 3 STRAIN GAGES ON THE STEEL GIRDER

Fig. 3.18 Plan view of strain gage location

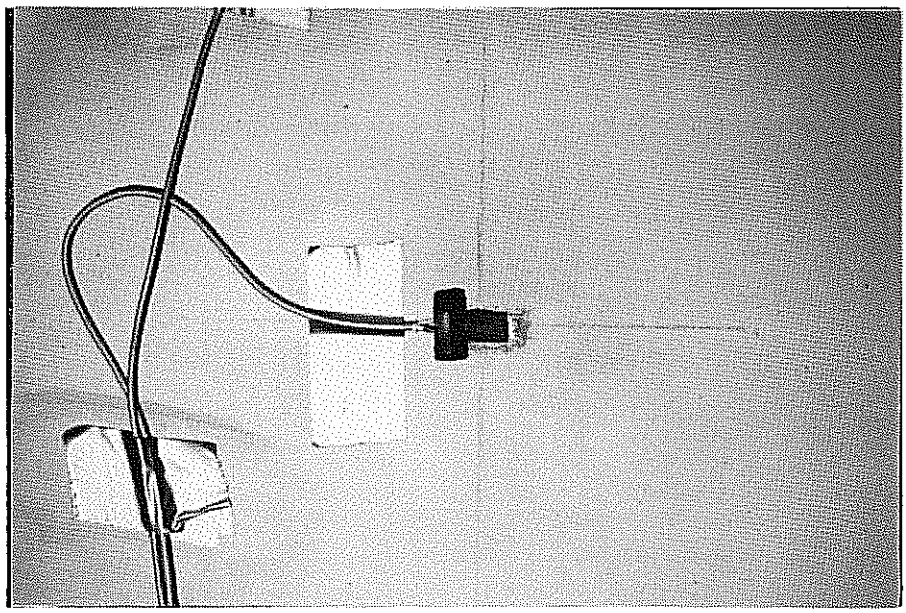

Fig. 3.19 Typical strain gage on steel girder

strain gage itself, were protected with M-Coat D waterproofing compound, and a Barrier-E rubber pad.

The data acquisition system for these 54 strain gages consisted of 6 switch and balance units and 2 strain indicator boxes. Three switch units, wired to one strain indicator unit, were used to read the gages for each girder.

3.5.2 Deflection and Slip Measurement. Vertical deflections along the steel girders were measured with dial gages and linear potentiometers, as shown in Figs. 3.20 and 3.21. Horizontal slip between the deck and girders was measured with dial gages and clip gages, as illustrated in Figs. 3.22 through 3.24.

3.5.3 Crack Measurement. Crack widths in the concrete deck were measured visually with a crack template. Crack propagation was followed by marking cracks as the test progressed.

3.6 Loading Sequence and Testing Procedure

Figure 3.25 outlines the loading sequence. The bridge was first loaded statically to 30 kips per ram in increments of 5 kips. The loading continued from 30 kips to a maximum of 60 kips in increments of 2.5 kips. The weld between the center diaphragm and the east girder failed when the peak load of 60 kips was attained, as shown in Figs. 3.9 and 3.26. The load was then decreased from 60 kips to 0 kips in increments of 20 kips. At each of these load stages, all gages were read. About 8 minutes were required per load stage to scan 54 channels on the switch and balance units and record the strains.

After re-welding the broken diaphragm, the structure was then subjected to 5 million cycles of fatigue loading. The load varied sinusoidally from 5 kips to 26 kips, the average load being 15.5 kips. The loading frequency was about 2 cycles per second, as shown in Fig. 3.27. The diaphragm welds broke again in several locations during the fatigue loading.

After the 5 million cycles had been attained, the diaphragms were again re-welded. The bridge was then loaded statically to 40 kips per ram in increments of 5 kips, and unloaded in increments of 10 kips. Readings were again taken at each load stage.

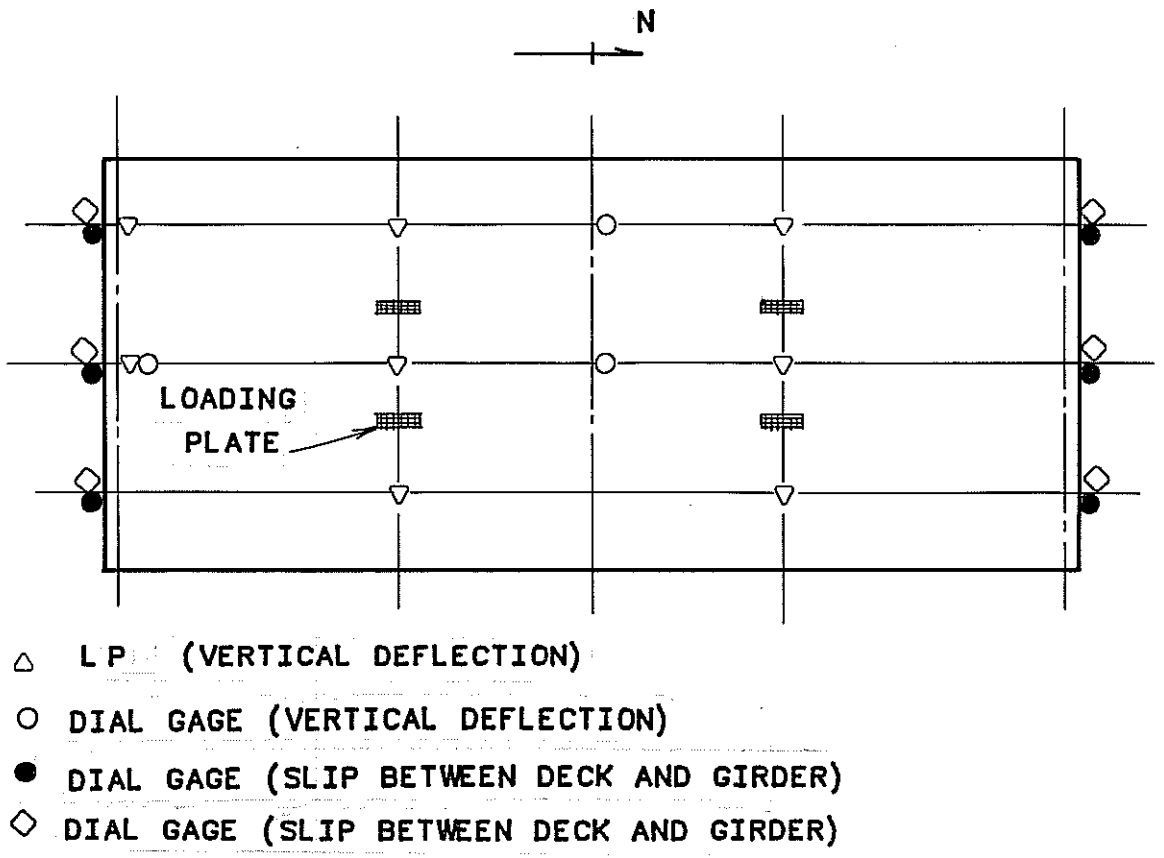

Fig. 3.20 Layout of deflection and slip instrumentation

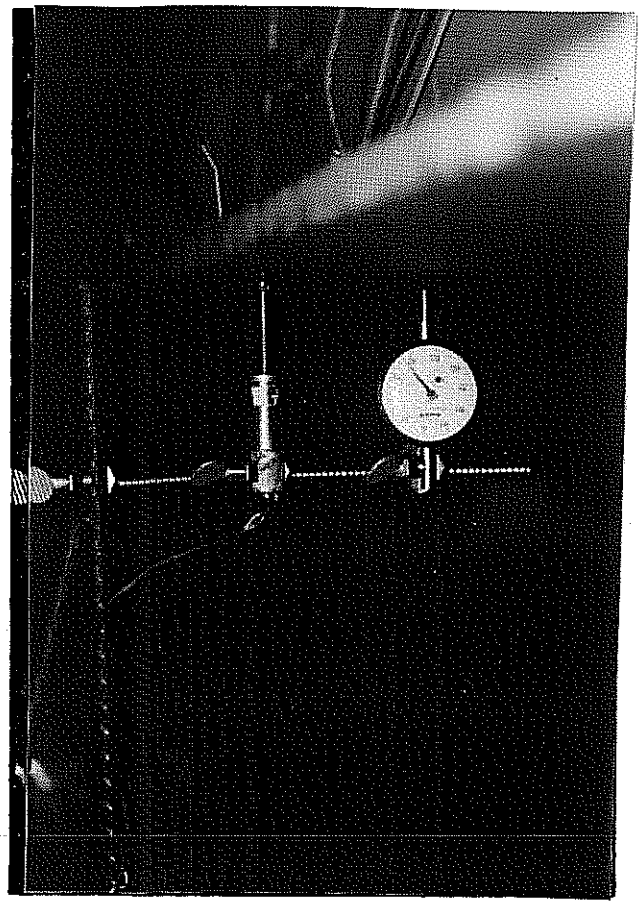

Fig. 3.21 Dial gage and linear potentiometer to measure vertical deflection of steel girders

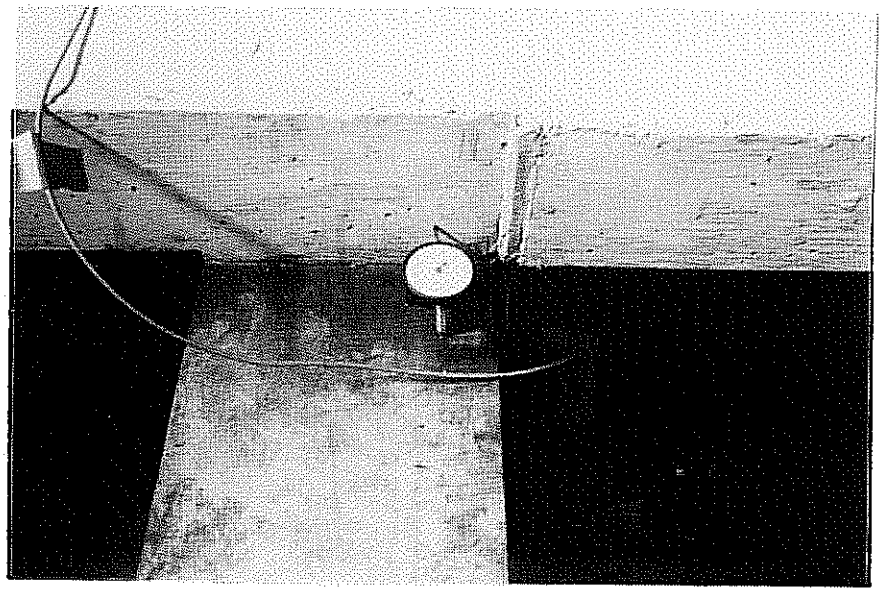

Fig. 3.22 Dial gage to measure slip between deck and girder

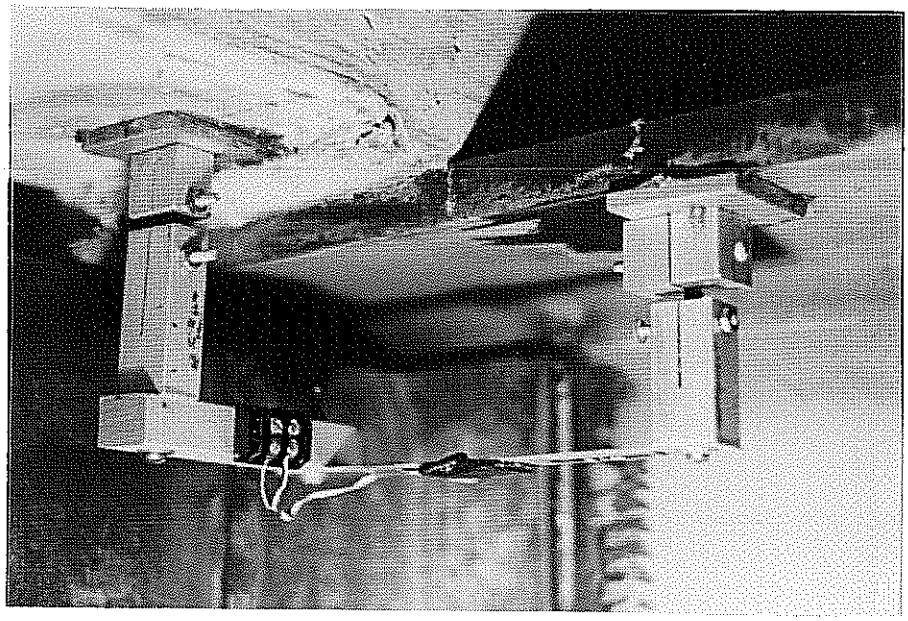

Fig. 3.23 Clip gage to measure slip between deck and girder

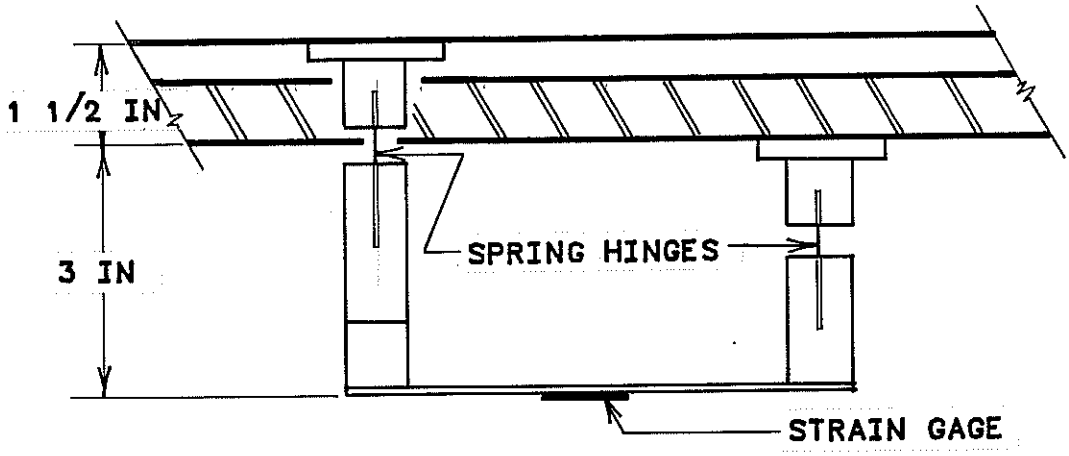

SIDE VIEW

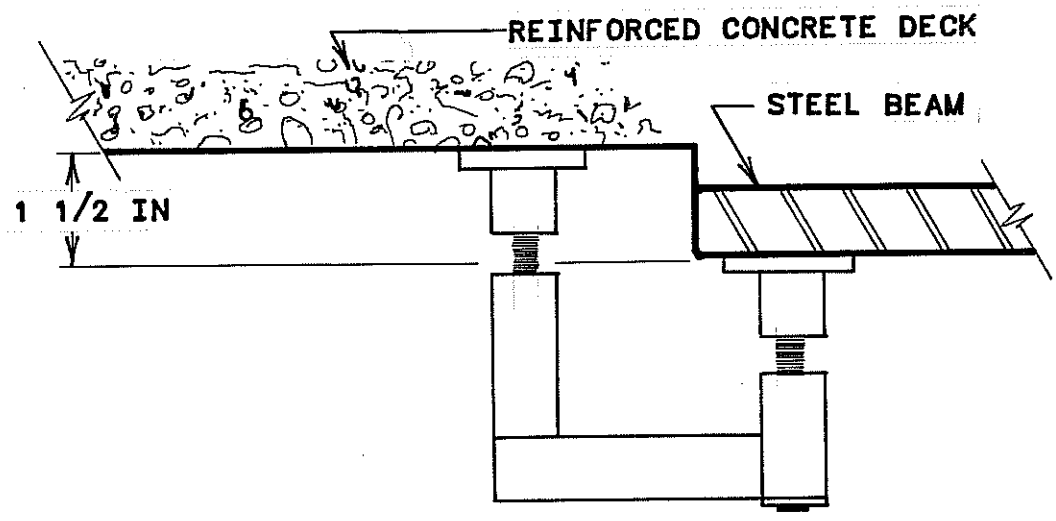

END VIEW

Fig. 3.24 Clip gage used for measuring slip between deck and girder

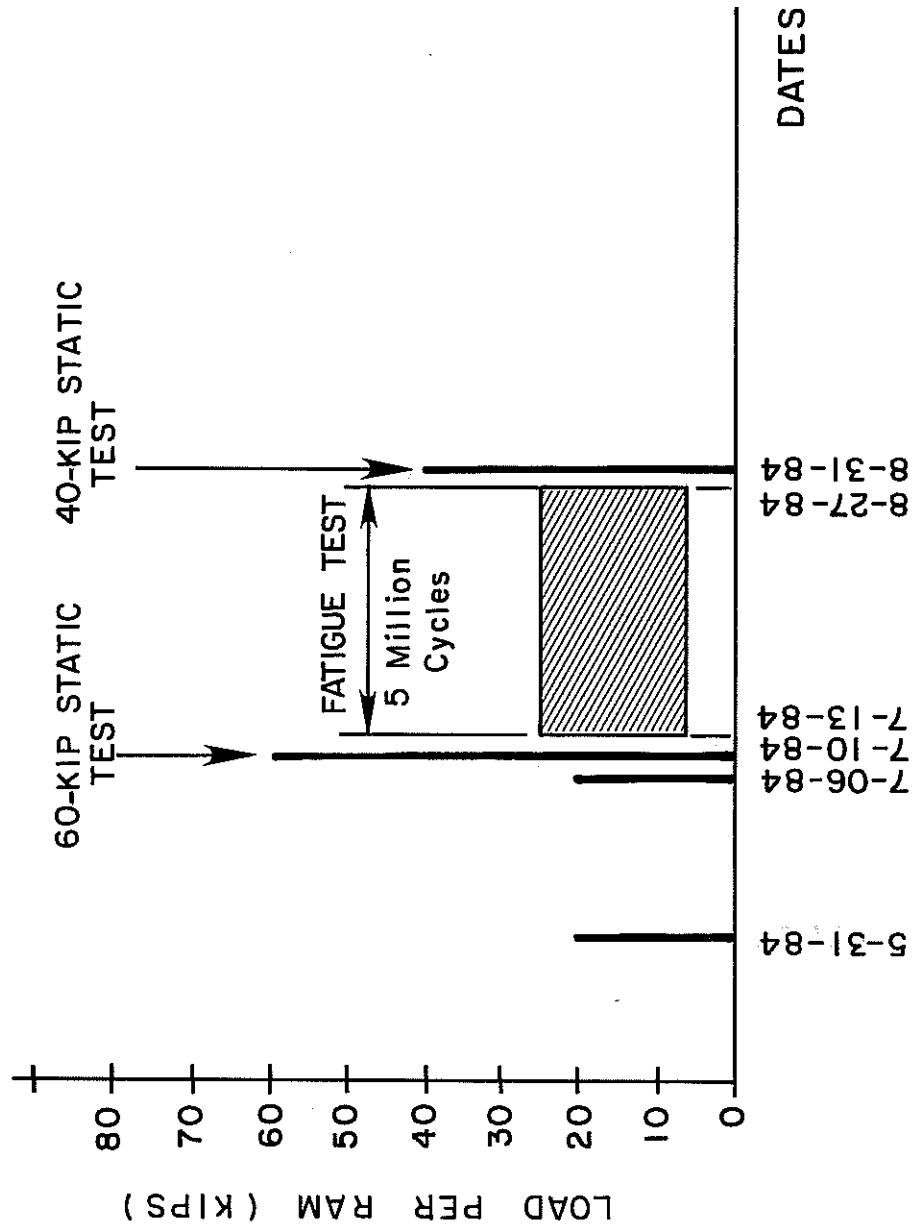

Fig. 3.25 History of loading

Fig. 3.26 Failed diaphragm weld

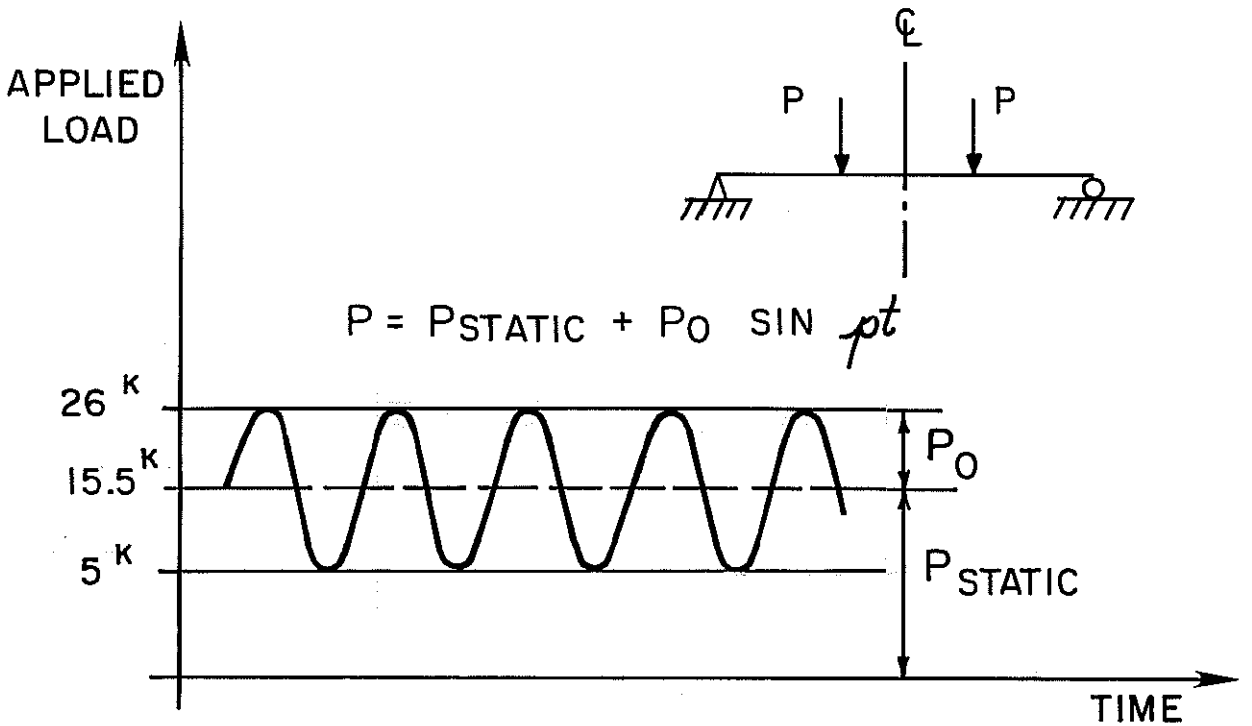

Fig. 3.27 Range of loading during fatigue test

CHAPTER 4

TEST RESULTS

4.1 General

The results of the pre-cracking and post-fatigue tests are presented in this chapter. The pre-cracking test was conducted in July 1984. The post-fatigue test was conducted in August 1984, after the structure had been subjected to several static tests (to a maximum load of 60 kips/ram), 5 million cycles of fatigue loading, and several more static tests to a maximum load of 40 kips/ram.

The distribution of girder loads was determined from strain readings. The procedure for doing this, discussed in detail in Section 4.5, involved the following steps:

1. longitudinal strains were measured in the girders at a series of evenly spaced points along the bridge, at 3 different heights at each point;

2. at each point, the strain variation with height was used to compute the curvatures of the girders along the bridge;

3. at each point, these curvatures were multiplied by the calculated flexural stiffness (EI) of the girder to determine the moment variations along the length of each girder; and

4. the moment variations were numerically differentiated twice to obtain the load applied to each girder over its length.

As will be discussed in Section 4.6, errors were introduced by the strain gages, and also from approximations used in the data reduction. Such errors are generally increased by the process of differentiation. In order to assess the accuracy of the above procedures for calculating girder loads, other types of data were also collected during the testing: vertical deflections of the steel girders; slip between the deck and the girders; and cracking patterns in the deck. These were used to check the validity of the numerical procedure, and also to check the internal consistency of the strain readings. These data are analyzed in Sections 4.2, 4.3 and 4.4, and the results are compared with the strain data in Section 4.5.

4.2 Deflections

4.2.1 Load vs. Deflection. Figures 4.1 and 4.2 show the curves of load vs. midspan deflection for the exterior and interior girders. Girder deflections varied linearly with applied load. One assumption (which will be discussed in Section 4.5), involving the procedure used to smooth the strain readings, was that the structure was linear and elastic. The linearity of Figs. 4.1 and 4.2 clearly substantiates this assumption.

In Fig. 4.1, the results of the pre-cracking test are shown by the solid line, and the post-fatigue test, by the dashed line. Vertical deflections of the girders were measured with dial gages, which registered deflections at the bottom flange of the steel girders, and were placed at the center of the span, at the loaded points, and over the supports. During the pre-cracking test, the dial gage at the center of the interior girder malfunctioned at the 40-kip load stage. Consequently, Figs. 4.1 and 4.2 show load-deflection data for both tests up to a maximum load of only 40 kips.

During the pre-cracking test, the girders had a linear load-deflection relationship under loads ranging from 0 kips up to about 35 kips. When the cracking load of 38 kips was attained, the solid lines shown in Figs. 4.1 and 4.2 exhibited a decrease in slope, reflecting the decreased flexural stiffness of the cracked deck.

The load-deflection plots for the post-fatigue test were similar to those for the pre-cracking test. Because the deck was already cracked, the load-deflection behavior was linear throughout the entire test. At each load stage, corresponding deflections increased by about 6 percent after the 5 million fatigue cycles, reflecting some softening as a result of the fatigue loading.

4.2.2 Variation of Deflection in Longitudinal Direction. The deflections shown in Figs. 4.1 and 4.2 were obtained from dial gages located at the girder midspans. As will be explained subsequently, vertical deflections at other points along the length of the girders were calculated from measured girder strains, in order to compare the calculated deflections with the experimentally determined ones, and to assess the accuracy of the strain gage readings.

The vertical deflections were calculated from measured girder strains (curvatures) using the moment-area theorems, and included the experimentally measured deformations of the bearing pads. The measured midspan deflections are compared with the calculated values in Figs. 4.3 through 4.6, and the centerline values are seen to agree within about 5 percent.

The fact that these deflections agreed so closely is important. The variation of deflection in the longitudinal direction was calculated

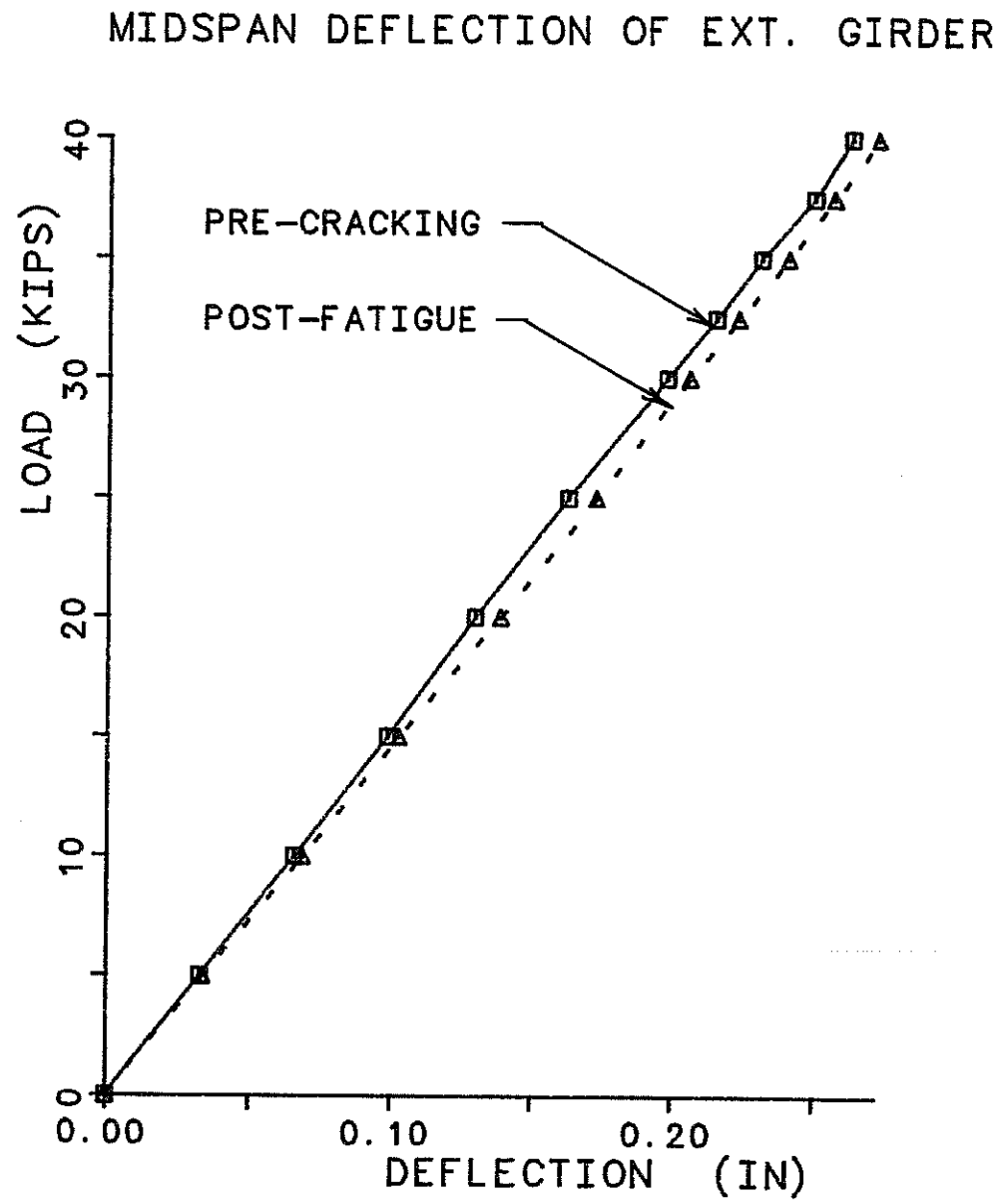

Fig. 4.1 Midspan deflection of exterior girder

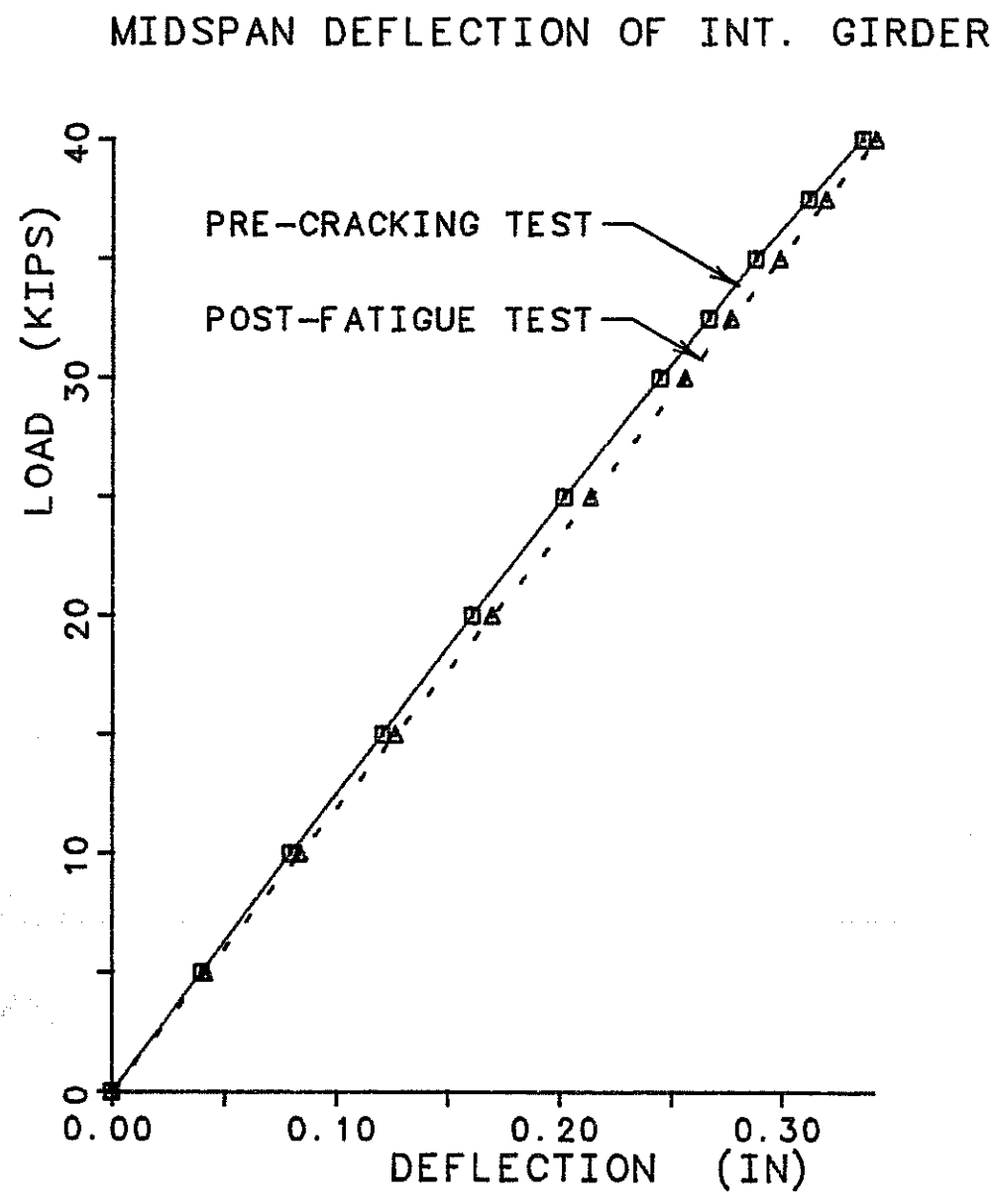

Fig. 4.2 Midspan deflection of interior girder

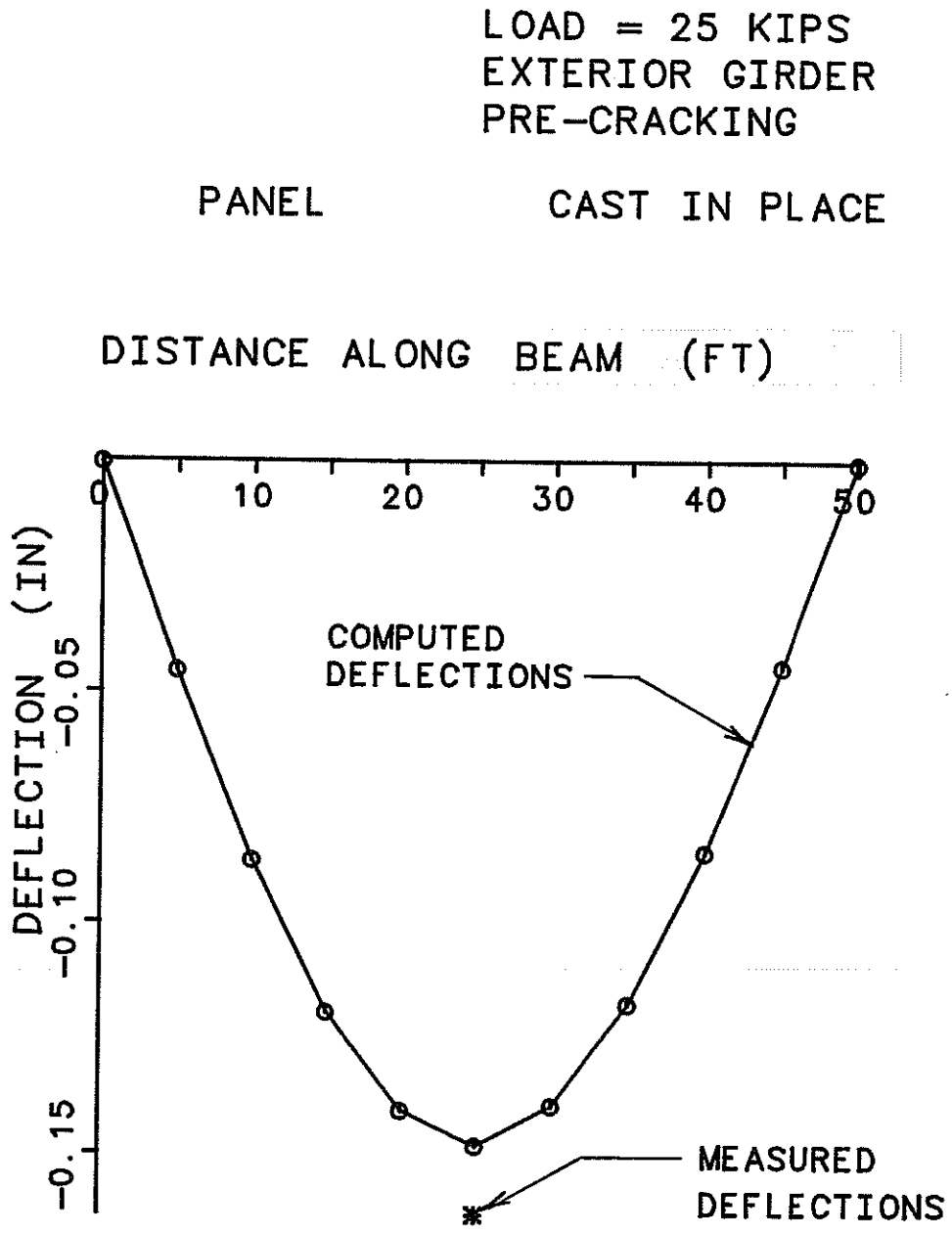

Fig. 4.3 Computed and measured deflections (pre-cracking), 25 kips, exterior girder

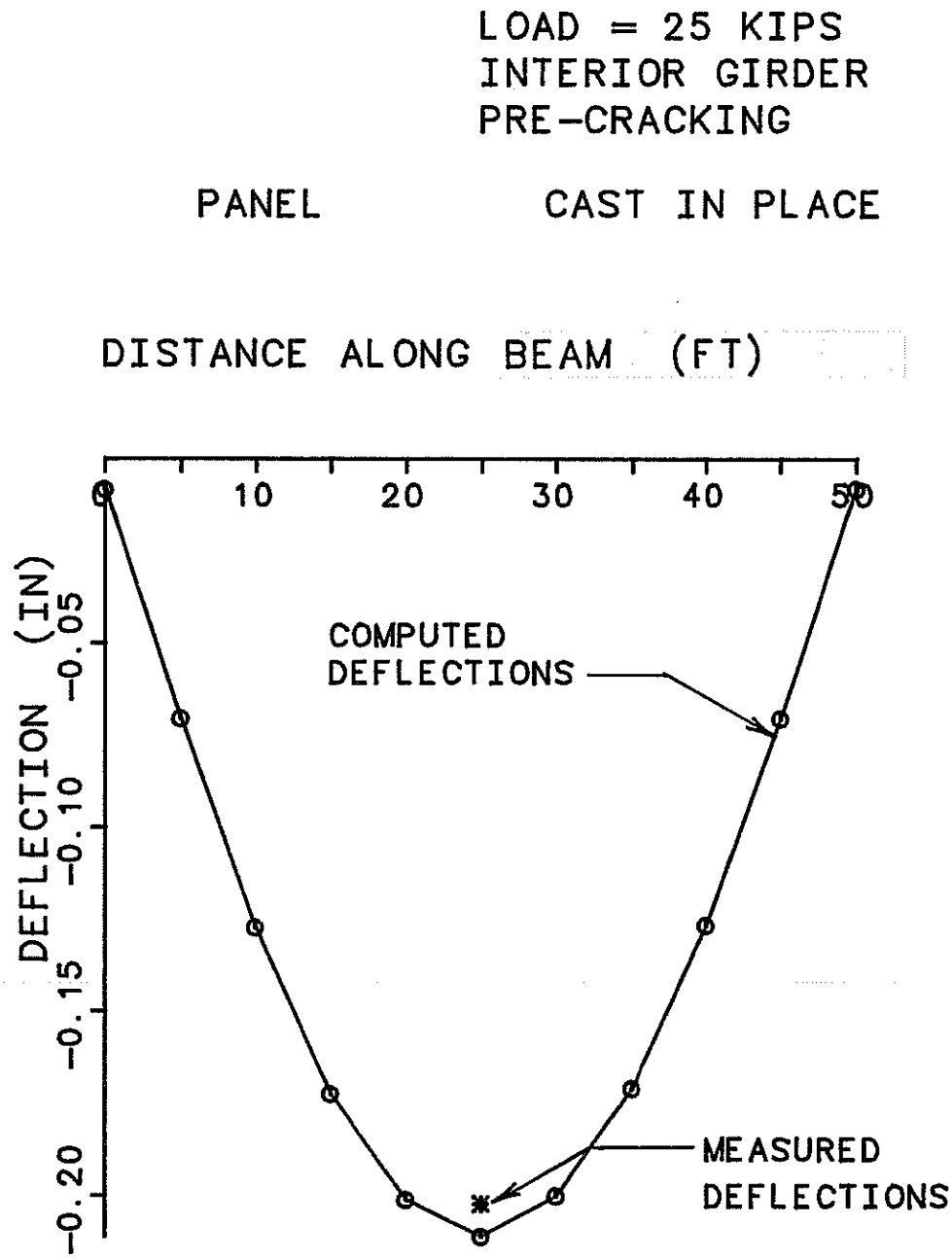

Fig. 4.4 Computed and measured deflections (pre-cracking), 25 kips, interior girder

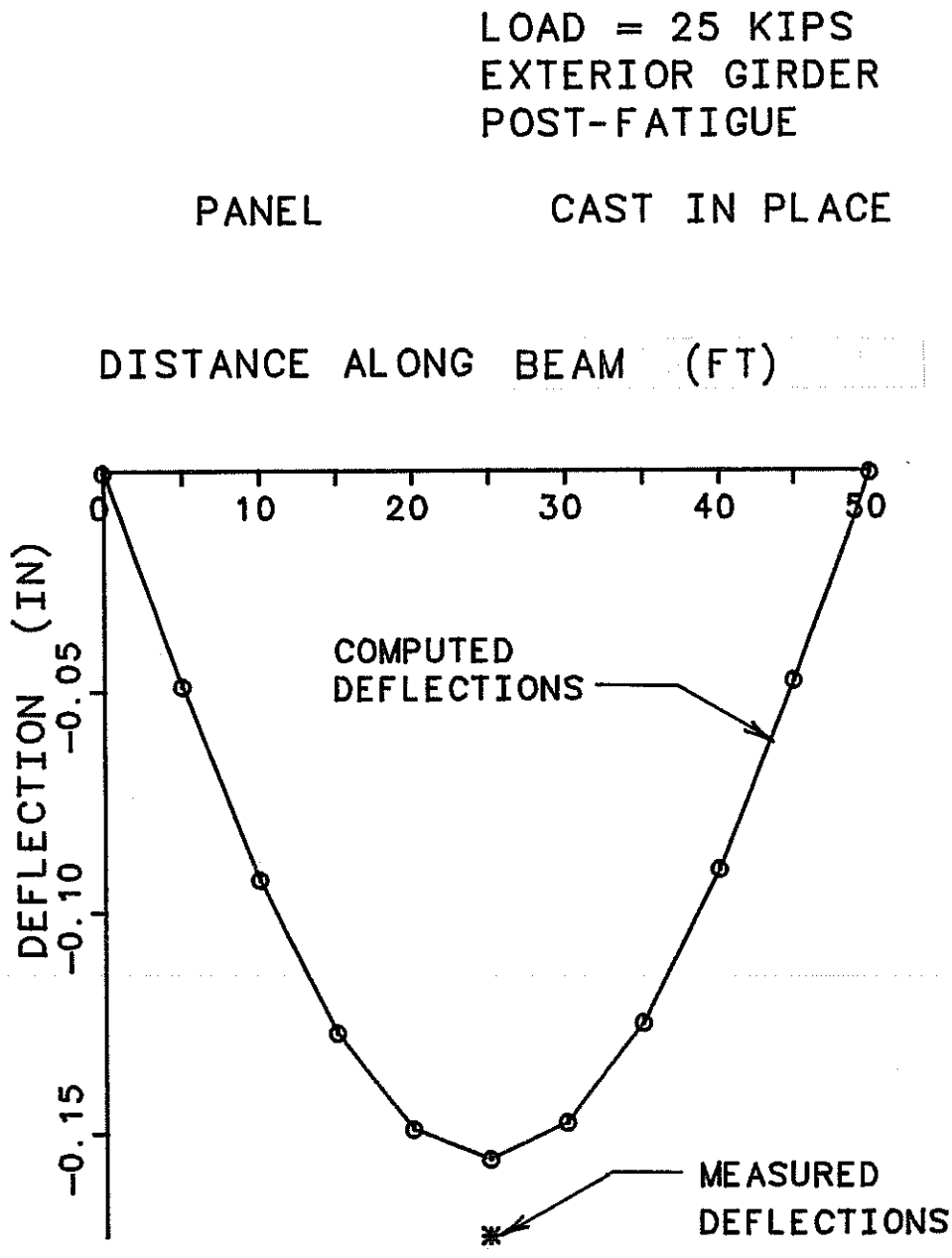

Fig. 4.5 Computed and measured deflections (post-fatigue), 25 kips, exterior girder

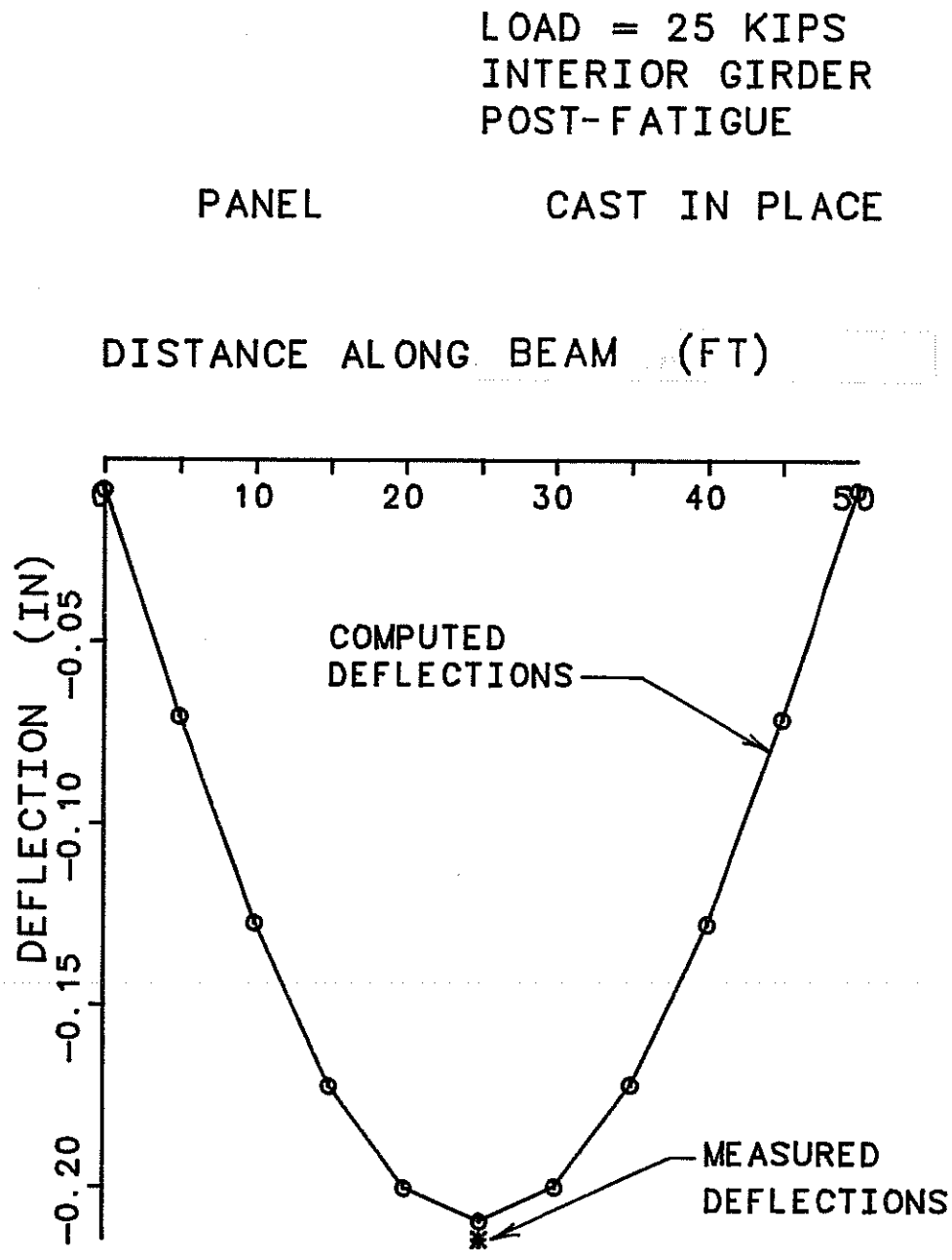

Fig. 4.6 Computed and measured deflections (post-fatigue), 25 kips, interior girder

using curvatures obtained from girder strain readings, and a comparison with the experimental deflections provides a check on the accuracy of the strain gage readings.

These strain gage readings are used in Section 4.5 to calculate the variation of moment and load in the longitudinal direction. Error was introduced by approximating the loads from the moments, and from several other sources. Based on the comparison of deflections presented here, it is concluded that a relatively small percentage of the total error was contributed by the strain gages themselves.

4.3 Slip Between Deck and Girders

The pre-cracking and post-fatigue slip between the deck and the steel girders is shown in Appendix B. In most cases the slip was small (less than 0.01 in.) indicating that the bridge was behaving as a composite structure.

Two typical load-slip diagrams, shown in Figs. 4.7 and 4.8, correspond to the northern (cast-in-place) end. Figure 4.7 shows the pre-cracked load-slip relationship, and Fig. 4.8 illustrates the load-slip behavior at the same point after fatigue loading.

The slip between the deck and the steel beams can be described by [43]:

$$d\gamma/dx = \epsilon_s \epsilon_b \qquad (4.1)$$

where: γ = slip between the deck and steel beam,

x = distance along the beam,

ϵ_s = longitudinal strain in the slab, and

ϵ_b = longitudinal strain in the beam.

The slip is zero at the center of the bridge, and increases to a maximum at the ends.

The pre-cracked plots indicate that the slip increased nonlinearly with increasing load. In general, the cast-in-place end seemed to slip more than the panel end, and the slab over the center girder slipped more than the slab over either of the two exterior girders. The largest slip occurred at the north end of the center girder.

The post-fatigue load-slip plots, shown in Appendix B, were also nonlinear, and the maximum slip was only 0.005 in. Slip at all load stages showed a slight but consistent decrease after 5 million

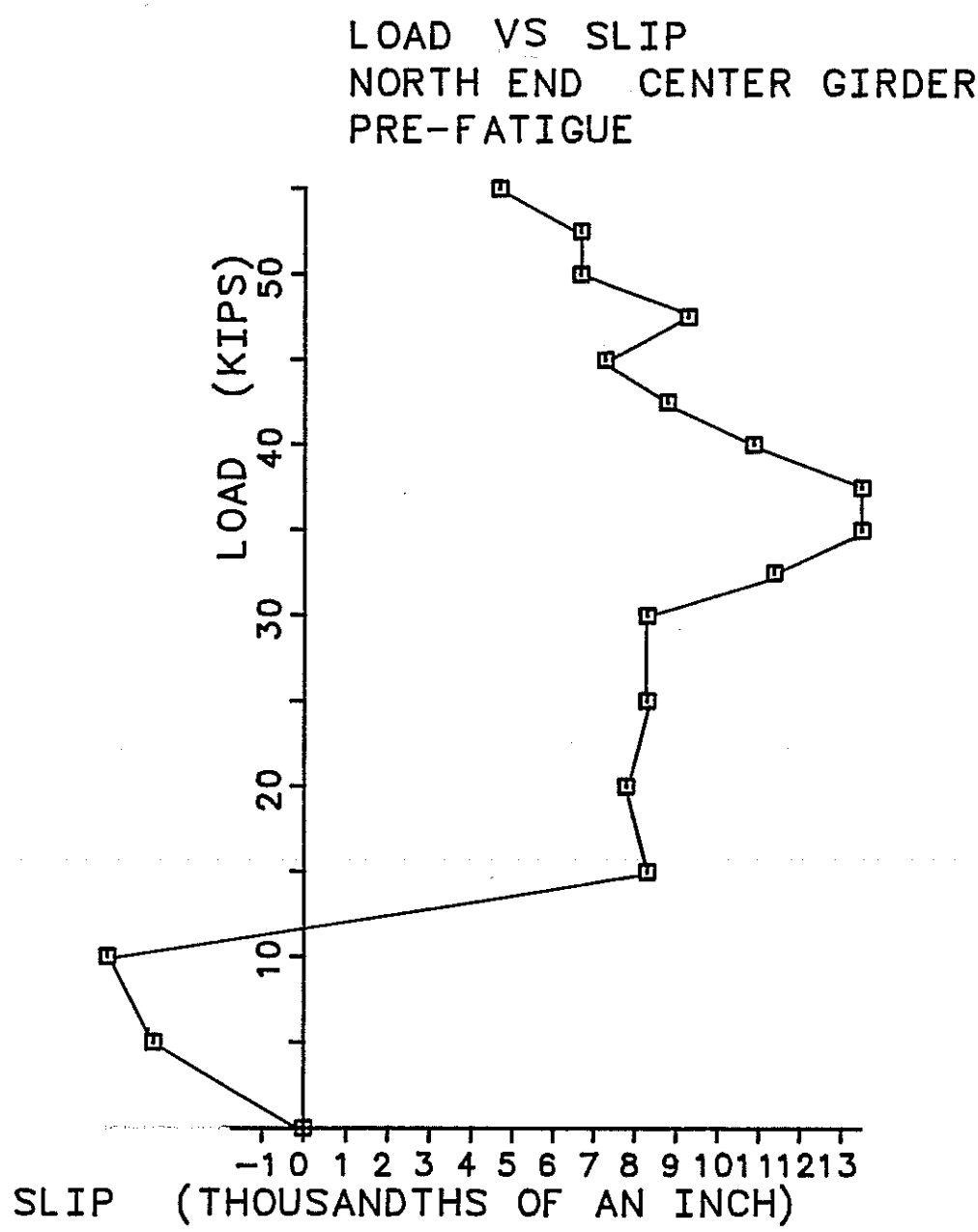

Fig. 4.7 Pre-cracked load-slip data, center girder, north end

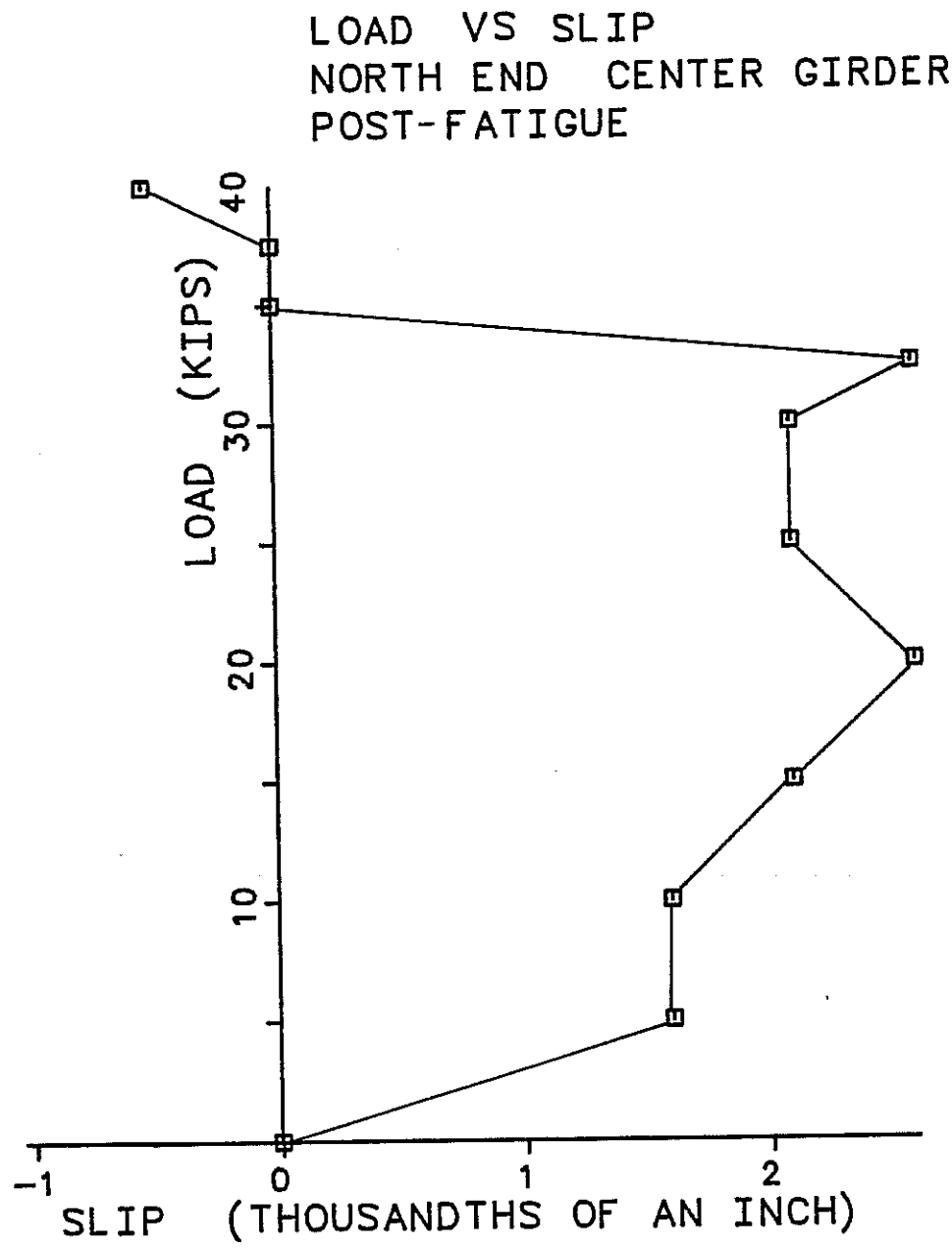

Fig. 4.8 Post-fatigue load-slip data, center girder, north end

cycles of fatigue loading. This decrease in slip under fatigue loading suggests that the composite behavior of the bridge did not deteriorate under fatigue. The reasons for the decrease are not clear. Although it might have been expected to result from a decrease in the in-plane stiffness of the deck owing to cracking, little change in overall bridge stiffness is apparent in Figs. 4.1 and 4.2.

4.4 Cracking Patterns in Deck

Cracking patterns in the deck are shown in Fig. 4.9 and 4.10. Strains and deflections were originally assumed to be equal in both exterior girders, and the symmetry of the cracking patterns about the center girder substantiated this assumption. The cracking patterns were non-symmetric about midspan, and the strains and deflections also differed from one end of the bridge to the other.

Most of the cracking occurred in the bottom of the deck at the cast-in-place end. Four short cracks formed on the bottom of the panel end, near the loaded points, and some cracks formed on the top surface of the deck over the panel joints. The 5 million cycles of fatigue loading extended many of the cracks, and produced several new ones.

Crack widths under load ranged from less than 0.005 in. to about 0.05 in. The narrowest cracks formed on the top of the deck, and were caused primarily by shrinkage of the concrete. The widest cracks were observed near the loaded points on the bottom of the cast-in-place deck. These wide cracks opened up as the load was applied, and closed almost completely when the load was removed.

The absence of longitudinal cracks over the exterior girders indicated that the slabs there, and the girders supporting them, rotated parallel to the longitudinal axis of the bridge as the load was applied. The pattern of cracks on the bottom of the cast-in-place end suggested the start of yield line fans on each side of the north end.

4.5 Calculation of Girder Loads from Strain Data

4.5.1 General. The distribution of girder loads was determined from steel strain readings. Usefulness of raw strain data was decreased by significant scatter as a result of errors caused by the gages themselves, and also by errors introduced in reading the data. Scatter was particularly noticeable for the gages near the supports, which registered small strains. As will be discussed subsequently, the steel strain readings were first smoothed, and the smoothed values were used to calculate girder curvatures and the longitudinal variation of girder moments and loads.

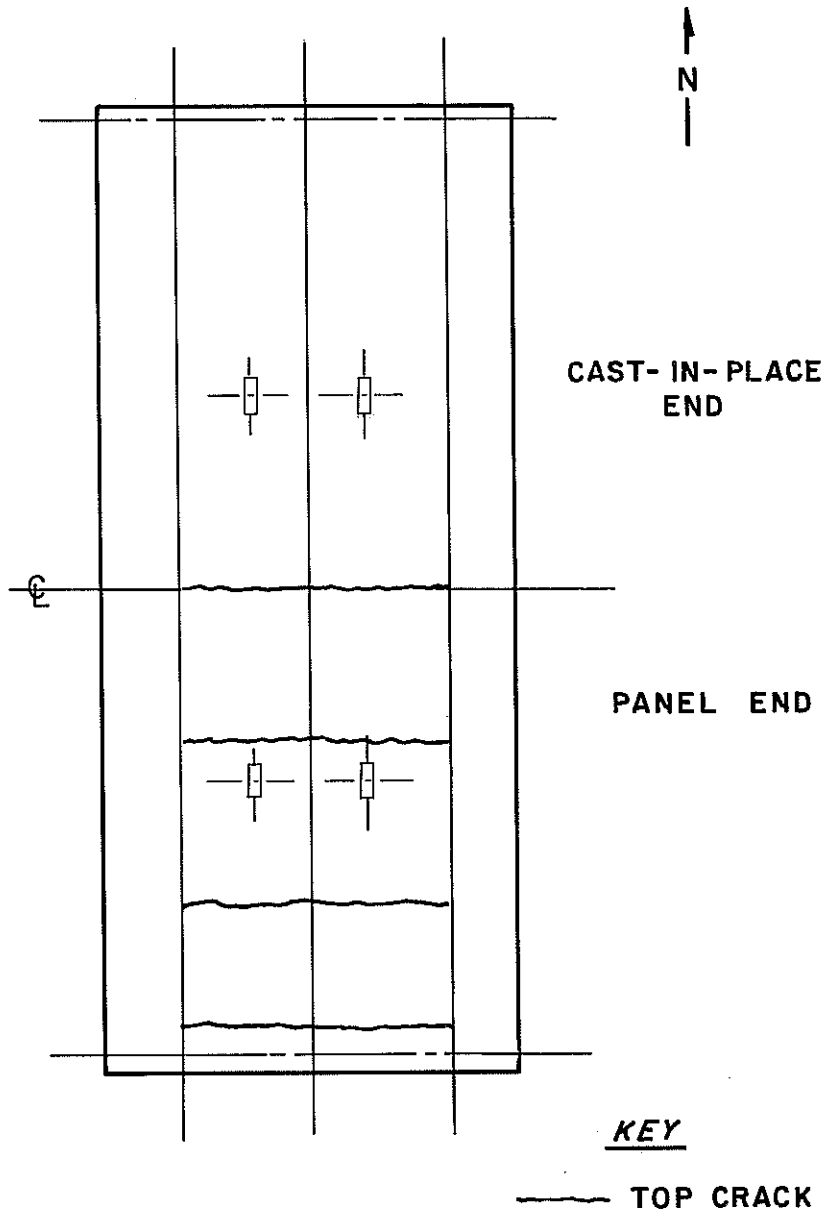

Fig. 4.9 Crack patterns in deck before testing

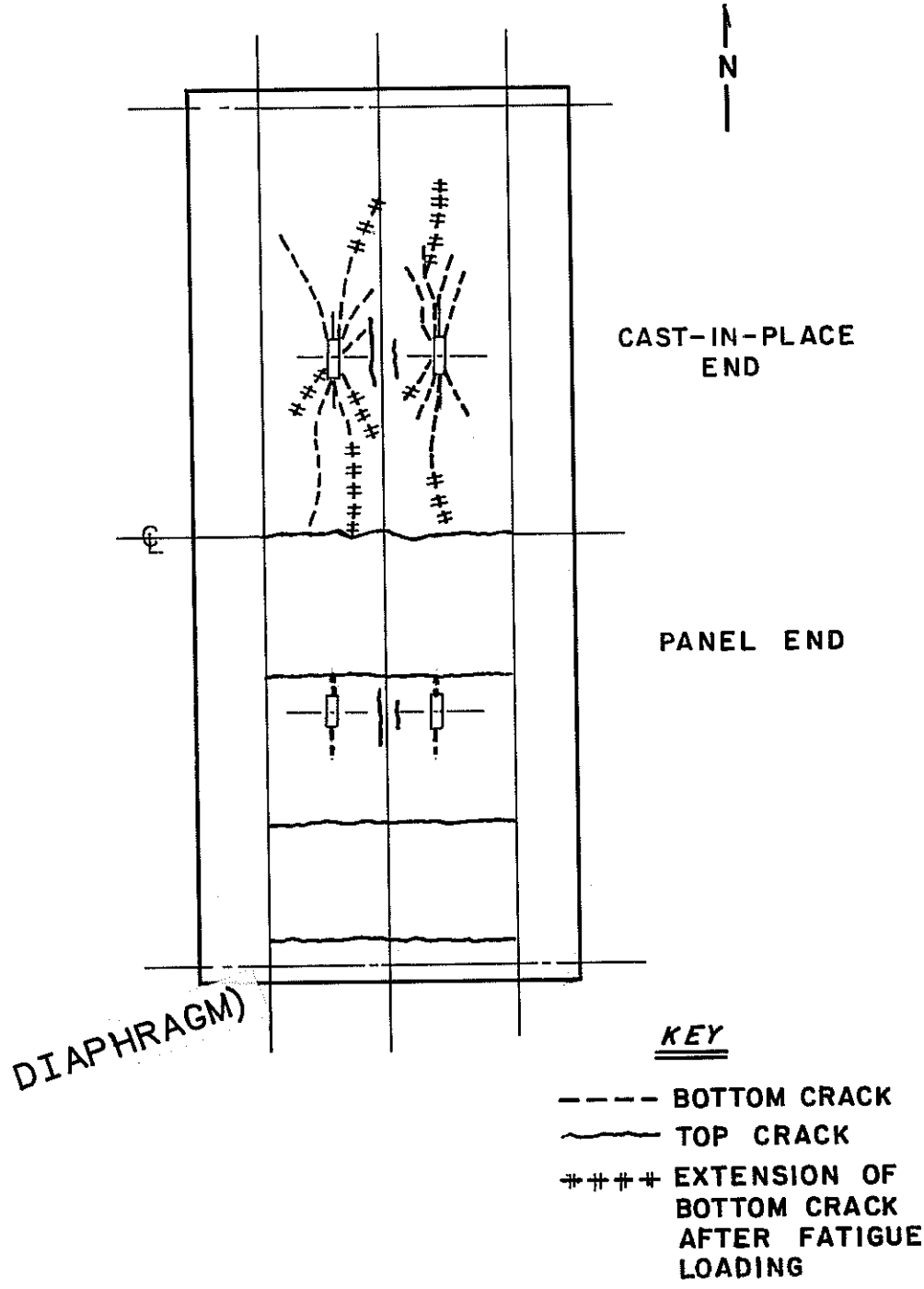

Fig. 4.10 Crack patterns in deck after testing

4.5.2 Load-Strain Diagrams. The 108 plots of load vs. girder strain data are shown in Appendices C and D. The plots in Appendix C correspond to the pre-cracking test, and the plots in Appendix D correspond to the post-fatigue test. A typical pre-cracking load-strain plot (for Strain Gage 19) is shown in Fig. 4.11. This strain gage was located on gage line 7, on the top flange of the west girder (refer to Fig. 3.18).

The triangles in Fig. 4.11, representing original load-strain data points, were rather scattered. It was reasoned that load-strain data from an ideal gage would lie on a straight line passing through the origin. The line shown in Fig. 4.11 represents load-strain data from such an ideal gage. It passes through the origin, and is drawn to minimize the sum of the squares of the deviations on the horizontal axis. This smoothing procedure was used for all 108 load-strain plots in Appendices C and D.

The smoothing procedure of Fig. 4.11 forced the experimentally recorded load-strain behavior of the girders to be linear and elastic. As noted earlier, this assumption is consistent with the linearity of the bridge's behavior as evidenced by load-deflection plots (Figs. 4.1 and 4.2), and the correspondence between measured deflections and those computed using linear elastic theory (Figs. 4.3 through 4.6).

4.5.3 Strain Gradient Diagrams. The strain gradients over the depth of the girders for the pre-cracking and post-fatigue tests are shown in Appendix E. Fig. 4.12 shows a typical strain gradient diagram for the interior girder near the supports on the panel end, at the 25-kip load stage. The three points on each strain gradient diagram are smoothed strains corresponding to the 25-kip load stage. Each gradient was then obtained as that line which would result in the smallest least-square error for the three strain readings. Because the smoothed load-strain curves were straight lines passing through the origin, the strain gradients at each point were proportional to the applied loads. If the load of 25 kips per ram were increased to 50 kips, then all smoothed strains would double, and so would the strain gradients. The location of the neutral axis of the composite section, read directly from the plots in Appendix E, ranged from 24 to 34 in. above the bottom fiber of the steel girders, with an average value of about 31 in.

The position of the neutral axis was also calculated assuming a fully composite section with an effective width of 84 in. as given by the AASHTO Specifications [1]. Because the concrete strains were small under the applied loads, it was thought that the initial tangent modulus should be used for concrete. The initial tangent modulus was calculated by modifying the current ACI formula [44] for the secant modulus at 0.5 f'_c as explained below:

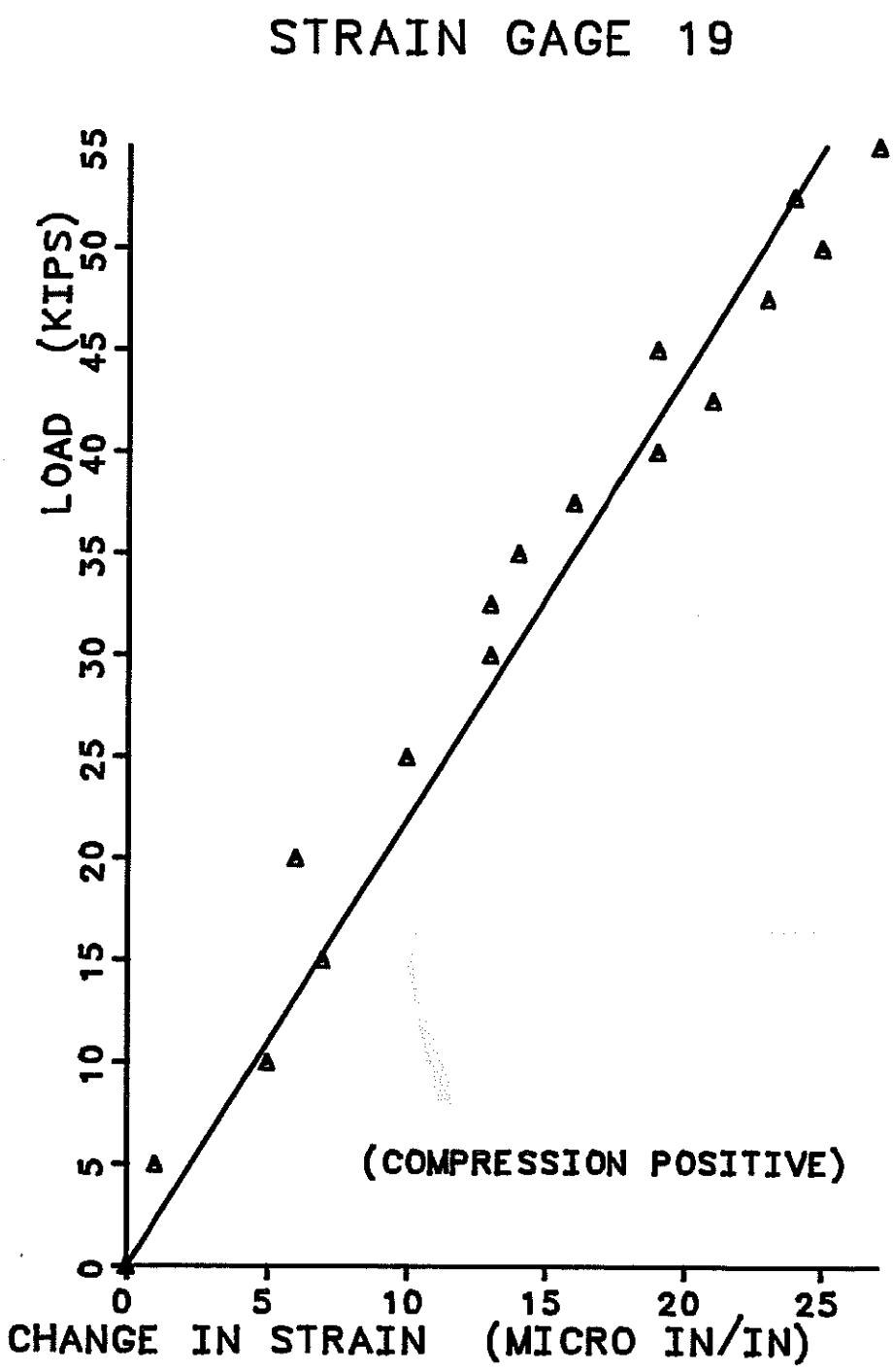

Fig. 4.11 Pre-cracking load vs. strain plot, strain gage 19

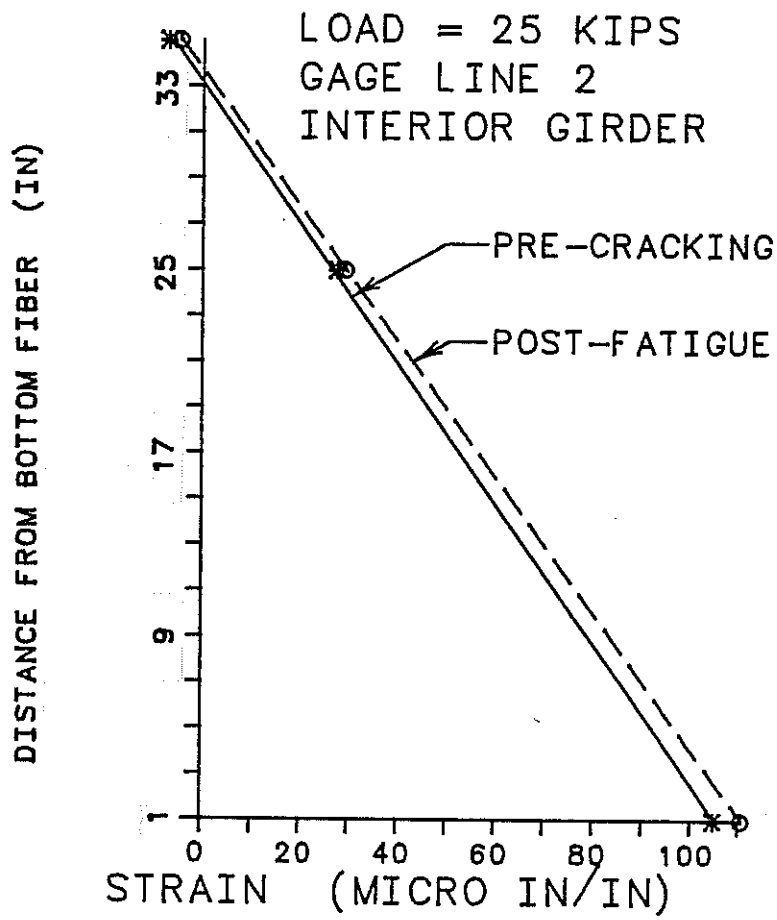

Fig. 4.12 Pre-cracking and post-fatigue strain gradient diagrams (25 kips, interior girder, gage line 2)

1. E_c was calculated using the current ACI formula [44],

$$E_c = W_c^{1.5}\ 33\ (f'_c)^{0.5}$$

2. Assuming a stress-strain curve of the form suggested by Hognestad [45], the ratio between E_c and E_T was calculated.

$$f_c = f'_c[2(\varepsilon_c/\varepsilon_o) - (\varepsilon_c/\varepsilon_o)^2],$$

when $\varepsilon_c = 0$, $E_T = 2(f'_c/\varepsilon_o)$,

when $\varepsilon_c = 0.5\ f'_c$, $2(\varepsilon_c/\varepsilon_o) - (\varepsilon_c/\varepsilon_o) = 0.5$

$2x - x^2 = 0.5$, $x = 0.293$

$E_T = 0.5f'_c/0.293\ \varepsilon_o$

$E_T/E_c = 2/(0.5/0.293) = 1.17$

3. E_T was computed by multiplying the current ACI value for E_c by that ratio:

$$E_T = 1.17\ E_c = 1.17\ (w_c^{1.5}33(f'_c)^{0.5})$$

Young's modulus for the steel girders was taken as 29,000 ksi, giving tangent modular ratios (E_S/E_T) of 5.76 and 4.86 for the cast-in-place and panel ends of the bridge, respectively. Using the AASHTO effective width of 84 in., and considering the contribution of the reinforcement in the deck, the theoretical position of the neutral axis was calculated to be about 33 in. from the bottom of the girder. This number was close to the average experimental value of 32 in. The calculation of the position of the neutral axis according to the AASHTO Specification assumes complete composite action. This assumption was substantiated by the slip data in Section 4.3. The small slip between the deck and the girders, shown in Figs. 4.7 and 4.8, indicated that the bridge was indeed behaving as a composite structure.

4.5.4 Moment Diagrams. Once the strain gradients had been determined, the longitudinal distribution of girder moments was calculated using the following procedure:

1. the curvatures (strain gradients in Fig. 4.12) were calculated at each point along the girder;

2. these curvatures were multiplied by the corresponding theoretical transformed EI values (calculated as discussed above) to obtain the moments according to Eq. 4.2 below:

$$E_S I_S = d^2y/dx^2 = M(x) \qquad (4.2)$$

where E_S = Young's modulus for steel;

I_S = moment of inertia of the composite section transformed to steel;

M(x) = moment

The calculated moment diagrams for the exterior and interior girders are shown in Figs. 4.13 and 4.14, for an applied load of 25 kips per ram. As a result of the smoothing procedure used for the load-strain data, the ordinates of each diagram are proportional to the applied load, and the moment at any other load stage can be obtained by scaling. The pre-cracking moment diagram is shown by the solid line, and the post-fatigue diagram, by the dashed line. Because the panel end experienced little cracking, the moment diagrams for that end were about the same before and after the fatigue loading. Adjacent to the loads, cracks formed over the girders on the cast-in-place end. These reduced the transverse stiffness of the deck near the loads, and transferred the load longitudinally to adjacent transverse slab strips. As a result, the load was smoothed out along the length of the girder after cracking; the moment diagrams reflected this behavior by also becoming smoother and more rounded after fatigue loading.

4.5.5 Load Diagrams. Girder loads were computed from the moments in Section 4.5.4 using the differential equation of a beam deforming in flexure:

$$(d^2(M(x))/dx^2 = W(x) \qquad (4.3)$$

where W(x) = load, and

M(x) = moment.

The previously discussed moment diagrams were numerically differentiated twice using the central difference operator:

$$W_i = (M_{i-1} - 2M_i + M_{i+1})/h^2 \qquad (4.4)$$

where W_i = load at the i^{th} point on the girder;

M_i = moment at the i^{th} point on the girder; and

h = uniform distance between points on the girder.

The load diagrams for the exterior and interior girders are shown in Figs. 4.15 and 4.16 for an applied load of 25 kips per ram. The pre-cracking load diagram is shown by the solid line, and the post-fatigue diagram, by the dashed line.

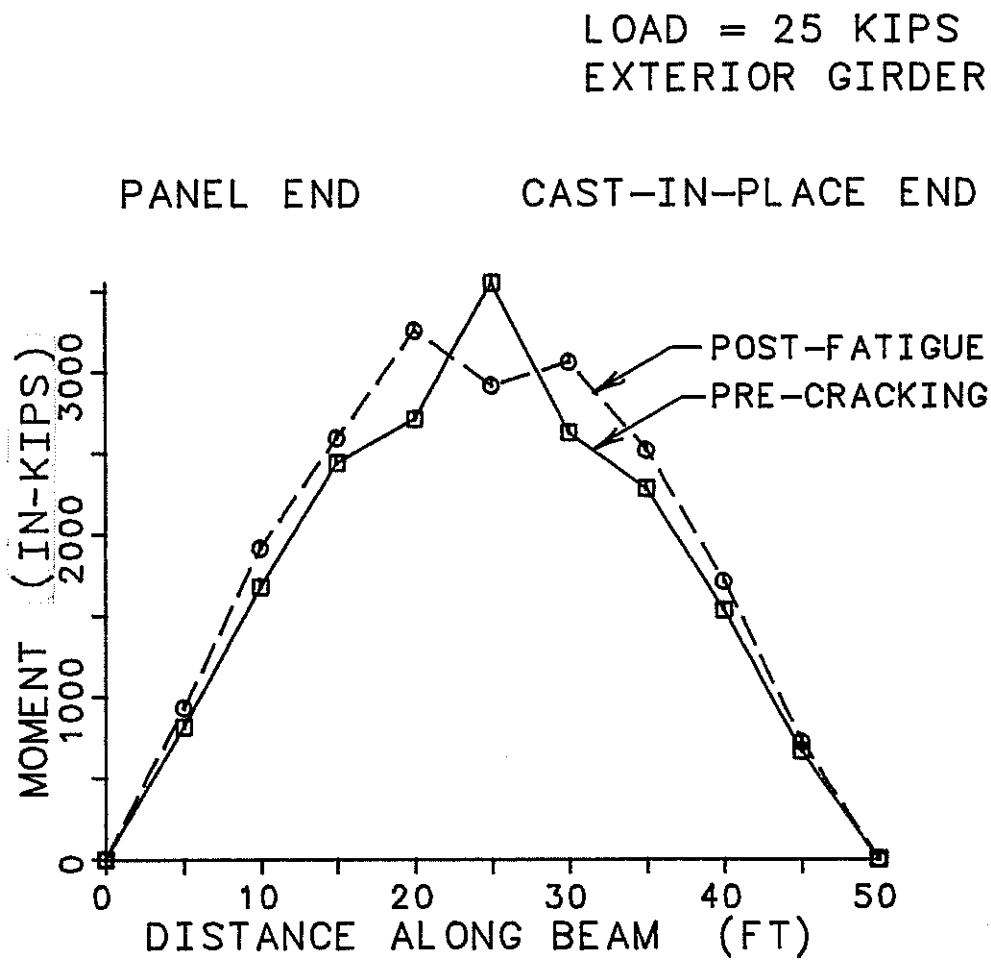

Fig. 4.13 Pre-cracking and post-fatigue moment diagrams (25 kips, exterior girder)

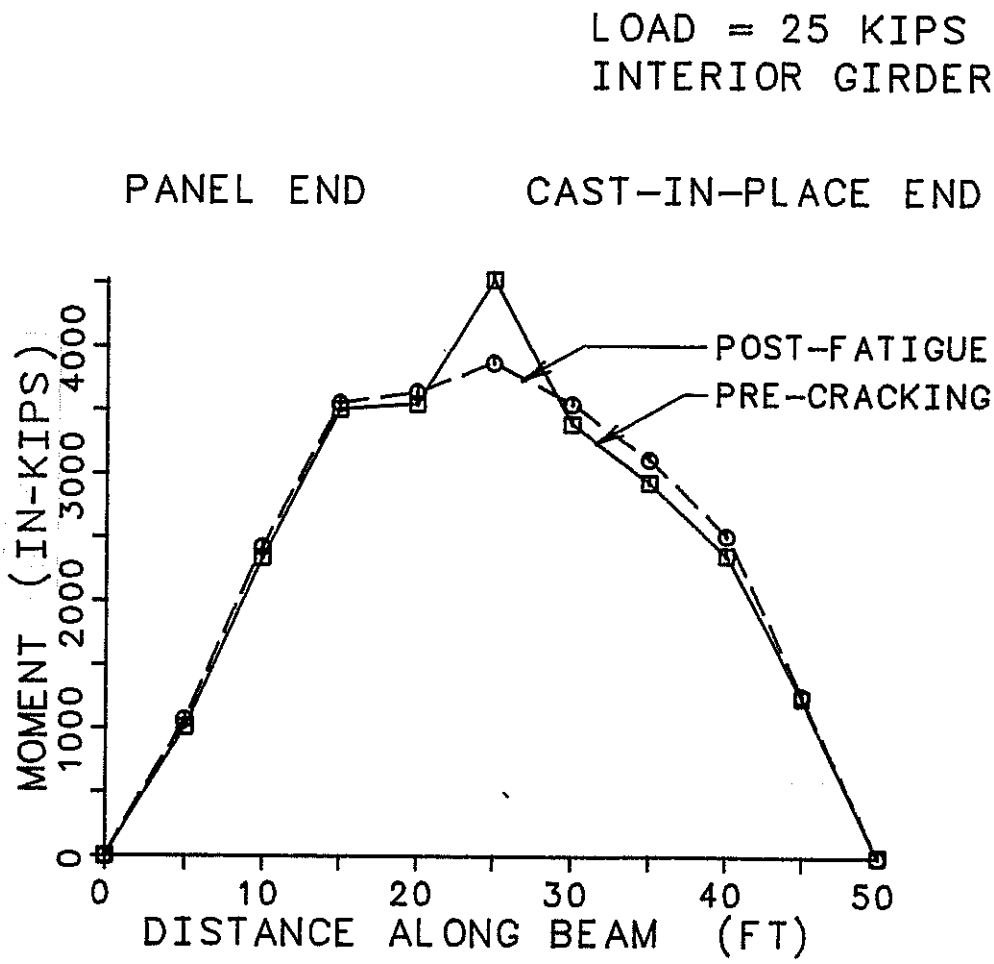

Fig. 4.14 Pre-cracking and post-fatigue moment diagrams (25 kips, interior girder)

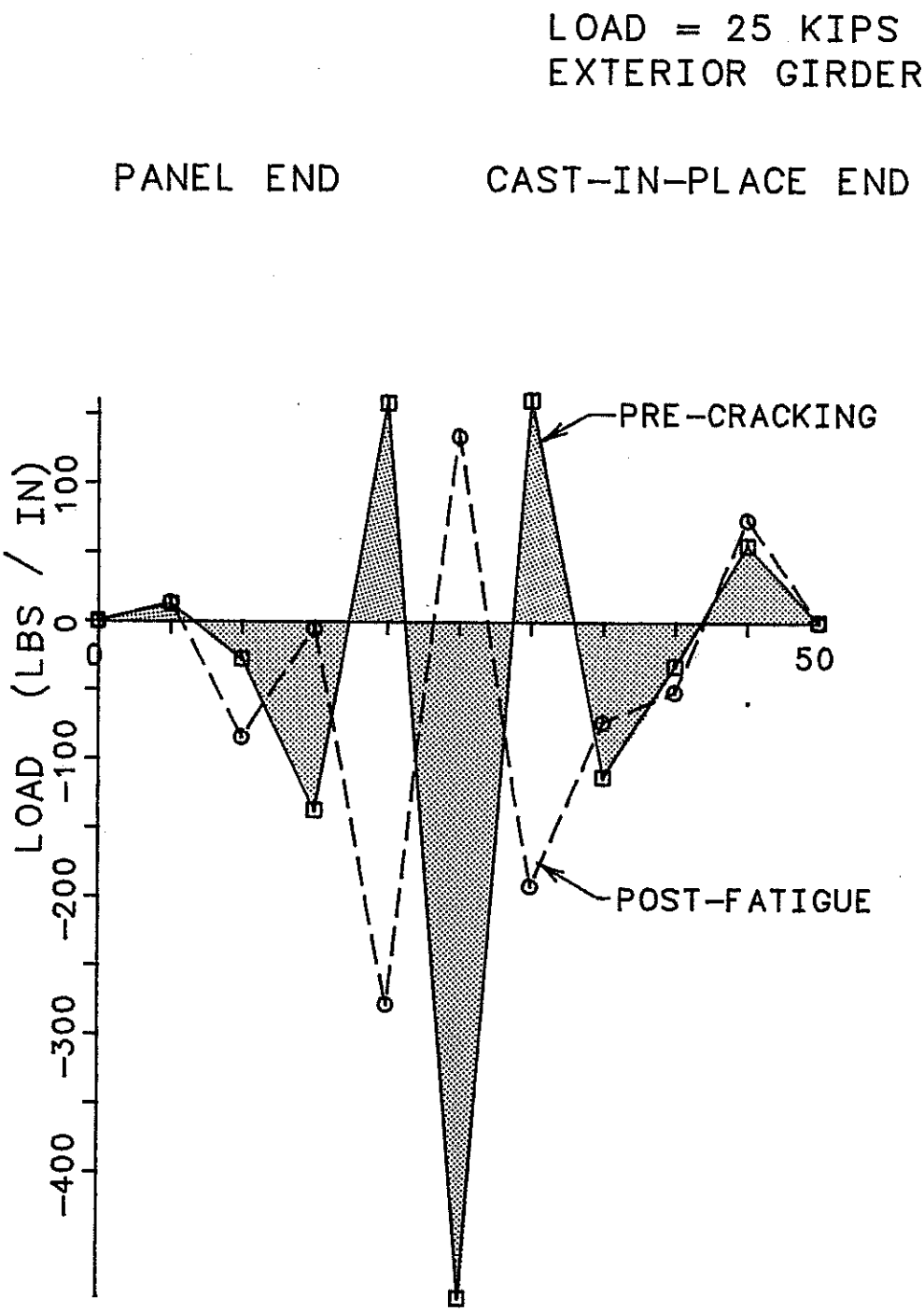

Fig. 4.15 Pre-cracking and post-fatigue load diagrams (25 kips, exterior girder)

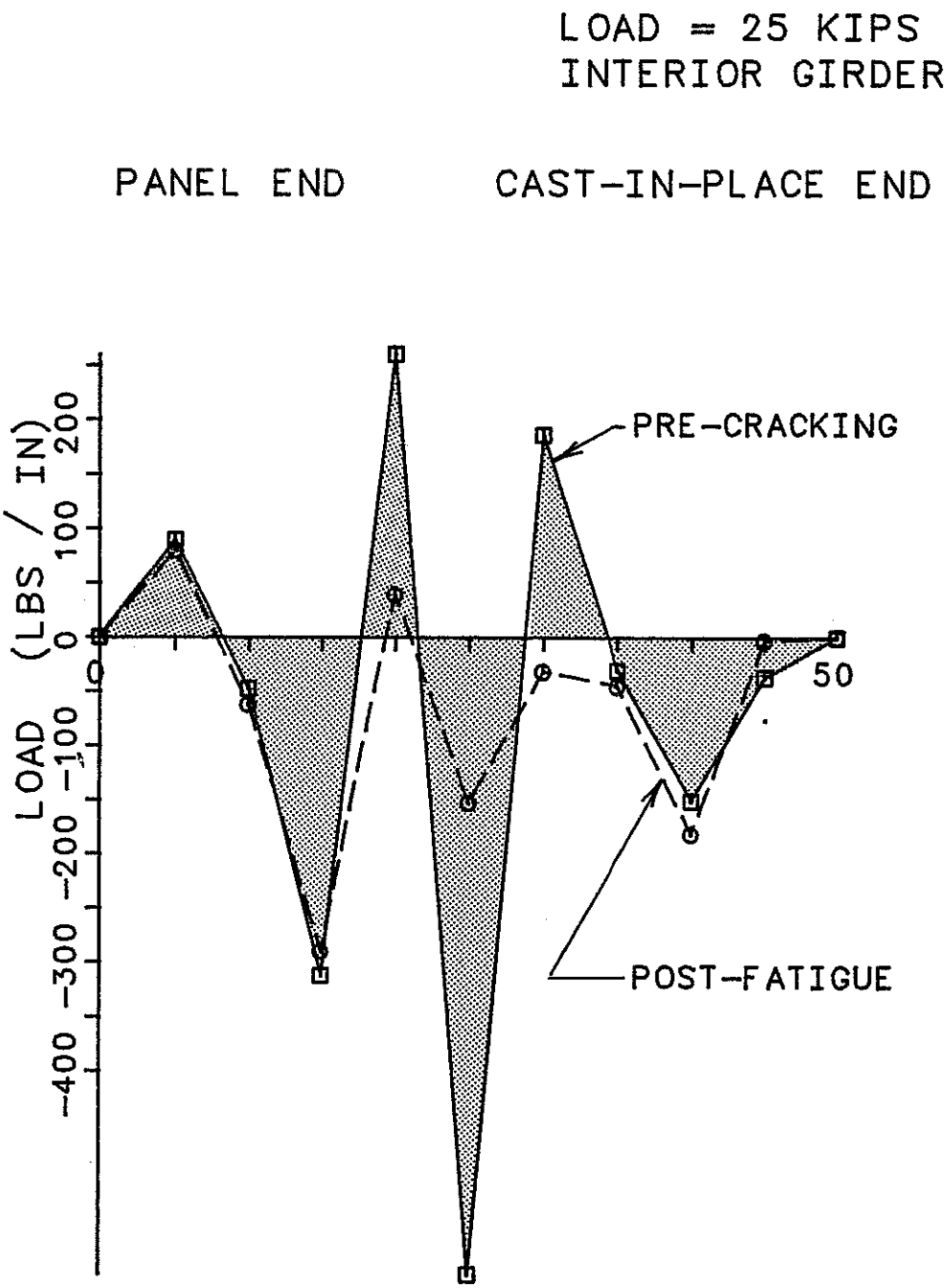

Fig. 4.16 Pre-cracking and post-fatigue load diagrams (25 kips, interior girder)

The panel deck on the southern end of the bridge was stiffer than the totally cast-in-place deck on the northern end, did not crack much, and did not exhibit the longitudinal redistribution of load shown by the cast-in-place end. As a result, the load diagrams for the panel end had peaks at the loaded points that were consistently higher than the corresponding peaks on the cast-in-place end.

Before the cast-in-place end cracked, it transferred the load transversely (between the girders), as shown in Figs. 4.15 and 4.16: the peak value at the loaded point was -110 lbs/in. for the exterior girder, and -150 lbs/in. for the interior girder. After the deck over the interior girder cracked, its transverse stiffness was reduced, and more load was transferred from the interior to the exterior girder. This behavior is shown in Fig. 4.15 by the increase in load on the exterior girder at the cast-in-place end from -110 lbs/in. to -190 lbs/in. at the loaded point.

4.6 Computed vs. Experimentally Determined Load Diagrams

The load diagrams shown in Figs. 4.15 and 4.16 were used for checking the accuracy of the techniques used to measure and reduce the experimental data. Using the trapezoidal rule, the area under the load diagrams was calculated (for both the interior and exterior girders), and the total load so calculated was compared with the total load actually applied at each load stage. This comparison, shown in Table 4.1, provided an overall check on the procedure used to compute girder loads from smoothed curvatures.

As shown in Table 4.1, the calculated load was 13 percent low in the pre-cracked test, and 6 percent low in the post-fatigue test.

TABLE 4.1 Comparison of Calculated Load with Actual Applied Load

	Calculated Load, kips			Actual Applied Load, kips	% Error
	Exterior Girder	Interior Girder	Total		
Pre-Cracking	24.7	37.6	87.0	100	13
Post-Fatigue	26.5	41.0	94.0	100	6

One possible source of error was the approximation of the actual area under the load diagram by a series of trapezoids. Another possible source of error was the fact that the data were collected from strain

gages using switching and balance units. Errors were introduced from the strain gages themselves, and from the recording of the strains during the testing.

The reduction in percent error (Table 4.1) from 13 percent before cracking to 6 percent after fatigue loading could be explained by the fact that the post-fatigue load plots are smoother than the pre-cracking plots. The smoothness would be expected to reduce the error in approximating the curved load diagrams by straight lines. The error in the experimentally determined loads was between 6 and 13 percent. Since the experimental load diagrams were obtained by differentiating the moments, the error in the moment diagrams is believed to be at most 6 to 13 percent. Because of this small error, the experimentally determined moment diagrams are used as a reference for the moment comparisons shown in the next chapter.

CHAPTER 5

COMPARISON OF EXPERIMENTALLY DETERMINED MOMENTS WITH THEORY

5.1 General

In this chapter, the moment diagrams derived using the procedures of the AASHTO Code, the Ontario Highway Bridge Design Code, and those obtained from a finite element model will be compared. As discussed in Chapter 1, the AASHTO design moments for a bridge girder are determined by loading the bridge with part of a truck load so as to produce a maximum stress in a particular girder, and the design moments in that girder are then calculated using a distribution factor times the moment in that girder acting alone. Because the loads on the test bridge were placed so as to produce a maximum stress in the center girder, those girder moments can meaningfully be compared with predicted code values.

5.2 Design Moments from AASHTO

The AASHTO procedure used to calculate girder moments for a bridge was outlined quantitatively in Chapter 1. This procedure is illustrated numerically in Fig. 5.1 for the center girder of the laboratory specimen. A pair of 25-kip loads were applied to the center girder, and multiplied by a distribution factor of (7/5.5), producing a peak design moment in the center girder of 5730 in.-kips. The experimental and theoretical moments are compared in Figs. 5.2 and 5.3. The shapes of the curves are clearly different, and the peak moment exceeds the experimentally determined value by about 80 percent.

5.3 Design Moments from Ontario Highway Bridge Code

The Ontario design approach for determining girder loads for a highway bridge is similar to that of the AASHTO Code, except that the distribution constant C is determined from charts. The design procedure for calculating the moments in the interior girder of the laboratory specimen is illustrated in Appendix F. The design moment for the center girder is also shown in Figs. 5.2 and 5.3. The peak value of 4230 in.-kips is higher than the experimental value by about 30 percent.

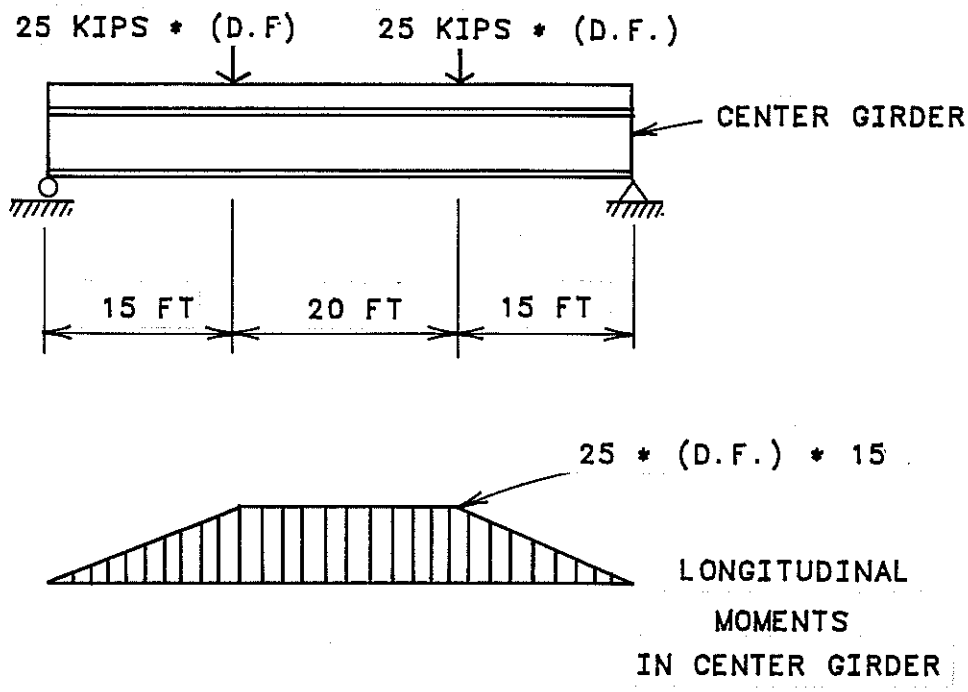

DESIGN MOMENT
FOR CENTER GIRDER = 25 * (7.0/5.5) * 15 * 12
= 5730 IN-KIPS

Fig. 5.1 Design moments from AASHTO Code, center girder of laboratory specimen

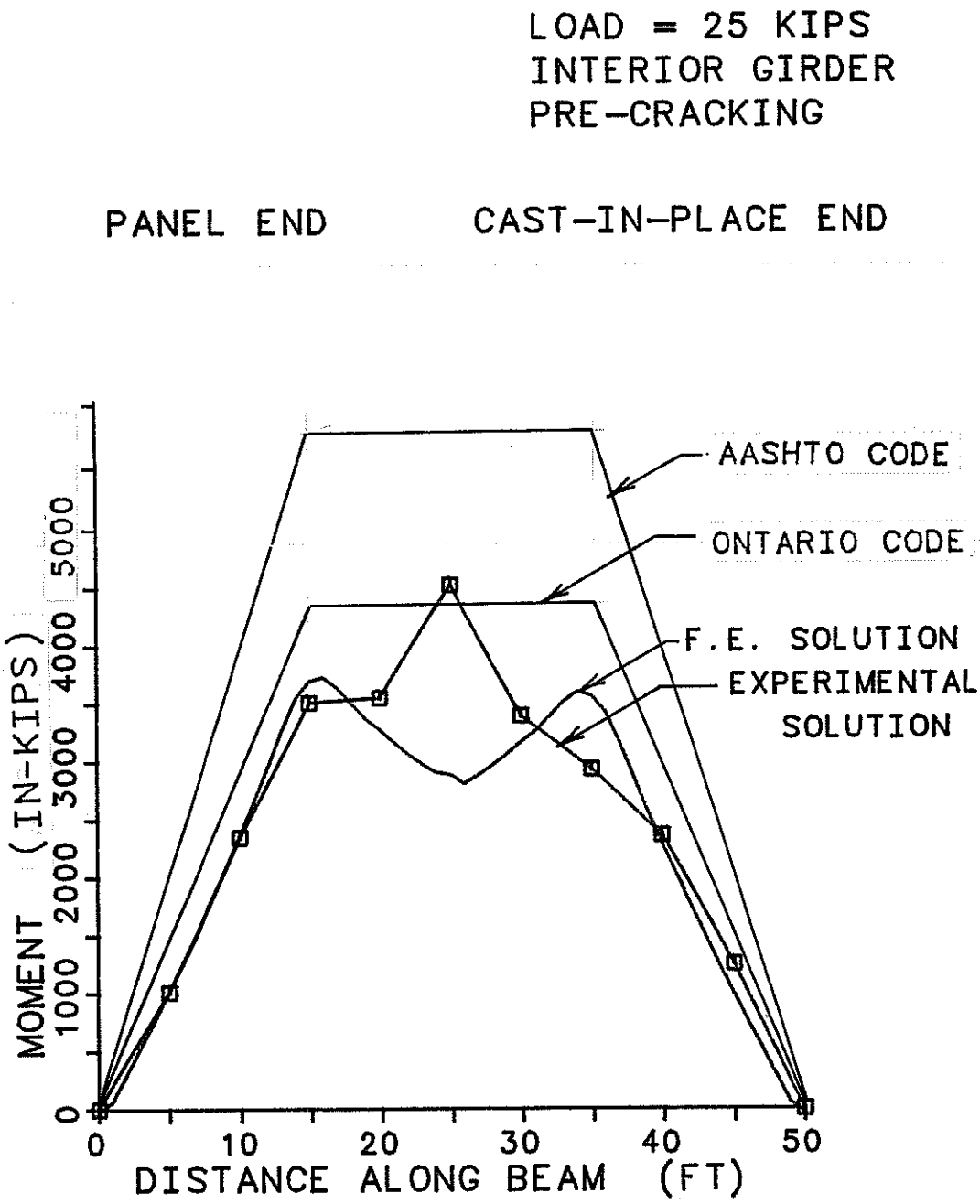

Fig. 5.2 Comparison of moment diagrams from experiment, AASHTO, Ontario Code, and finite element analysis (25 kips, interior girder, pre-cracking)

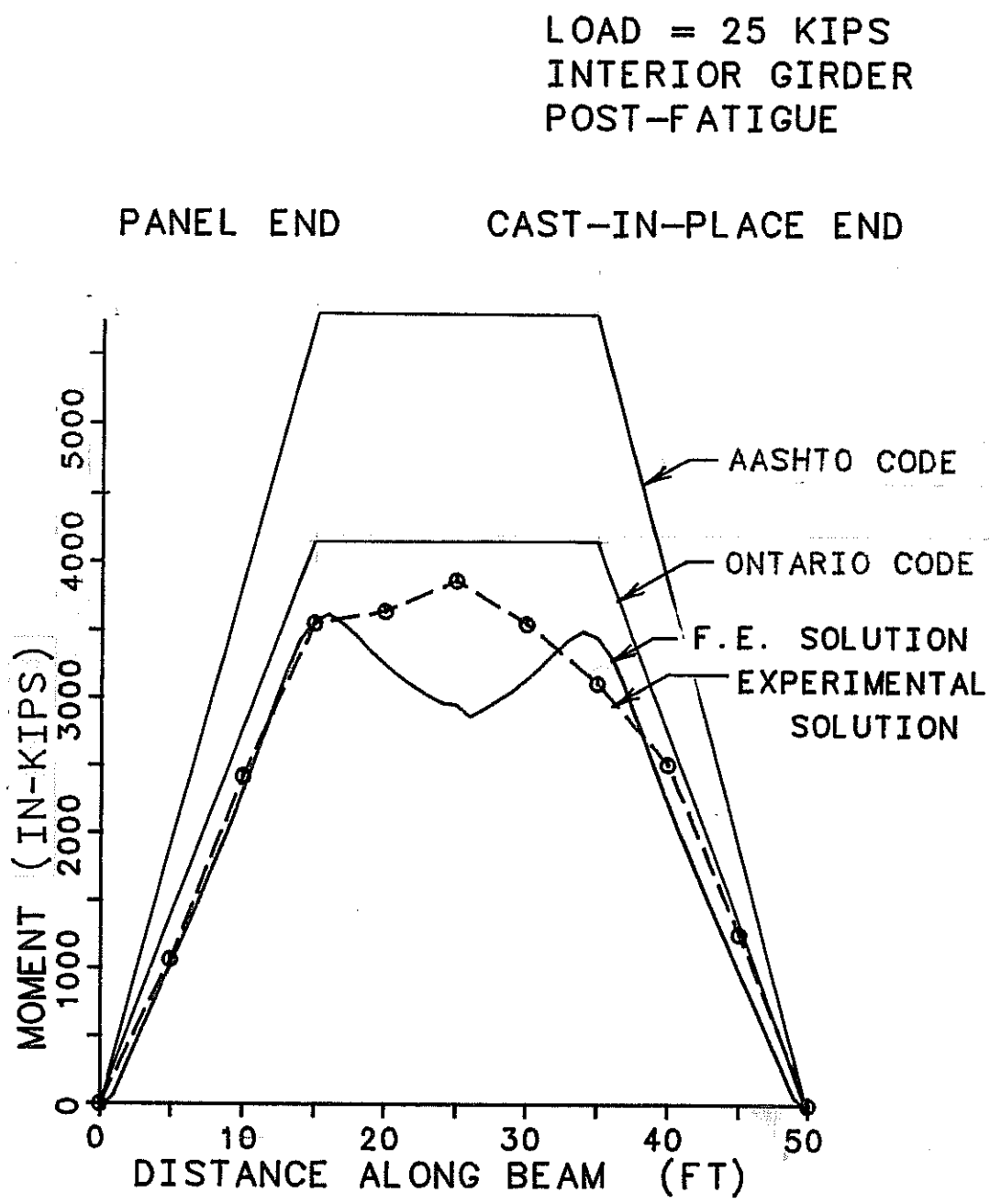

Fig. 5.3 Comparison of moment diagrams from experiment, AASHTO, Ontario Code, and finite element analysis (25 kips, interior girder, post-fatigue)

5.4 Moments from Finite Element Method

The laboratory specimen was modeled using the finite element method, which can closely approximate the actual solution for a wide range of structures with complex geometry, connectivity, and material characteristics.

The finite element model was developed as part of another investigation [46]. In this finite element model, two types of elements are used to model the composite bridge. The reinforced concrete deck is modeled by two layers of thick shell elements in order to follow the cracking of the deck at top and bottom surfaces. The steel girder is modeled by three-dimensional beam elements. The computer program used for this analysis, SAPIV [47], was designed for linear elastic analyses only, and its application to the nonlinear analysis of reinforced concrete was achieved using a sequential linear elastic technique. Cracking of the deck was modeled using a smeared cracking model [48].

The finite element program gave moments for the steel girders, but computation of overall longitudinal moments in the composite girders was difficult and time-consuming. Examination of the output from the finite element program showed that transverse sections through the steel girder and concrete deck remained plane under load. Because plane sections remained plane, composite girder moments were calculated from steel beam moments by multiplying the steel beam moments by the ratio of the flexural stiffness of the composite girders to the flexural stiffness of the steel beam.

Moments so obtained from the finite element model are shown in Figs. 5.2 and 5.3. The finite element moment diagrams follow the experimental diagrams in the outer two 15-ft sections of the bridge, nearest the supports. Adjacent to the loaded points, the finite element solution is still close to the experimental solution. In the middle 20 ft, however, between the loaded points, the peak finite element moments are 40 percent lower than the experimental values for the precracked case, and 28 percent lower after cracking. In this middle portion, the shape of the finite element solution also differs significantly from the experimental data.

The reasons for this are not clear. Other comparisons [46] showed that local finite element results agreed very well with experimental values. The most logical explanation is that the procedure used to calculate overall girder moments (multiplying steel beam moments by the ratio of overall girder EI to steel beam EI) was not sufficiently accurate in regions of the bridge subjected to higher local deformations under concentrated loads. While it might have been possible to use more precise procedures, this was not attempted due to lack of time, and because a more exact comparison was not essential to the scope of this study.

CHAPTER 6

SUMMARY AND CONCLUSIONS

6.1 Summary

The objectives of this thesis, given in Chapter 1, were as follows:

1. to measure the girder loads and bending moments in a full-scale bridge;

2. to compare the experimental girder bending moments with those predicted using some of the available analytical methods; and

3. based on this comparison, to assess the relative merits of the procedures studied.

Background material on refined and simplified methods for the analysis of bridge superstructures was presented in Chapter 2. Seven methods were briefly described: five refined methods and two simplified methods. An experimental test program for a slab and girder bridge was described in Chapter 3, and the test data were presented and discussed in Chapter 4. Although many plots and figures were described in Chapter 4, the test data were used primarily to obtain plots of the longitudinal moments (both pre-cracking and post-fatigue) for the center girder. In order to confirm the validity of the data reduction program, computed girder loads were compared with those actually applied. Other data, such as load-deflection or load-slip plots, were useful for checking purposes. The experimentally determined girder moments of Chapter 4 were compared with the moments obtained from the AASHTO Specifications, from the Ontario Highway Bridge Design Code, and from a finite element model of the bridge. These comparisons are presented in Chapter 5.

6.2 Conclusions

No method for determining girder design moments is clearly superior for all applications. Each has advantages and disadvantages.

One advantage of the experimental procedure is its accuracy. The error in girder moments (probably within 13 percent) was considered low enough to permit the use of the experimental moment diagrams as a basis against which to compare the other moment diagrams. A disadvantage of this approach, however, was the time and expense involved in testing

a full-scale model, and the difficulty in applying the laboratory results to other structures.

The finite element method is more suited for analysis than typical design. One advantage of the finite element method was that the predicted moments were very close to the experimental values for some regions along the girder. It is believed that more precise procedures for computing overall girder moments from finite element results would have given good accuracy for the entire girder span. A second advantage of the finite element method was its ability to predict the cracking behavior of the deck. Disadvantages included: the need to use a computer; the time required to develop a model; and the need for prior knowledge of member sizes and material properties.

The AASHTO load distribution method is a simplified design procedure which calculates girder design moments as though each girder were acting alone. As a result, the shape of the AASHTO-predicted moment diagram will not match the shape of the experimental diagram, and predicted peak moments can be expected to differ significantly from actual values. In the experiment described here, the peak moment value predicted by AASHTO was 80 percent higher than the experimental value (uncracked case). One advantage of the AASHTO load distribution method, however, is its speed. The load distribution fractions are simply read from a table. A second advantage is the fact that the designer does not have to know the relative stiffnesses of the bridge members. The only parameters needed for design are the beam type, the stringer spacing, and the number of lanes. The convenience of the AASHTO Code, and its long history of successful use in this country have led to general acceptance by U.S. highway designers.

Like the AASHTO Code, the Ontario Bridge Code provides a simplified method of design that determines the girder design moments assuming the girder to act alone. It can therefore be expected to show the same kinds of inaccuracies as the AASHTO procedure. The Ontario procedure attempts to offer the designer more precise moment estimates. For the bridge studied here, Ontario-predicted peak moments were 30 percent higher than experimental values. This prediction was not only much more accurate than that of AASHTO, it also compares favorably with the solution obtained using the finite element method. However, the Ontario Bridge Code has several disadvantages: 1) determination of girder moments required much more extensive calculations than needed for AASHTO; and 2) the designer had to know beforehand the relative stiffnesses of the girders and deck.

Accuracy should not be the only criterion by which these methods are judged. When predicted moments are used for design, the overall factor of safety of the resulting structure will depend on the accuracy of the analysis and the conservatism of the design, and also on the degree of indeterminacy and quality of construction of the

structure. Without looking at this total picture, it is not possible to define the desired degree of accuracy of a given method.

In assessing the proper role of these methods for estimating girder moments, it is important to recognize that each method has its place. A method such as AASHTO (or perhaps a simplification of the Ontario procedure) is necessary for preliminary design. After preliminary deck and girder sizes have been picked, a method such as the Ontario procedure can be used to produce a more efficient revised design. The finite element method appears advantageous primarily for checking local behavior.

6.3 Suggestions for Further Research

In the course of this experiment, a number of questions arose which were not directly within the scope of this thesis. While time was not available to answer them here, the author feels that the following issues deserve further study:

1. The behavior of the clip gages. In this and other related studies, clip gages (used here for detecting slip) showed erratic behavior at low strain levels. Ways of reducing this erratic behavior should be found, or the gages should be supplemented with surface strain gages.

2. Finite element girder moments. Different techniques should be investigated for calculating overall composite girder moments from the finite element output. Results achieved here (by multiplying by EI ratios) were reasonably successful, but less accurate than would have been expected based on other comparisons of finite element and experimental results.

3. Use of finite element procedures for design. Using parameter studies with finite element bridge models, it should be possible to develop design charts similar to, and perhaps more accurate than, those currently used in the Ontario Code.

4. Diaphragm behavior. It would be useful to know more about diaphragm behavior, in order to improve diaphragm design and detailing, and to prevent the early diaphragm failures observed in these tests.

5. Design procedures for other situations. It would be useful to conduct studies similar to this one on a bridge with continuous girders.

A P P E N D I X A

MATERIAL PROPERTIES

TABLE A.1 Concrete Mix Design for Cast-in-Place Deck

Design Strength:	3600 psi
Water-Cement Ratio:	0.485
Slump:	3 in.
Type I Cement:	0.36%
Water:	0.42%
Aggregate:	0.22%
Added Water:	0%
Admixture:	6% air entrained

TABLE A.2 Cast-in-Place Deck Properties

Concrete		
Cast date:		2/28/84
f_c:	14 day:	3510 psi
	28 day:	4240 psi
	180 day:	5160 psi
Slump:		3 in.
Steel		
Size:		#4
Grade:		60
Tested yield strength:		73 ksi

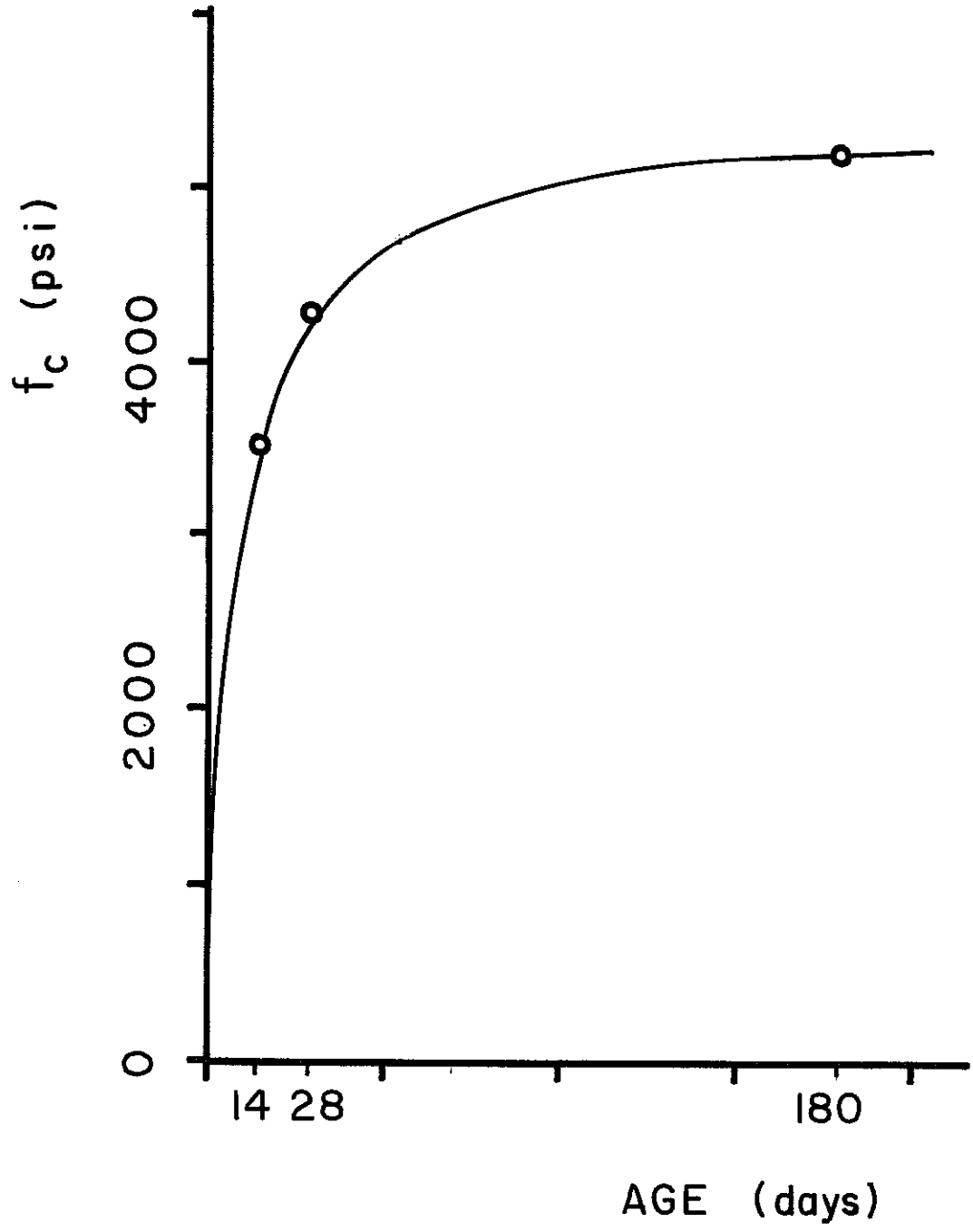

Fig. A.1 Strength vs. age for cast-in-place concrete

TABLE A.3 Precast, Prestressed Panel Properties

Concrete	
Release strength:	4000 psi
Design strength:	6000 psi
Type:	Texas Class H, Type III (high early strength) cement, 6-1/2 sacks/cu.yd.
Casting date:	2/2/84
f_c: 48 hr:	5104 psi
7 day:	6593 psi
Slump:	4 in.
Prestressing Steel:	
Size of strand:	3/8-in. diameter
Type:	7-wire
Grade:	270, stress relieved
Prestress force per strand:	16.1 kips

TABLE A.4 Seven-Day Modulus of Rupture Data

Beam No.	Breaking Load P (lbs)	Modulus of Rupture (psi)
1	3465	433
2	3470	434
3	4050	506
4	3890	486
5	2880	360
6	3080	385
7	3040	380
8	3580	448
9	3700	463

Average: 433 psi
S.D.: 49.6 psi

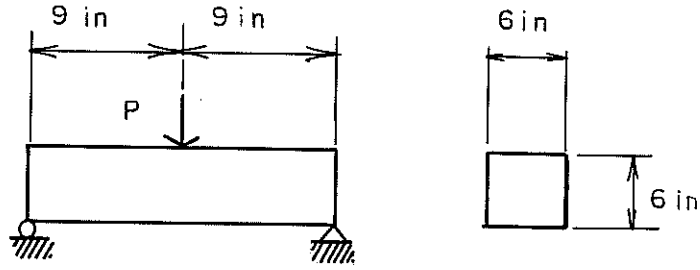

$$f_t = M_y/I = ((18P/4)3)/(6^4/12) = P/8 \text{ (psi)}$$

A P P E N D I X B

LOAD VS. SLIP PLOTS

STRAIN GAGE 9

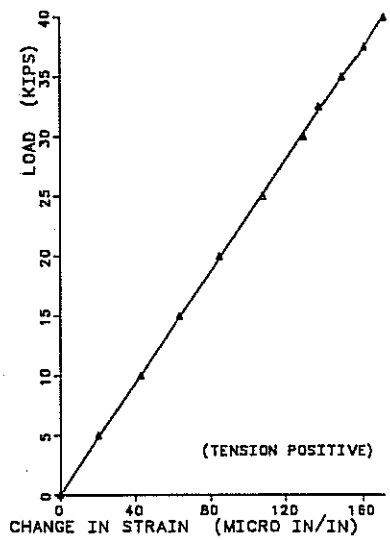

STRAIN GAGE 10

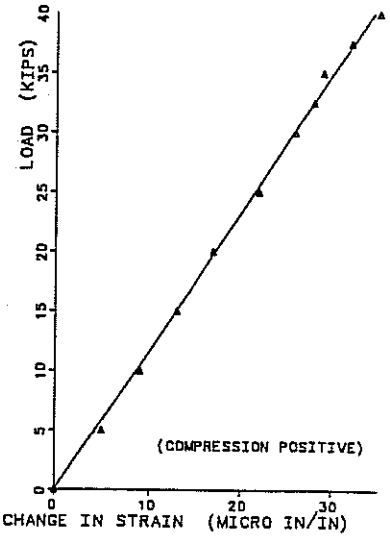

STRAIN GAGE 11

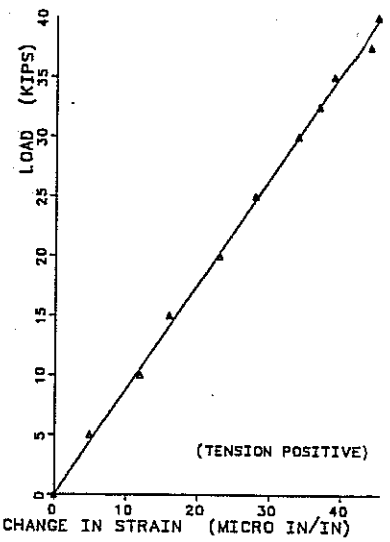

STRAIN GAGE 12

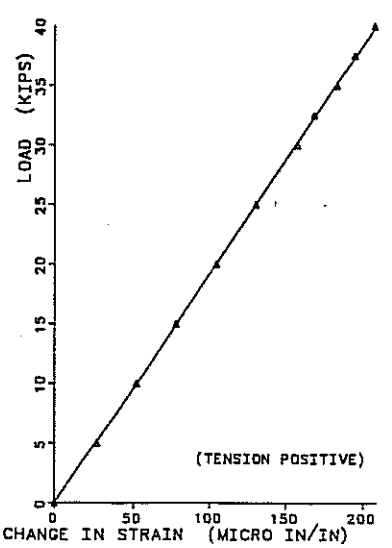

STRAIN GAGE 13

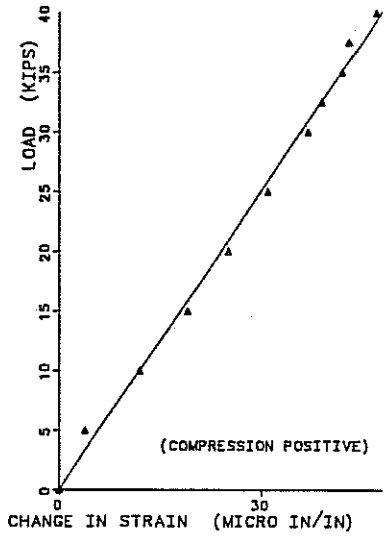

STRAIN GAGE 14

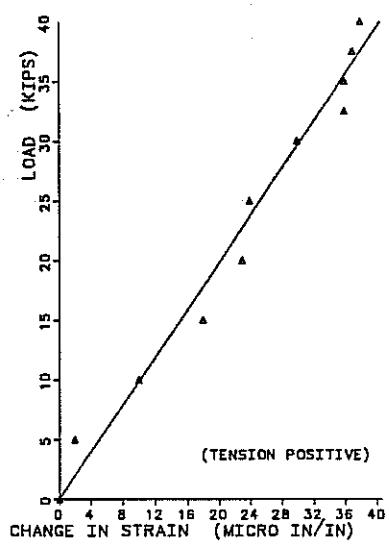

STRAIN GAGE 15

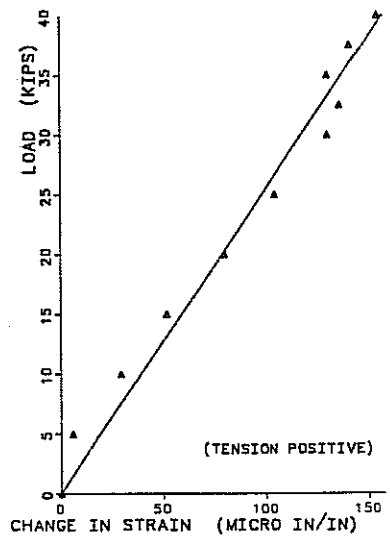

STRAIN GAGE 16

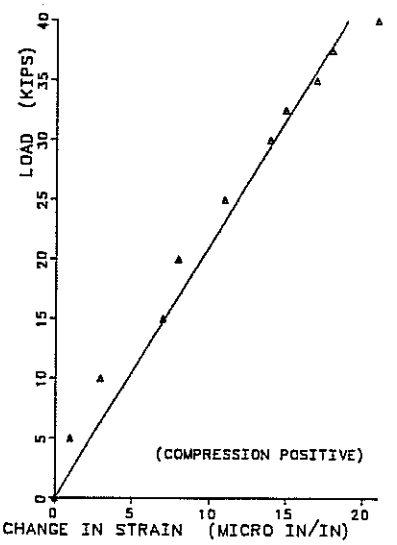

STRAIN GAGE 17

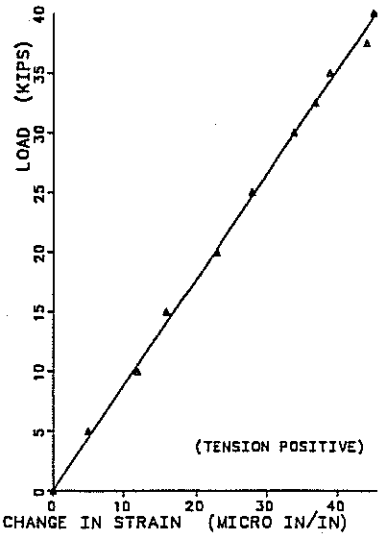

STRAIN GAGE 18

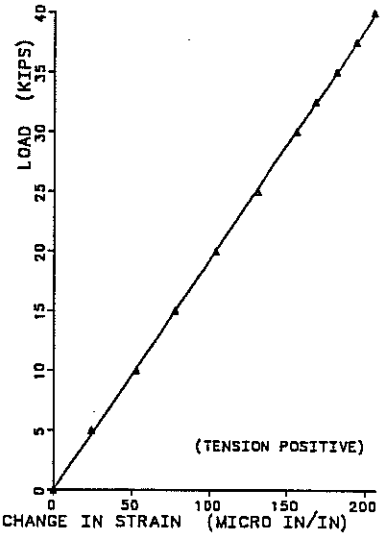

STRAIN GAGE 19

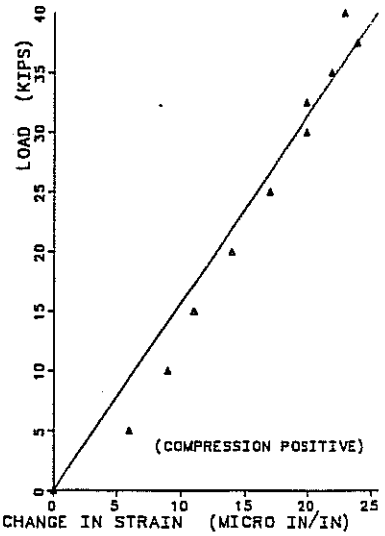

STRAIN GAGE 20

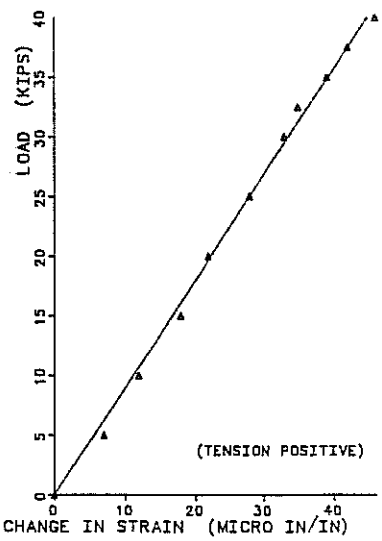

STRAIN GAGE 21

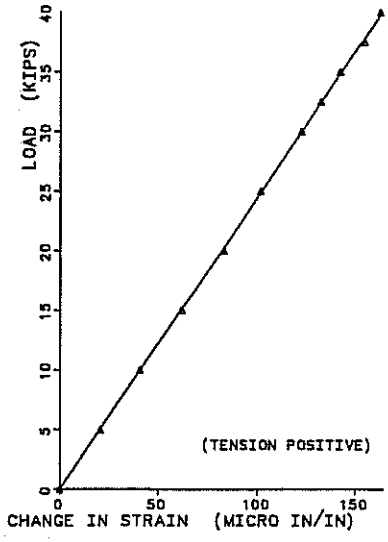

STRAIN GAGE 22

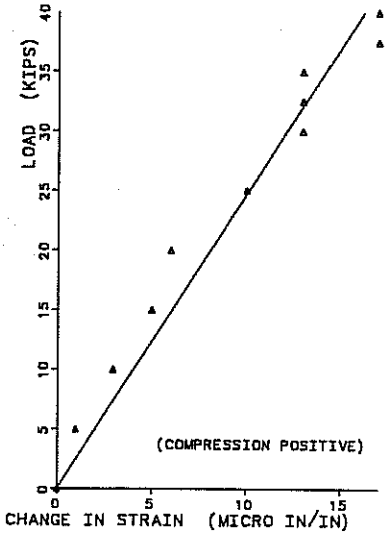

STRAIN GAGE 23

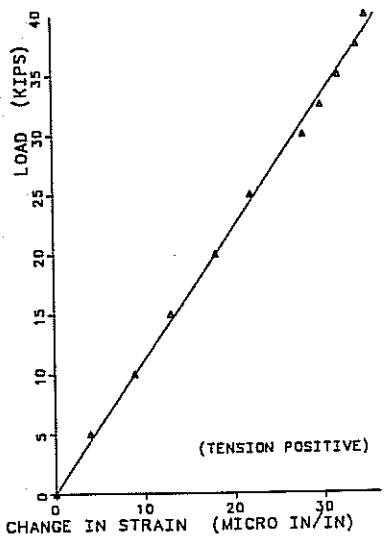

STRAIN GAGE 24

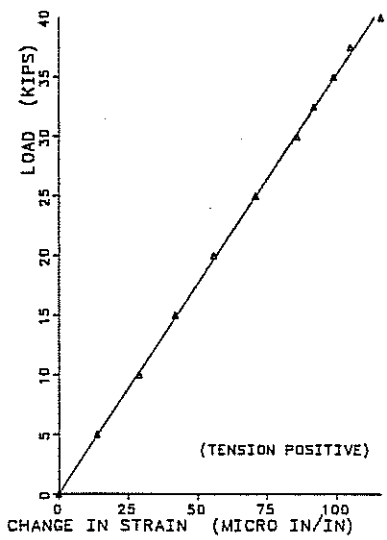

STRAIN GAGE 25

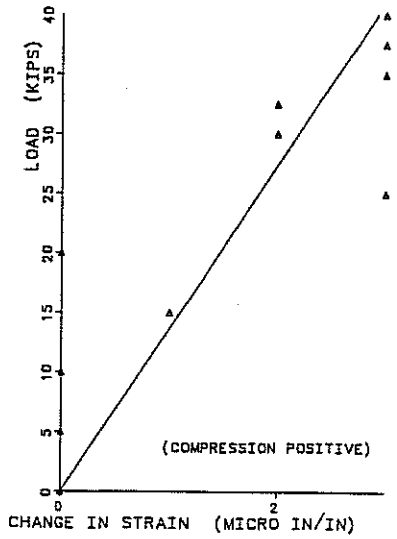

STRAIN GAGE 26

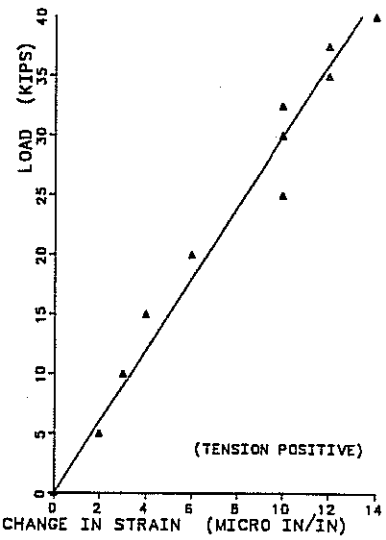

STRAIN GAGE 27

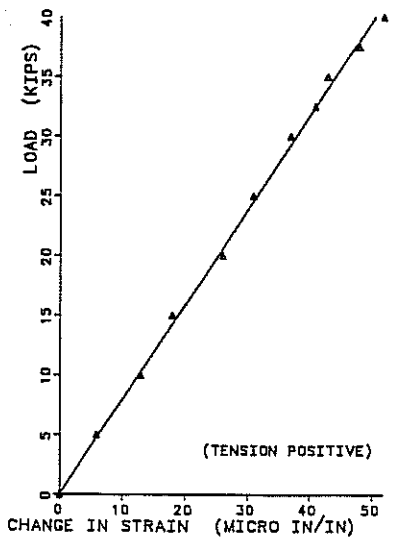

STRAIN GAGE 28

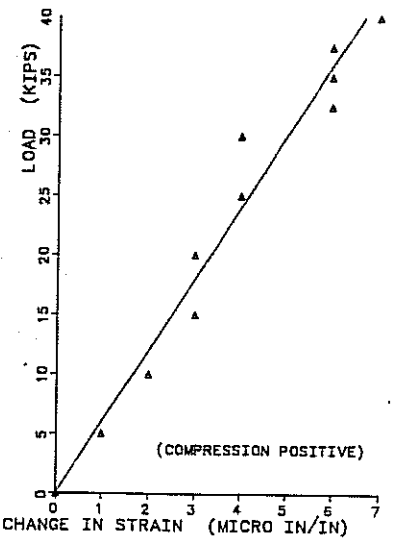

STRAIN GAGE 29

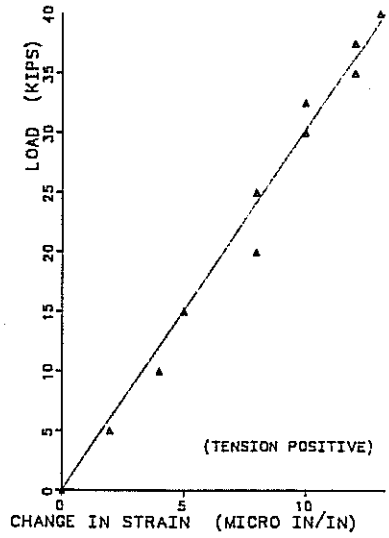

STRAIN GAGE 30

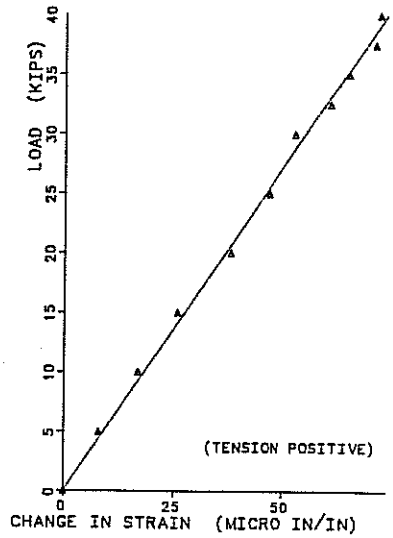

STRAIN GAGE 31

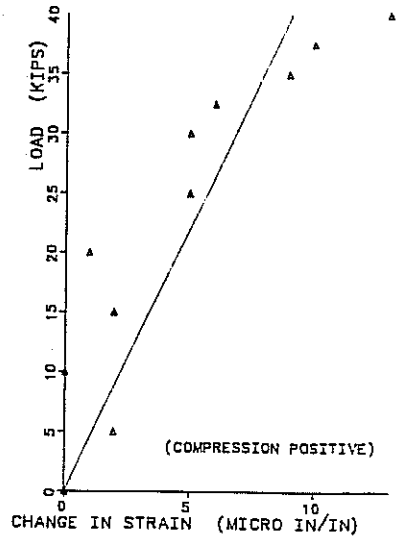

STRAIN GAGE 32

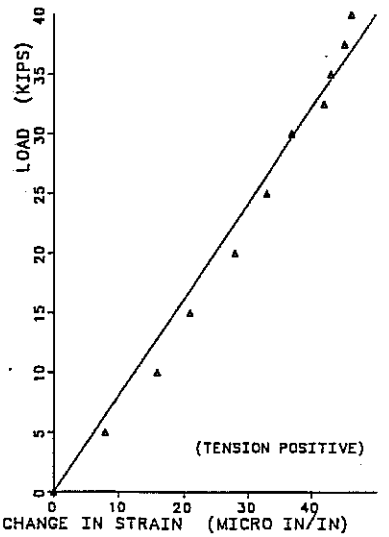

STRAIN GAGE 33

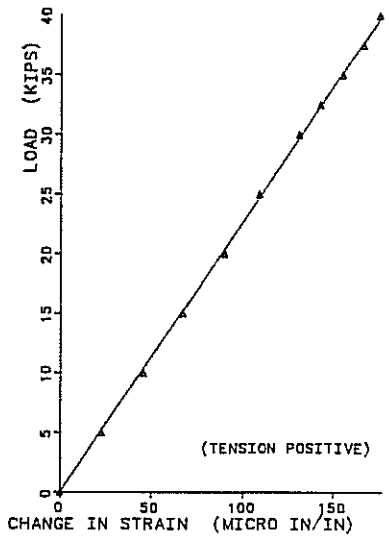

STRAIN GAGE 34

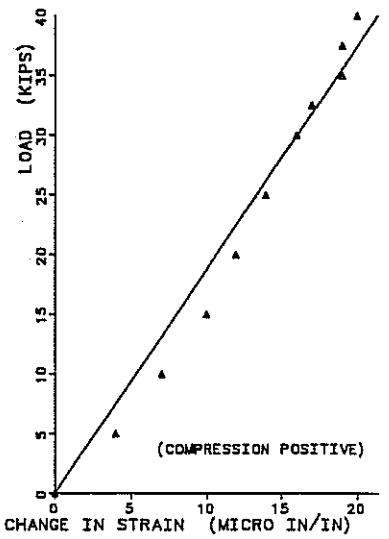

STRAIN GAGE 35

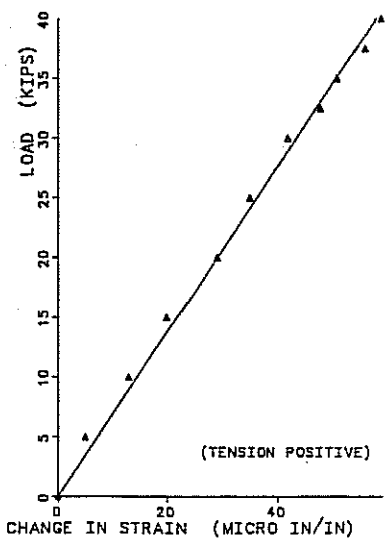

STRAIN GAGE 36

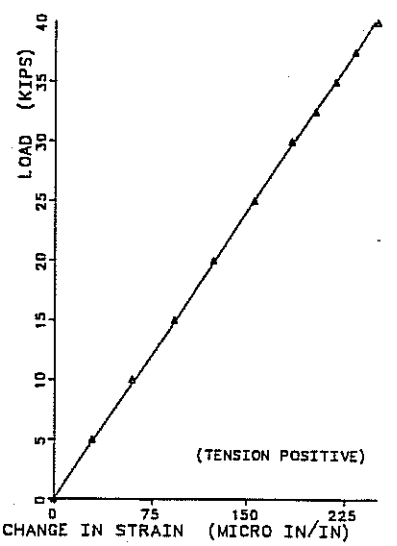

STRAIN GAGE 37

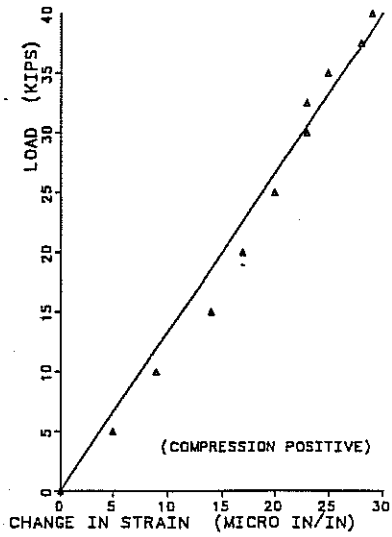

STRAIN GAGE 38

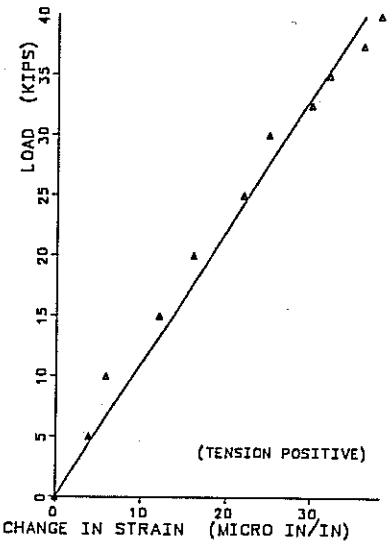

STRAIN GAGE 39

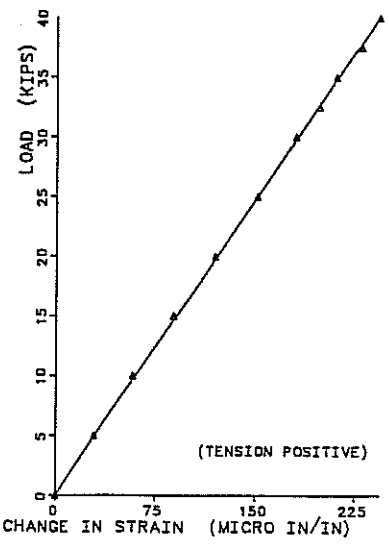

STRAIN GAGE 40

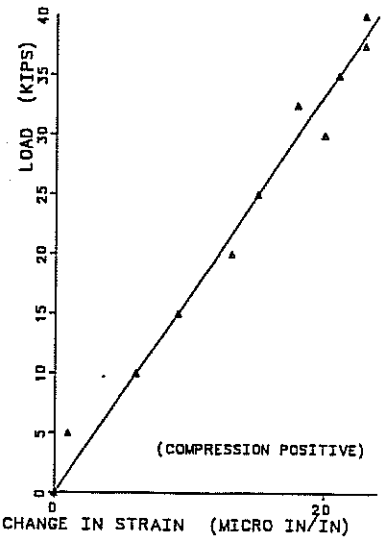

STRAIN GAGE 41

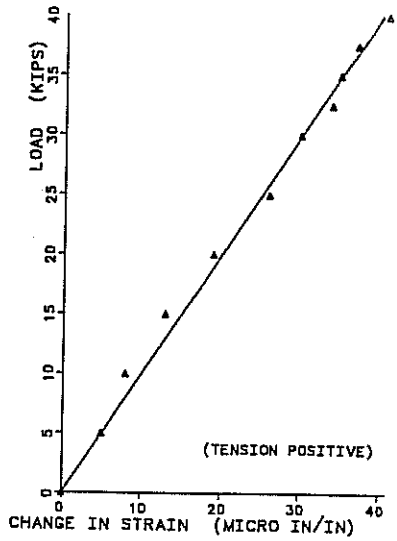

STRAIN GAGE 42

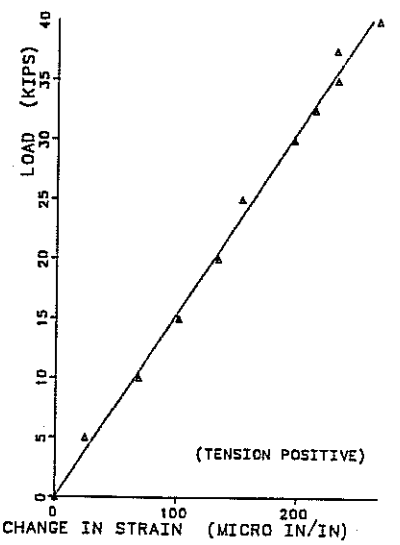

STRAIN GAGE 43

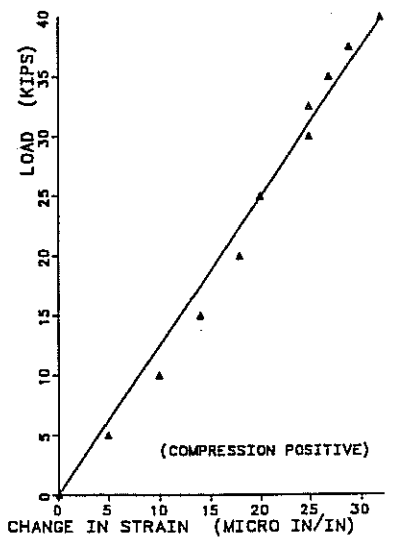

STRAIN GAGE 44

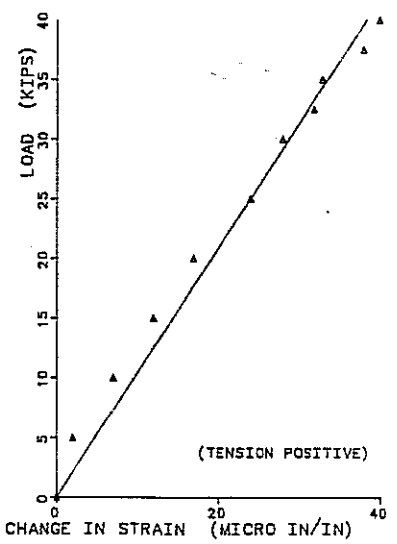

STRAIN GAGE 45

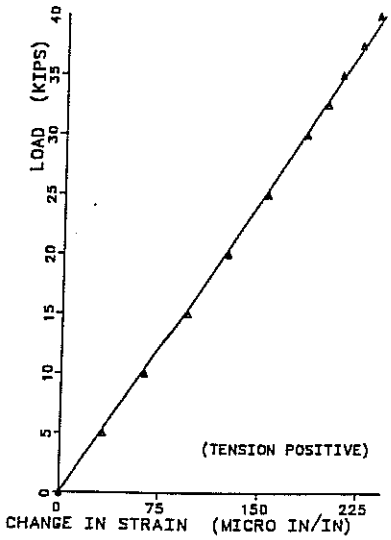

STRAIN GAGE 46

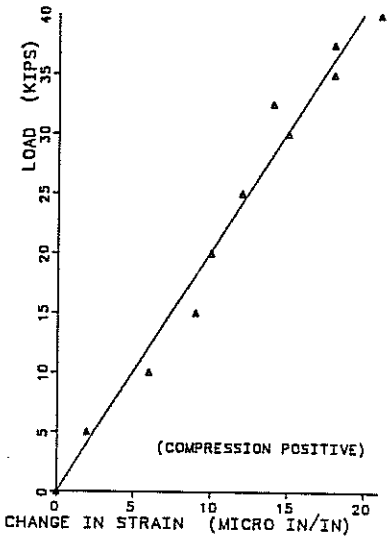

STRAIN GAGE 47

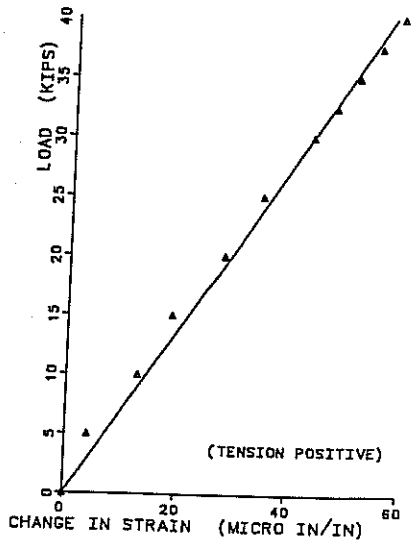

STRAIN GAGE 48

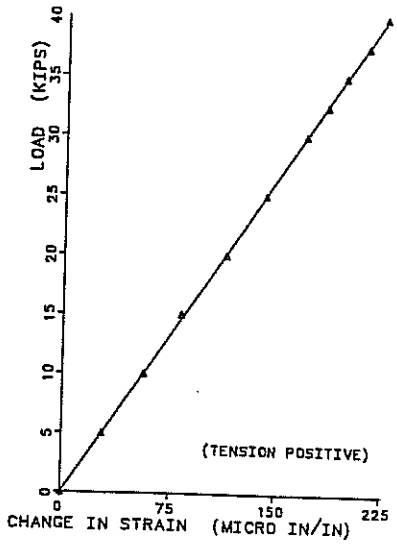

STRAIN GAGE 49

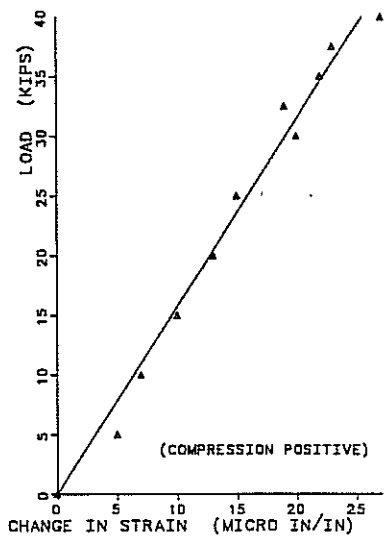

STRAIN GAGE 50

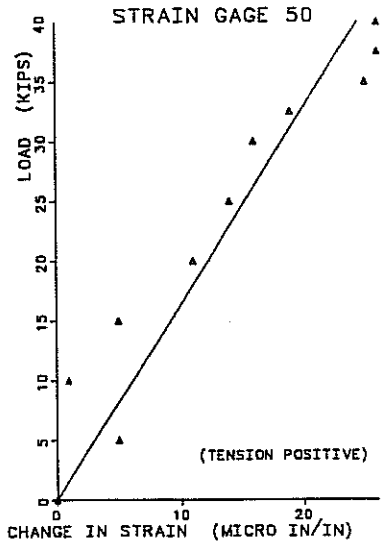

STRAIN GAGE 51

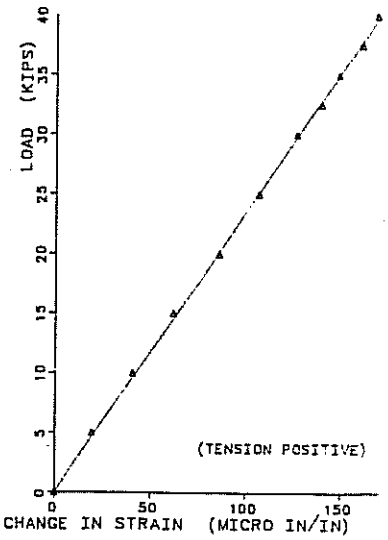

STRAIN GAGE 52

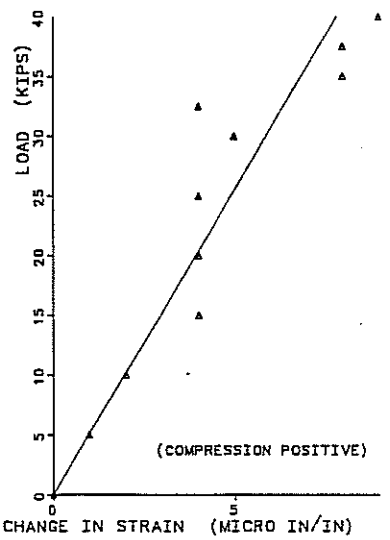

STRAIN GAGE 53

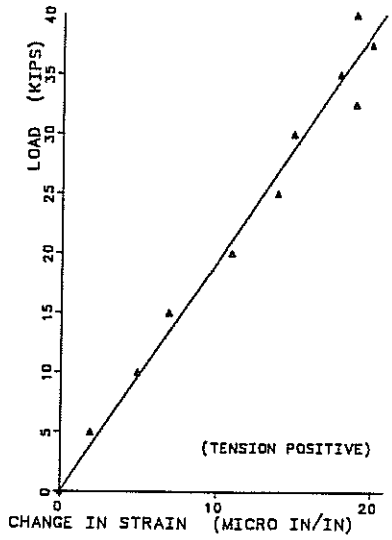

STRAIN GAGE 54

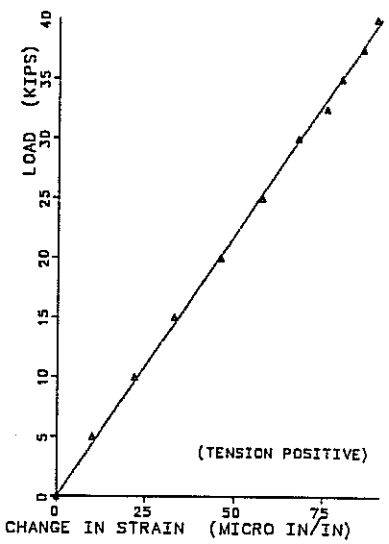

A P P E N D I X E

STRAIN GRADIENT DIAGRAMS

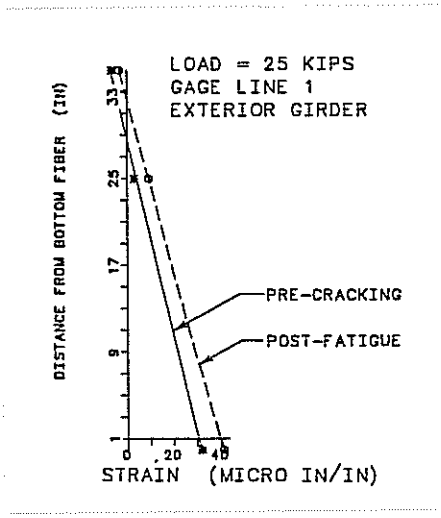
LOAD = 25 KIPS
GAGE LINE 1
EXTERIOR GIRDER
PRE-CRACKING
POST-FATIGUE
DISTANCE FROM BOTTOM FIBER (IN)
STRAIN (MICRO IN/IN)

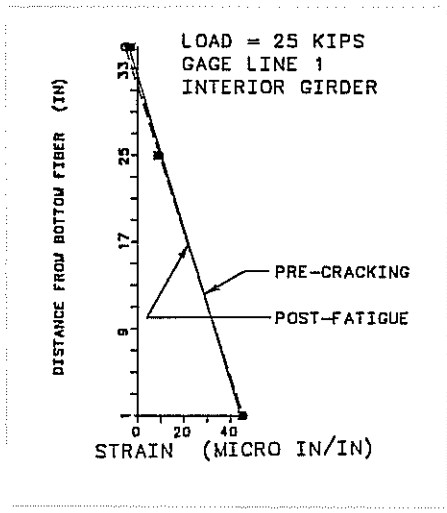
LOAD = 25 KIPS
GAGE LINE 1
INTERIOR GIRDER
PRE-CRACKING
POST-FATIGUE
DISTANCE FROM BOTTOM FIBER (IN)
STRAIN (MICRO IN/IN)

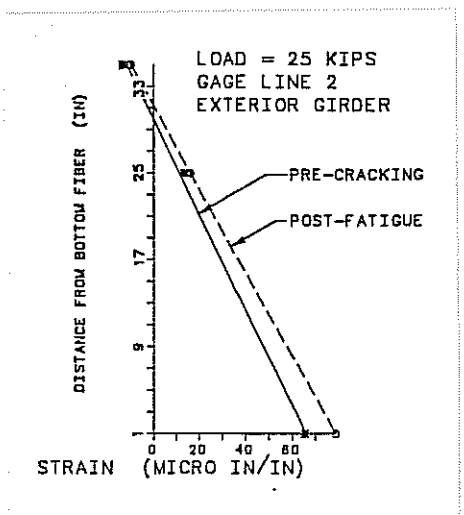
LOAD = 25 KIPS
GAGE LINE 2
EXTERIOR GIRDER
PRE-CRACKING
POST-FATIGUE
DISTANCE FROM BOTTOM FIBER (IN)
STRAIN (MICRO IN/IN)

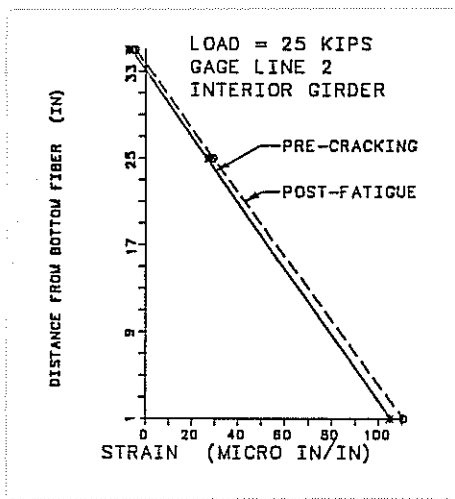
LOAD = 25 KIPS
GAGE LINE 2
INTERIOR GIRDER
PRE-CRACKING
POST-FATIGUE
DISTANCE FROM BOTTOM FIBER (IN)
STRAIN (MICRO IN/IN)

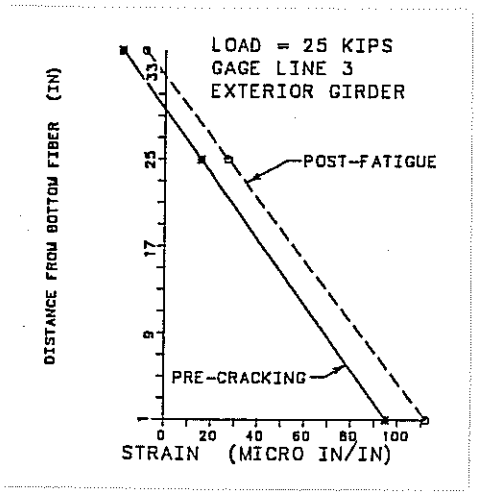
LOAD = 25 KIPS
GAGE LINE 3
EXTERIOR GIRDER
POST-FATIGUE
PRE-CRACKING
DISTANCE FROM BOTTOM FIBER (IN)
STRAIN (MICRO IN/IN)

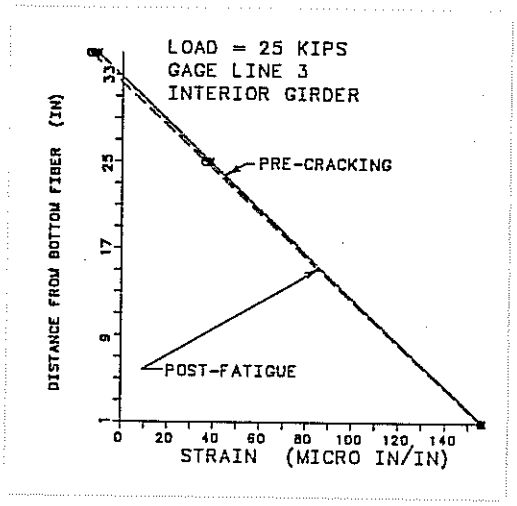
LOAD = 25 KIPS
GAGE LINE 3
INTERIOR GIRDER
PRE-CRACKING
POST-FATIGUE
DISTANCE FROM BOTTOM FIBER (IN)
STRAIN (MICRO IN/IN)

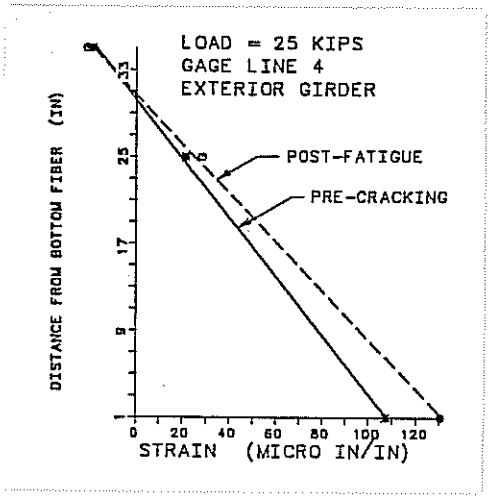
LOAD = 25 KIPS
GAGE LINE 4
EXTERIOR GIRDER
POST-FATIGUE
PRE-CRACKING
DISTANCE FROM BOTTOM FIBER (IN)
STRAIN (MICRO IN/IN)

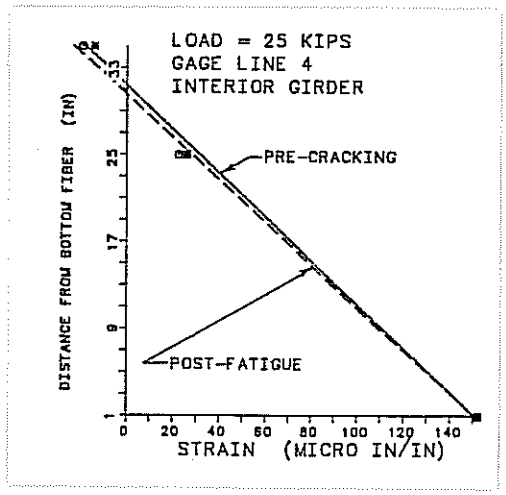
LOAD = 25 KIPS
GAGE LINE 4
INTERIOR GIRDER
PRE-CRACKING
POST-FATIGUE
DISTANCE FROM BOTTOM FIBER (IN)
STRAIN (MICRO IN/IN)

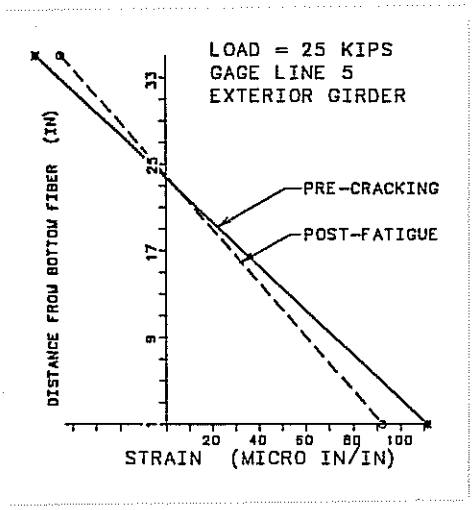
LOAD = 25 KIPS
GAGE LINE 5
EXTERIOR GIRDER
PRE-CRACKING
POST-FATIGUE
DISTANCE FROM BOTTOM FIBER (IN)
STRAIN (MICRO IN/IN)

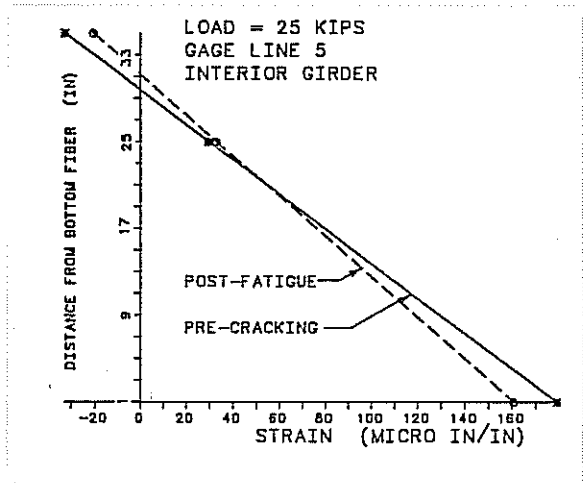
LOAD = 25 KIPS
GAGE LINE 5
INTERIOR GIRDER
POST-FATIGUE
PRE-CRACKING
DISTANCE FROM BOTTOM FIBER (IN)
STRAIN (MICRO IN/IN)

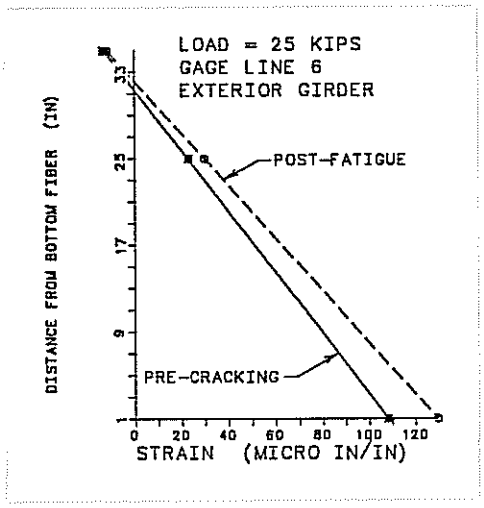
LOAD = 25 KIPS
GAGE LINE 6
EXTERIOR GIRDER
POST-FATIGUE
PRE-CRACKING
DISTANCE FROM BOTTOM FIBER (IN)
STRAIN (MICRO IN/IN)

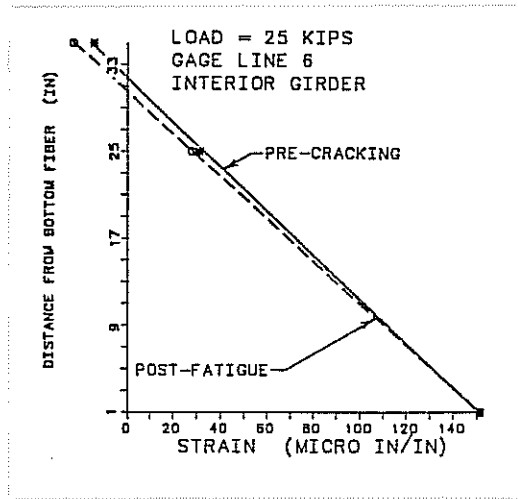
LOAD = 25 KIPS
GAGE LINE 6
INTERIOR GIRDER
PRE-CRACKING
POST-FATIGUE
DISTANCE FROM BOTTOM FIBER (IN)
STRAIN (MICRO IN/IN)

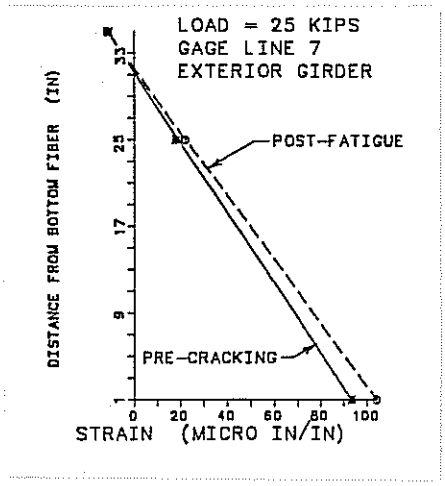
LOAD = 25 KIPS
GAGE LINE 7
EXTERIOR GIRDER
POST-FATIGUE
PRE-CRACKING
DISTANCE FROM BOTTOM FIBER (IN)
STRAIN (MICRO IN/IN)

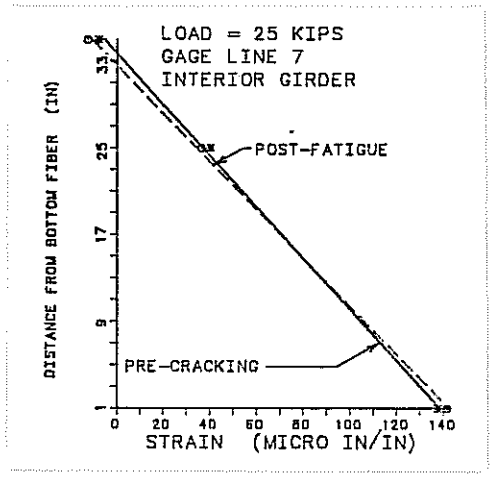
LOAD = 25 KIPS
GAGE LINE 7
INTERIOR GIRDER
POST-FATIGUE
PRE-CRACKING
DISTANCE FROM BOTTOM FIBER (IN)
STRAIN (MICRO IN/IN)

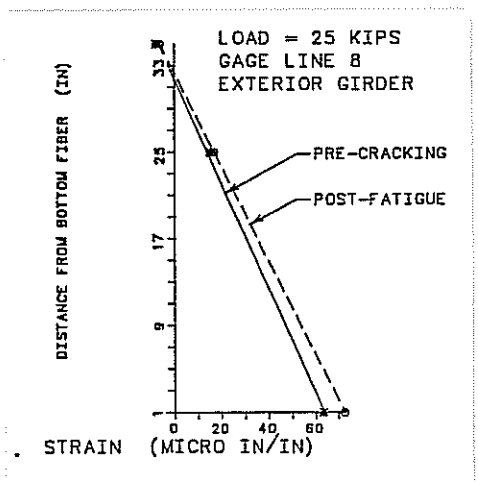
LOAD = 25 KIPS
GAGE LINE 8
EXTERIOR GIRDER
PRE-CRACKING
POST-FATIGUE
DISTANCE FROM BOTTOM FIBER (IN)
STRAIN (MICRO IN/IN)

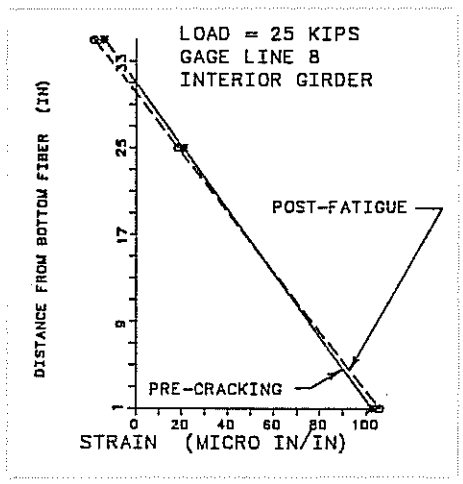
LOAD = 25 KIPS
GAGE LINE 8
INTERIOR GIRDER
POST-FATIGUE
PRE-CRACKING
DISTANCE FROM BOTTOM FIBER (IN)
STRAIN (MICRO IN/IN)

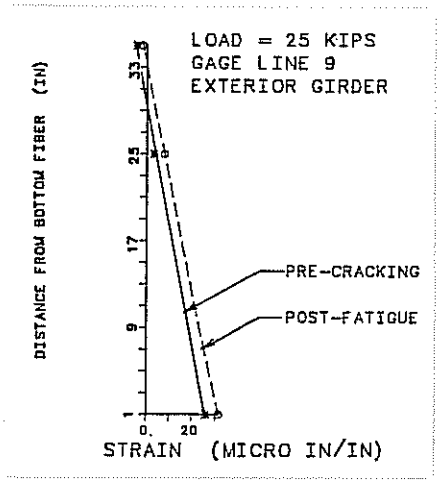
LOAD = 25 KIPS
GAGE LINE 9
EXTERIOR GIRDER
DISTANCE FROM BOTTOM FIBER (IN)
33
25
17
9
1
0
20
PRE-CRACKING
POST-FATIGUE
STRAIN (MICRO IN/IN)

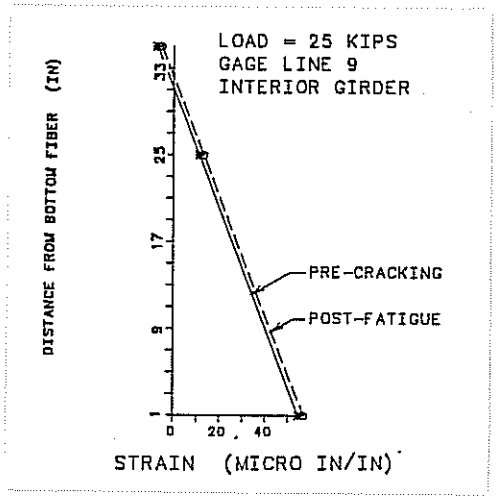
LOAD = 25 KIPS
GAGE LINE 9
INTERIOR GIRDER
DISTANCE FROM BOTTOM FIBER (IN)
33
25
17
9
1
0
20
40
PRE-CRACKING
POST-FATIGUE
STRAIN (MICRO IN/IN)

A P P E N D I X F

CALCULATIONS FOR DETERMINING GIRDER DESIGN MOMENTS

BY THE ONTARIO BRIDGE CODE

CALCULATIONS FOR INTERIOR GIRDER OF HIGHWAY BRIDGE MODEL

The design procedure for calculating the moments in the interior girder of the laboratory specimen according to the Ontario Highway Bridge Design Code [2] are shown below. The notation used is listed at the end of this appendix, and is taken directly from Ref. 2.

The first step in the Ontario procedure is to calculate the parameter Dx for the interior girder:

$$D_x = EI \;/\; \text{beam spacing}$$

$$D_x = (E \cdot (25{,}000 \text{ in.}^4) \cdot (3 \text{ beams}) \cdot (2.54 \text{ cm/in.})^4) \;/\; 213.4 \text{ cm}$$

$$D_x = 14{,}630 \cdot E \text{ cm}^4$$

D is then calculated as:

$$D_y = (E \times (\text{slab thickness})^3) \;/\; 12$$

$$D_y = (E\ (19.05 \text{ cm})^3) \;/\; 12$$

$$D_y = 576 \cdot E$$

Neglecting the contribution of the steel beam to the torsional moment of inertia:

$$D_{xy} = D_{yx} = (G\ (\text{slab thickness})^3) \;/\; 6$$

$$D_{xy} = (E \times (19.05)^3) \;/\; (2 \cdot (1 + 0.15) \cdot 6)$$

$$D_{xy} = 501 \cdot E$$

$$D_1 = D_2 = \nu \times (\text{lesser of } D_x \text{ and } D_y)$$

$$D_1 = 0.15\ (576 \cdot E)$$

$$D_1 = 86 \cdot E$$

The parameters α and θ are then calculated as:

$$\alpha = (D_{xy} + D_{yx} + D_1 + D_2) \; / \; (2 \times (D_x \cdot D_y)^{0.5})$$

$$\alpha = ((501 + 501 + 86 + 86) \cdot E) \; / \; (2((14{,}630 \cdot E) \cdot (576E))^{0.5})$$

$$\alpha = 0.202$$

$$\theta = b/L \; (D_x/D_y)^{0.25}$$

$$\theta = 305\text{cm}/1524\text{cm} \; ((14{,}530 \cdot E)/(576 \cdot E)^{0.25}$$

$$\theta = 0.449$$

With $\alpha = 0.202$ and $\theta = 0.449$, the values of D and C_t can be read from Fig. 3.7.1.2.2(b) of Ref. 2 (Fig. F.1):

$$D = 2.35$$

$$C_t = 9.0$$

The width of a design lane is calculated as:

$$W_e = W_c/n$$

$$W_e = 6.10\text{m}/2$$

$$W_e = 3.05\text{m}$$

The value of μ is calculated as:

$$\mu = (W_e - 3.3)/0.6 \leq 1.0$$

$$\mu = (3.05 - 3.3)/0.6$$

$$\mu = -0.417$$

The Ontario load distribution factor, which is analogous to the value 5.5 from the AASHTO Specifications, is calculated as:

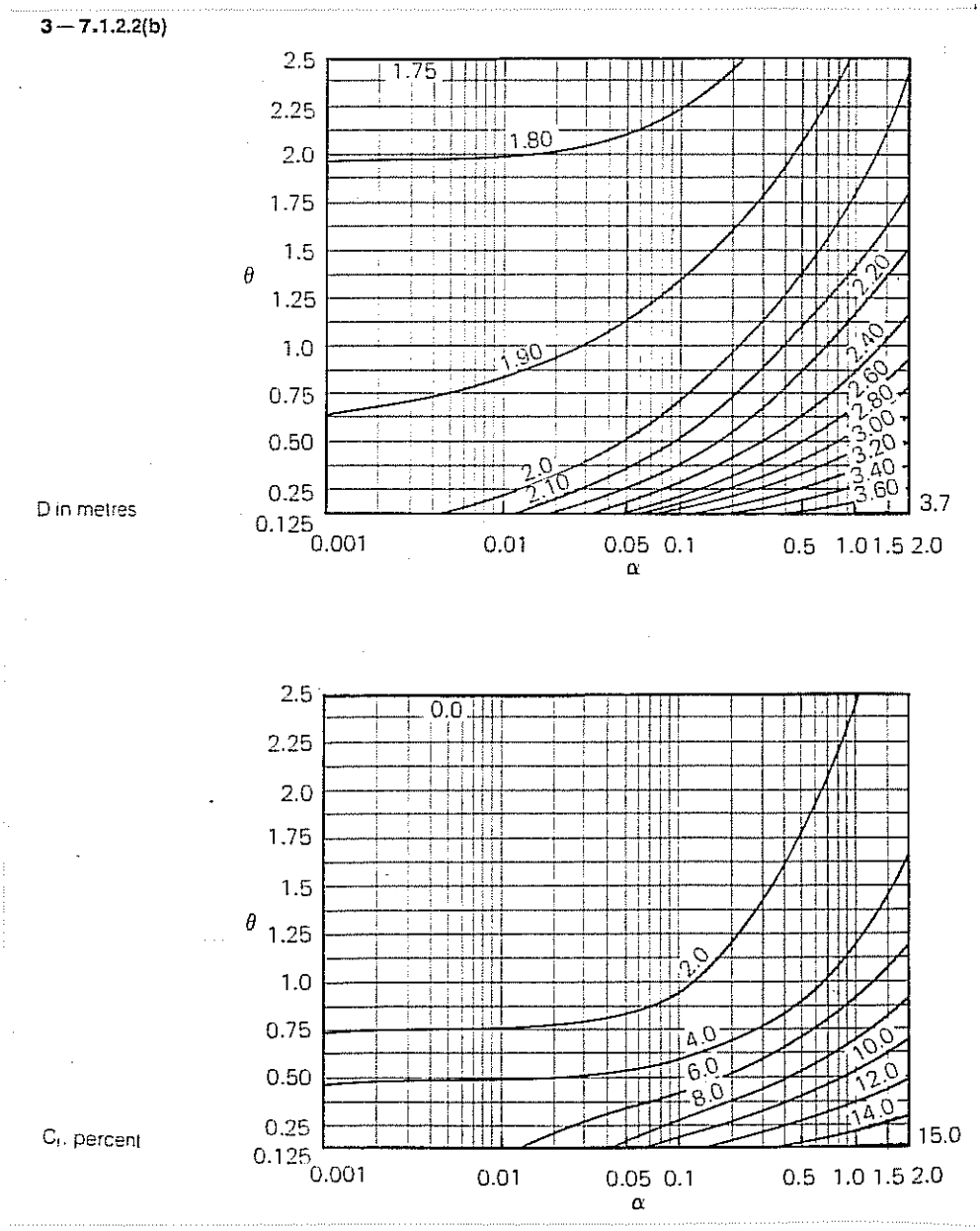

Fig. F.1 Charts for C and D (Fig. 3-7.1.2.2(b) Ref. [2])

$$D_d = D\ (1 + (\mu C_t/100))$$

$$D_d = 2.35\ (1 - (0.417\ (9)/100))$$

$$D_d = 2.26\ m$$

$$D_d = 7.41\ ft\ (3.280\ ft = 1\ in.)$$

According to the Ontario Code, the design moment for the center girder is then:

$$\text{Design moment} = P\ (15\ ft)\ (S/C)$$

$$= 25\ k\ (15\ ft)\ (7.0/7.41)\ 12$$

$$= 4230\ in.\text{-}k$$

The following notation is used in the calculation of girder design moments by the Ontario Bridge Code:

C_1 a correction factor used to adjust the D value for longitudinal moment and longitudinal shear

D the load distribution factor

D_d the load distribution factor modified for design

D_1 the coupling rigidity per unit width

D_2 the coupling rigidity per unit length

D_x the longitudinal flexural rigidity per unit width

D_{xy} the longitudinal torsional rigidity per unit width

D_y the transverse flexural rigidity per unit length

D_{yx} the transverse torsional rigidity per unit length

E the modulus of elasticity

G the shear modulus

L the span of a bridge

W_c the bridge deck width, m

W_e the width of a design lane, m

b the half-width of a bridge

α torsional parameter = $(D_{xy} + D_{yx} + D_1 + D_2)/2([D_x D_y]^{0.5}$

θ a flexural parameter = $(b/L)\ [D_x/D_y]^{0.25}$

μ $(W_e - 3.3)/0.6 > 1.0$

ν Poisson's ratio

REFERENCES

1. Standard Specification for Highway Bridges, Thirteenth Edition, American Association of State Highway and Transportation Officials, Washington, D.C., 1984.

2. Ontario Highway Bridge Design Code and Commentary, Second Edition, Ontario Ministry of Transportation and Communication, Ontario, Canada, 1983.

3. Burns, N.H., and Klingner, R.E., "Research Study Proposal, Project 3-5-83-350 to Texas Department of Highways and Public Transportation from Center for Transportation Research, The University of Texas at Austin," 1982, pp. 1-14.

4. Chu, Kuang-Han, and Krishnamoorthy, C., "Bridge Analysis Using Orthotropic Plate Theory," Journal of the Structural Division, ASCE, February 1968.

5. Cusens, A.R., and Pama, R.P., "Distribution of Concentrated Loads on Orthotropic Bridge Decks," The Structural Engineer, September 1969.

6. Heins, C.P., and Looney, C.T.C., "Bridge Analysis Using Orthotropic Plate Theory," Journal of the Structural Division, ASCE, February 1968.

7. Hendry, A.W., and Jaeger, L.B., "The Analysis of Interconnected Bridge Girders by the Distribution of Harmonics," Structural Engineer, Vol. 34, No. 7, 1956, pp. 241-266.

8. Jaeger, L.G., and Bakht, B., "The Grillage Analogy in Bridge Analysis," Canadian Journal of Civil Engineering, Vol, 9, No. 3, 1982.

9. Sawko, F., and Mosley, W.H., "Grillage Analysis of Composite Box Girder Bridge Decks," Civil Engineering (London), Vol. 64, No. 759, October 1969.

10. West, R., "The Use of Grillage Analogy for the Analysis of Slab and Pseudo-Slab Bridge Decks," Research Report 21, Cement and Concrete Association, London, England, 1973.

11. Hambly, E.C., and Pannels, E., "Grillage Analysis Applied to Cellular Bridge Decks," The Structural Engineer, July 1975.

12. Zienkiewicz, O.C., and Cheung, Y.K., "The Finite Element Method for Analysis of Elastic Isotropic and Orthotropic Slabs," Proc. Instn. Civil Engr., August 1964.

13. Moore, T.A., and Can, A.G., "Finite Element Analysis of Box and Plate Girder Bridges," Proc. of the International Conference of Finite Element Methods in Engineering, December 6-8, 1976.

14. Davies, J.D., Somerville, I.J., and Zienkiewicz, O.C., "Analysis of Various Types of Bridges by the Finite Element Method," Proc. Conference on Developments in Bridge Design and Construction, Cardiff, March-April 1971, Crossby Lockwood, London.

15. Cheung, M.S., and Cheung, Y.K., "Analysis of Curved Box Girder Bridges by Finite Strip Method," IABSE Publications, Vol. 31-1, Zurich, June 1971.

16. Loo, Y.C., and Cusens, A.R., "Development of the Finite Strip Method in the Analysis of Bridge Decks," Proc. Conference on Developments in Bridge Design and Construction, Cardiff, 1971, Crossby Lockwood, London.

17. Cheung, M.S., Cheung, Y.K., and Ghali, A., "Analysis of Slab and Girder Bridges by the Finite Strip Method," Building Science, 5, p. 95, 1970.

18. Scordelis, A.C., "A Matric Formulation of the Folded Plate Equations," Journal of the Structural Division, ASCE, ST-10, October 1960.

19. Scordelis, A.C., "Analysis of Continuous Box Girder Bridges," University of California, Berkeley, Structural Engineering and Structural Mechanics, No. SESM 6.7-5, November 1967.

20. Evans, H.R., and Rockley, K.C., "A Folded Plate Approach to the Analysis of Box Girders," Proc. Conference on Developments in Bridge Design and Construction, Cardiff, 1971, Crossby Lockwood, London.

21. Timoshenko, S., and Woinowsky-Kreiger, S., Theory of Plates and Shells (Engineering Society Monographs), 2nd Edition, McGraw-Hill, New York, 1959.

22. Guyon, Y., "Calcul des ponts larges a poritres multiples solidarisees par des entretoises," Annales des Ponts et Chaussees, No. 24, September-October 1946.

23. Guyon, Y., "Calcul des ponts dalls," Annales des Ponts et Chaussees, Vol. 119, No. 29, 1949.

24. Massonnet, C., "Methode de calcul des ponts a poutres multiples tenant compte de leur resistance a la torsion," (Methods of Calculation of Bridges with Several Longitudinal Beams, Taking into Consideration Their Torsional Resistance), Zurich, International Association for Bridge and Structural Engineering, Publications Vol. 10, 1950.

25. Leyendecker, E.V., and Breen, J.E., "Behavior of Concrete Slab and Girder Bridges," Research Report 94-3F, Center for Transportation Research, The University of Texas at Austin, May 1969.

26. Mouce, P.B., and Little, G., "Load Distribution in Prestressed Concrete Bridge Systems," The Structural Engineer, Vol. 32, No. 3, March 1954.

27. Morris, P.B., and Little, G., "Analysis of Right Bridge Decks Subjected to Abnormal Loading," Cement and Concrete Association, London, England, July 1956.

28. Rowe, R.E., "A Load Distribution Theory for Bridge Slabs Allowing for the Effect of Poisson's Ratio," Magazine of Concrete Research, Vol. 7, No. 20, July 1955.

29. Morris, P.B., Little, G., and Rowe, R.E., "Design Curves for the Effects of Concentrated Loads on Concrete Bridge Decks," Cement and Concrete Association, London, July 1956.

30. Arendts, J.G., "Study of Experimental and Theoretical Load Distribution in Highway Bridges," unpublished M.S. Thesis, Iowa State University, 1968.

31. Zienkiewicz, O.C., The Finite Element Method of Engineering Science, McGraw-Hill Publishing Company, LTD., London, 1971.

32. Motarjemi, D., and Van Horn, D.A., "Theoretical Analysis of Load Distribution in Prestressed Concrete Box-Beam Bridges," Fritz Engineering Laboratory Report No. 315.9, Lehigh University, October 1969.

33. Goldberg, J.E., and Leve, H.L., "Theory of Prismatic Folded Plate Structures," International Association of Bridge and Structural Engineers, Publication Vol. 17, 1957, pp. 59-86.

34. Sanders, W.W., "Distribution of Wheel Loads on Highway Bridges," Report furnished for review by members of the National Cooperative Highway Research Program, Transportation Research Board, 1983.

35. Standard Specifications for Highway Bridges and Incidental Structures, First Edition, American Association of State Highway Officials, Washington, D.C., 1931.

36. Standard Specifications for Highway Bridges, Seventh Edition, American Association of State Highway Officials, Washington, D.C., 1957.

37. Newmark, N.M., "A Distribution Procedure for the Analysis of Slabs Continuous over Flexible Beams," Engineering Experiment Station Bulletin 304, University of Illinois, Urbana, 1938.

38. Texas Highway Department, "Standard Specifications for Construction of Highways, Streets, and Bridges," September 1, 1982.

39. Texas State Department of Highways and Public Transportation, Bridge Division, Drawing File 1284, Research Project 3-5-83-350, April 14, 1982.

40. Operating Manual, Dennison 800 Series Variable Volume Pump, Model No. PV08-035-51R, 02-X381, Abex Corp., 1160 Dudlin Rd., Columbus, Ohio 43216.

41. Operating Manual, Sundstrand 1200RPM, Pressure Compensated Variable Volume Pump, Model No. S/SPV22-7012, Sundstrand Company, Ames, Iowa.

42. Precision Measurement Company, P.O. Box 7676, Ann Arbor, Michigan.

43. Newmark, N.M., et al., "Tests and Analysis of a Composite I-Beam," Proceedings of the Society for Experimental Stress Analysis, Vol. IX, No. 1, 1951, pp. 75-92.

44. Building Code Requirements for Reinforced Concrete, ACI Standard 318-83, American Concrete Institute, Detroit, Michigan, 1984.

45. Hognestad, E., "A Study of Combined Bending and Axial Load in Reinforced Concrete Members," University of Illinois Bulletin No. 399, 1951.

46. Fang, I-Kuang, "The Verification of Ontario Highway Bridge Deck Design on Steel Girders (With and Without Precast Panels)," Ph.D. Dissertation (in progress), The University of Texas at Austin, January 1985.

47. Bathe, K.J., Wilson, E.L., and Peterson, F.E., "SAPVI: A Structural Analysis Program for Static and Dynamic Response of Linear Systems," Report No. EERC 73-11, Earthquake Engineering Research Center, University of California at Berkeley, 1973.

48. Finite Element Analysis of Reinforced Concrete, American Society of Civil Engineers, New York, 1982.

NOTATION

C = specified constant for various bridge types

D.F. = distribution factor

E_c = secant modulus of elasticity of concrete at $0.5f'_c$

E_S = modulus of elasticity of steel (29,000 ksi)

EI = calculated flexural stiffness of girder

E_T = initial tangent modulus of elasticity of concrete

f_c = compressive stress in concrete

f'_c = 28-day compressive strength of 6-in. by 12-in. concrete cylinders

S = average girder spacing (ft)

h = uniform distance between points on the girder

I_S = calculated moment of inertia of composite girder section, transformed to steel

L = span length

M_i = moment at the i^{th} point on the girder

M(x) = moment at distance x along girder

P = concentrated load

W_c = unit weight of concrete (pcf)

W_i = load at the i^{th} point on the girder

W(x) = load at distance x along girder

γ = slip between deck and steel beam

ϵ_b = longitudinal strain in the beam

ϵ_c = strain in concrete

ϵ_o = compressive strain in concrete corresponding to maximum stress

ϵ_s = longitudinal strain in the slab